

**Design of membrane systems for
fractionation of particle suspensions**

Stellingen

1. Transmissie van deeltjes is een onderbelicht aspect van microfiltratie.
(dit proefschrift)
2. Een “quick en dirty” experiment met microzeven is bij voorbaat al mislukt.
(hoofdstuk 4)
3. Als de werkelijkheid voldoet aan een model, hoeft het mechanisme niet te kloppen.
4. De kracht van simuleren is niet zozeer het voorspellen van de werkelijkheid maar het afschatten van het effect van veranderingen.
5. Als je niet weet waar je naar toe gaat, kom je waarschijnlijk ergens anders terecht.
(Laurence J. Peter)
6. TomTom wijst de weg naar de Nederlandse kenniseconomie.

Stellingen behorend bij het proefschrift:

Design of membrane systems for fractionation of particle suspensions

Gerben Brans

Wageningen, 31 maart 2006

**Design of membrane systems for
fractionation of particle suspensions**

Promotor

Prof. dr. ir. R.M. Boom

Hoogleraar Levensmiddelenproceskunde, Wageningen Universiteit

Co-promotoren

Dr. ir. C.G.P.H. Schroën

Universitair docent, sectie Proceskunde, Wageningen Universiteit

Dr. ir. R.G.M. van der Sman

Universitair docent, sectie Proceskunde, Wageningen Universiteit

Promotiecommissie

Prof. dr. ir. H.E.A. van den Akker

Technische Universiteit Delft

Dr. R. Bos

Royal Friesland Foods Deventer

Dr. ir. R. G. H. Lammertink

Universiteit Twente

Prof. dr. E. van der Linden

Wageningen Universiteit

Dit onderzoek is uitgevoerd binnen de onderzoekschool OSPT.

Gerben Brans

**Design of membrane systems
for fractionation of particle suspensions**

Proefschrift

ter verkrijging van de graad van doctor
op gezag van de rector magnificus
van Wageningen Universiteit,
Prof. dr. M.J. Kropff,
in het openbaar te verdedigen
op vrijdag 31 maart 2006
des namiddags te vier uur in de Aula.

Gerben Brans (2006) Design of membrane systems for fractionation of particle suspensions

PhD. Thesis, Wageningen University, The Netherlands - with summary in Dutch.

ISBN: 90-8504-379-4

Contents

1	Introduction to membrane fractionation systems	1
2	Membrane fractionation of milk, state of the art and challenges	9
3	Optimization of the pore geometry and membrane design for micro-machined membranes	33
4	Evaluation of microsieve membrane design	63
5	Transmission and fractionation of micro-sized particle suspensions	75
6	A suspension flow model for hydrodynamics and concentration polarization in cross flow microfiltration	99
7	3D Lattice Boltzmann sub-grid particle method for suspension flow	127
8	Concluding remarks, towards fractionation on production scale	141

Summary

Samenvatting

Dankwoord

Curriculum vitae

Chapter 1: Introduction to membrane fractionation systems

Introduction

The development towards more sustainable production methods will lead to a more efficient use of renewable natural resources and agrotechnological products. This is not only important for the production of foods products, but also for the development of new biotechnological production routes for specialty and bulk chemicals.

Many applications demand the availability of pure components or a specific fraction of the feedstock, such as functional proteins from milk or enzymes produced by solid-state fermentation. Since the desired components are often part of heterogeneous mixtures, separation technology has gained more attention. Purification can often be achieved by separation based on a difference in physical properties, as is illustrated in table 1.

Because many feed streams in the food industry consist of suspended micro particles in a liquid (e.g. milk) or a liquid (water) is used as a processing aid (e.g. wheat processing), we focus on separation of these individual phases. This is in contrast to molecular separation, where components are mixed on a molecular scale, and different methods are required for fractionation.

Table 1: Principles for separation and examples of separation processes [1].

	Principle	Processes
Phase separation	Density Size Surface properties Surface tension	Centrifugation, sedimentation, flotation Sieving, filtration, microfiltration, ultrafiltration shear induced fractionation Flotation, interfacial partitioning Coalescers
Molecular separation	Surface adsorption Complexation Solubility Volatility Membranes (solubility and diffusivity)	Chromatography, adsorption Ion exchange, reversible chemical complexation Extraction, crystallization Distillation, drying Nanofiltration, reverse osmosis, dialysis, electro dialysis, gas separation, pervaporation.

For suspended micro particles (0.1 - 10 μm), fractionation by centrifugation is hardly possible, because their sedimentation velocity is too low and would therefore require very high centrifugation velocities and high energy input. If the particles in the mentioned size range have approximately the same charge, separation with an electric field is not effective. For many systems, therefore, separation on size is the method of choice, which can be realized by microfiltration. Further, microfiltration is suitable for large scale production processes, because it is relatively easy to scale up by parallelization of identical membrane modules (linear scale up).

Membranes

Microfiltration membranes are available in different varieties and can be characterized by their morphology (structure, thickness) and pore geometry (size, size distribution), which are both affected by the production method [2]. Morphology can be symmetric (homogeneous) or asymmetric. Asymmetric membranes consist of a support layer with large pore size, which is covered with a thin skin layer with small pores. This results in a membrane with small pore size, while maintaining high permeability and sufficient mechanical strength. High permeability is advantageous, because the membrane can be operated at low transmembrane pressures. This reduces the suction force acting on deposited particles on a pore and promotes the release of such deposits.

The pores can be circular and straight (cylindrical pores), or form a connected sponge-like network (tortuous path). Tortuous path membranes have no unique pore size, but their pore size has a broad distribution, e.g. between 0.1 to 10 times their nominal size, which makes them less suitable for fractionation purposes. Recently developed membranes, such as metal membranes and microsieves can have cylindrical pores with a well-defined pore shape and more uniform pore size (deviation few %), and show high potential for fractionation purposes.

Microfiltration membranes are made from different materials, such as polymers, ceramics, glass, metal and silicon, and are manufactured with different techniques: phase-inversion (e.g. diffusion induced phase separation from vapor or liquid, or thermally induced phase separation), track-etching, sintering (ceramic membranes), spinodal decomposition (glass membranes), electro-deposition (metal membranes), and photolithographic etching (microsieves), but this list is not exhaustive [2].

In this research, we worked with conventional polymer membranes and microsieves (fig. 1). The polymer membranes are produced by phase inversion and have a tortuous structure with a broad pore size distribution. Phase-inversion membranes are produced on commercial scale by different manufacturers and are relatively inexpensive.

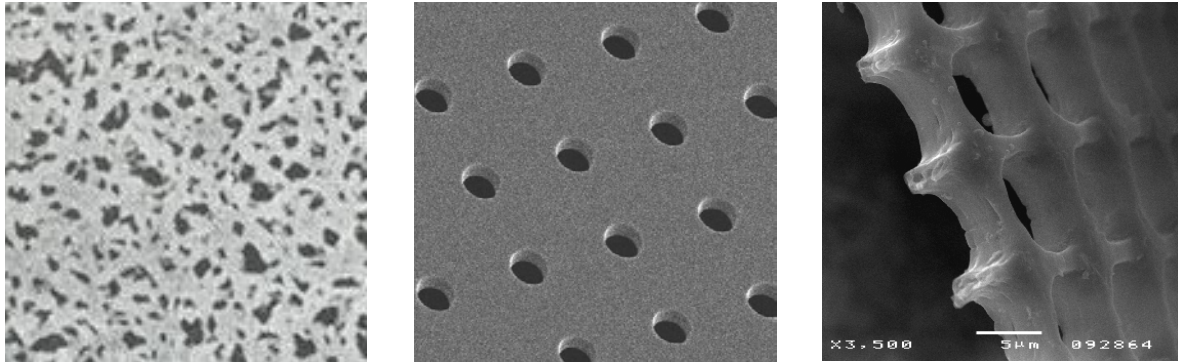


Figure 1: SEM photos of different membranes. Conventional polymer membrane (left), silicon microsieve (middle), and polymer microsieve (right).

Microsieves are a novel type of membrane, which are manufactured from silicon wafers with photolithographic techniques developed in the semi-conductor industry [3, 4]. Because of their extremely thin active top layer, their relatively large porosity, and their open support structure, the fluxes can be two or three orders of magnitude larger than conventional membranes, even when using very low transmembrane pressures.

Furthermore, these membranes have a flat silicon-nitride surface that is expected to have minimal particle adsorption and a uniform pore size. These unique features make microsieves interesting for membrane fractionation purposes. However, because microsieve technology is relatively new, silicon microsieves are costly. Microsieves are expected to become more price attractive when they can be mass produced. The newest development in this field is the polymer microsieve that combines properties of the silicon based microsieve (uniform pore size) with the use of conventional polymer membranes (production by immersion precipitation) [5]. This will also contribute to the attractiveness of microsieves.

Fractionation

In most current applications of microfiltration, it is sufficient to retain all particles from the liquid. The purpose of fractionation of particle suspensions is however the separation of smaller and larger particles. This is more complex, since the retention of large particles should be combined with transmission of smaller particles through the membrane (fig. 2).

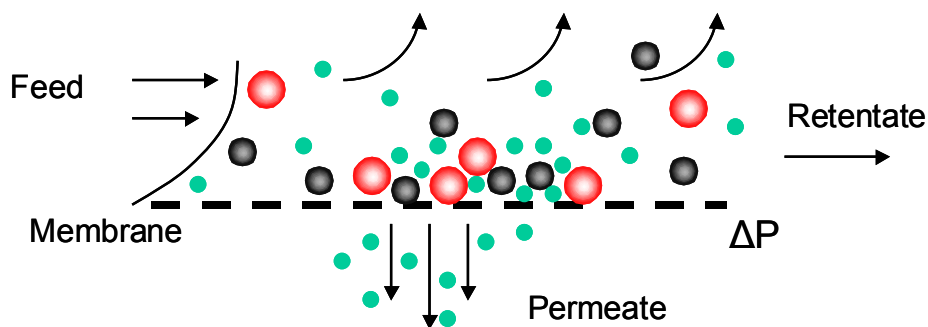


Figure 2: Schematic representation of membrane fractionation in cross flow.

Particle retention is based on size exclusion of the particles from the pores in the membrane. It can be carried out in dead end and in cross flow mode. In dead end, all the liquid is pushed through the membrane. The particles accumulate on the membrane surface and form a cake layer. Initially, the membrane determines particle retention, but as the pores in the cake layer are usually smaller than the membrane pores, the cake layer will determine the retention of small particles soon afterwards. In addition, the growing cake layer also increases the flow resistance. It is clear that this situation is not desired. Therefore, cross flow filtration of the feed suspension tangentially over the membrane is often applied. The cross flow mode induces backtransport of particles from the membrane surface into the bulk of the feed. Depending on the filtration regime (critical or sub-critical) [6], particles are taken up by the cross flow again [7] or they may remain close to the membrane.

Besides the retention of larger particles, fractionation implies the transmission of smaller particles through the membrane. However, even when the membrane pore size allows the passage of the smaller particles through the membrane, they may still be retained by a number of effects:

- 1) Large particles that are retained by the membrane can plug or block a pore, thus preventing passage of liquid and/or smaller particles (complete blocking mechanism). A tangential flow of the feed over the membrane will exert a

tangential force on the large particle, and when this force is sufficiently large, the particle will be taken up by the feed stream. However, if the particle is too firmly attached to (or sucked on) the pore, it cannot be removed.

- 2) When large particles do not block individual pores, but are still retained, they continue to accumulate on the membrane surface: a cake layer is formed. A cake layer of larger particles on the membrane will have smaller internal pores than the membrane, thus preventing the passage of smaller particles through the cake layer, and through the membrane.
- 3) Even when the larger particles have no influence, the smaller particles that ought to pass the membrane may cause plugging. Plugging of membrane pores can occur by the formation of a bridge of smaller particles.
- 4) Besides bridging, the small particles can adsorb to the pore walls inside the pores. This will reduce the effective pores size and may thus cause retention of particles that are smaller than the original pore size.

All these effects have to be prevented for the realization of an effective and efficient fractionation process. Effects 1 and 2 have been well described for membrane filtration (for both dead end and cross flow filtration), while 3 and 4 were mainly investigated for suspension flow through porous media in dead end mode. The occurrence of these combined effects depends strongly on the feed composition (relative particle sizes and concentrations), the membrane properties (surface properties and interactions with feed liquid and particles) and the process conditions (e.g. the flow velocity through the membrane and concentration [8, 9]). However, discussion of the combination of retention and transmission processes is still relatively scarce in literature and the interactions between particles of different sizes during membrane fractionation are largely unknown. Therefore, fractionation of particle suspensions clearly needs more investigation.

Aim of the research

The aim of the research reported in this thesis was to obtain more insight in microfiltration processes for the fractionation of micro-sized particles (0.1 - 10 μm) with small size differences. Given their potential especially for fractionation purposes, special attention was paid to microsieves as an alternative for conventional polymer and ceramic membranes.

The effects of microsieve design and process conditions (transmembrane pressure, cross flow velocity) on particle deposition need to be investigated in depth for the successful application of microsieves. The influence of flow dynamics was

investigated on pore/particle scale and on the scale of a microsieve pore field with Computational Fluid Dynamics (CFD). These CFD simulations were performed with the lattice Boltzmann (LB) method. Besides computer simulations, experimental validation was performed. The effects of process conditions and feed composition on fractionation were studied for polymer membranes and microsieves.

Outline of the thesis

A schematic outline of this thesis is depicted in figure 3. Chapter 2 describes different fractionation stages for milk that are currently known from literature. In this review, there is special attention to fouling and fouling control. Further, new membrane technologies and the value of computer simulations are touched upon.

In chapter 3, the effects of pore size, pore geometry, and inter-pore distance are evaluated with LB simulations. These effects were captured in a general criterion for critical flux, which relates the microsieve pore design to the choice of process conditions. Depending on the membrane process (filtration or fractionation) and the filtration regime, different pore designs are recommended. This work is especially relevant for the design of microsieves, since current micro-machining technology allows the preparation of microsieves with pores of almost any shape.

In chapter 4, the design of a microsieve is evaluated on the scale of the complete membrane or module, again with LB simulations. It was found that the design, and more specifically the design of the support structure, is important for flux maximization. The effect of the support structure on the flow was also demonstrated experimentally.

Chapter 5 describes experiments on the transmission of mono-disperse latex particles through polymer microsieves and conventional polymer membranes, and the fractionation of bi- and tri-disperse latex suspensions. The feed composition and process conditions (the transmembrane pressure and cross flow velocity) are related to particle transmission and fractionation processes.

In chapter 6, a new method for 2D suspension flow is introduced in LB. Suspended particles are treated as a continuous density field and the mass transfer is described with a convection-diffusion model. Concentration polarization and cake layer formation could be described accurately, and further, the model is used to evaluate the effect of turbulence promoters and corrugated membranes.

Chapter 7 describes a 3D discrete particle simulation method that ultimately is to be used for microfiltration. Because the particles are smaller than the grid cells on which the fluid flow is solved, this approach is called a sub-grid particle method.

The thesis is concluded in chapter 8 with a discussion of some practical implications for membrane fractionation on industrial scale, and an outlook is given on the use of computer simulations for the design and further understanding of fractionation processes.

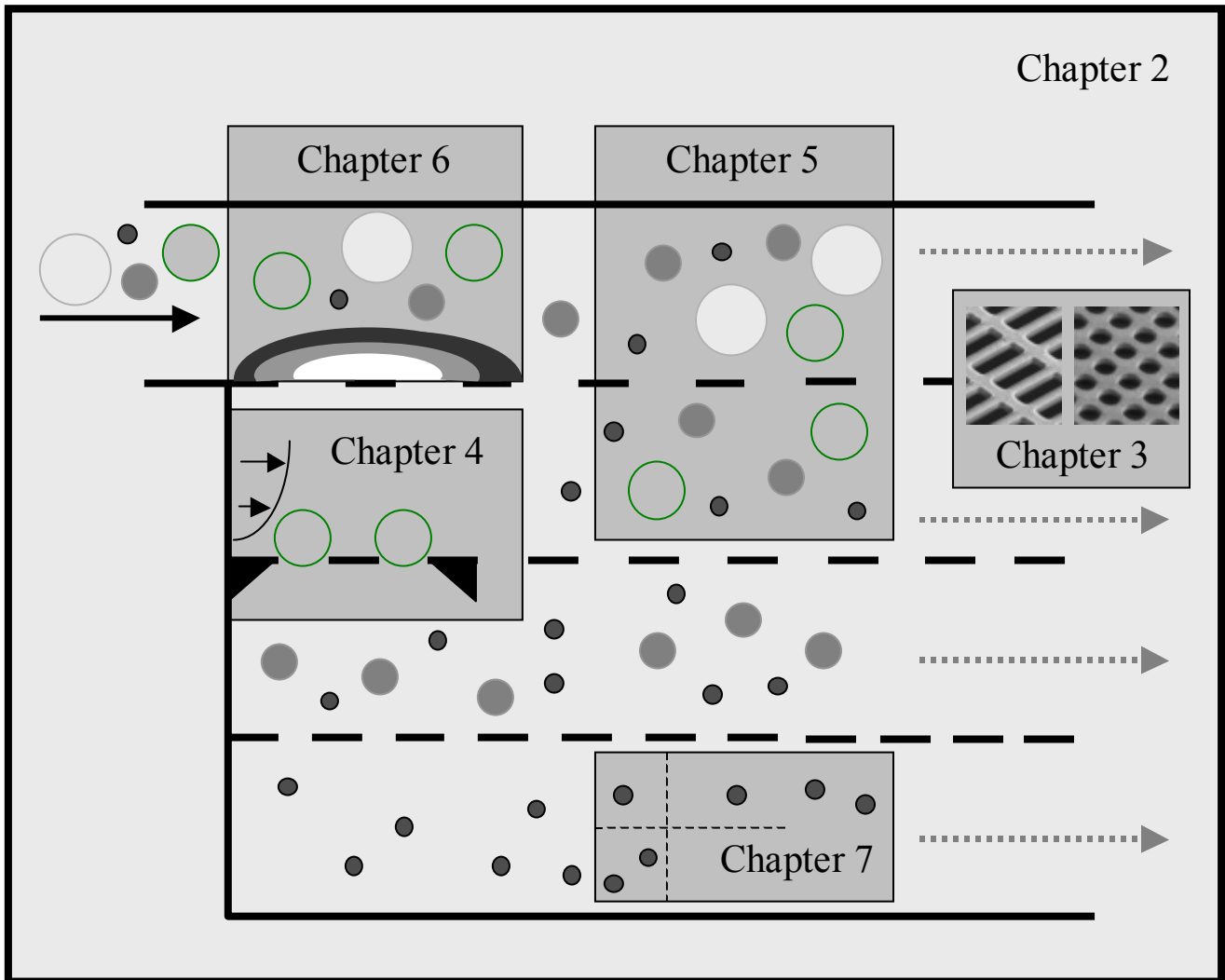


Figure 3: Schematic outline of this thesis: Chapter 1 introduction; Chapter 2 review about membrane fractionation of milk; Chapter 3 pore geometry and pore field design; Chapter 4 microsieve design and pore-blocking; Chapter 5 transmission and fractionation of particle suspensions; Chapter 6 model for suspension flow and concentration polarization; Chapter 7 discrete particle model with sub-grid particles.

Acknowledgement

The research was part of the D-force project that investigates the fractionation of milk with membrane technology (EETK 20033). We like to thank our project partners for interesting discussions and fruitful collaboration: Friesland Foods BV, Aquamarijn Micro Filtration BV, and Membrane Technology Group of Twente University.

References

- [1] A.S. Grandison, M.J. Lewis, Separation processes in the food and biotechnology industries: principles and applications. Woodhead, Cambridge (1996).
- [2] M. Mulder, Basic principles of membrane technology. Kluwer Academic Publishers (1991), Dordrecht, the Netherlands.
- [3] C.J.M. van Rijn, M.C. Elwenspoek, Micro filtration membrane sieve with silicon micro machining for industrial and biomedical applications. Proceedings of Micro Electro Mechanical Systems (MEMS) (1995) 83, Amsterdam, the Netherlands.
- [4] C.J.M. van Rijn, Nano and micro engineered membrane technology, Elsevier Amsterdam (2004), ISBN 0444-51489 9.
- [5] C.J.M. van Rijn, L. Vogelaar, W. Nijdam, J.N. Barsema, M. Wessling, Method of making a product with a micro or nano size structure WO0243937 (2002).
- [6] R.W. Field, D. Wu, J.A. Howell and B.B. Gupta, Critical flux concept for microfiltration fouling. J. Membrane Sci., 100 (1995) 259.
- [7] G. Belfort, R.H. Davis, A.L. Zydney, The behavior of suspensions and macromolecular solutions in cross flow microfiltration. J. Membrane Sci., 96 (1994) 1.
- [8] V.B. Pandya, S. Bhuniya, K.C. Khilar, Existence of a critical particle concentration in plugging of a packed bed. AIChE Journal 44 (1998) 978.
- [9] V. Ramachandran, H.S. Fogler, Plugging by hydrodynamic bridging during flow of stable colloidal particles within cylindrical pores. J. Fluid Mech. 385 (1999) 129.

Chapter 2: Membrane fractionation of milk, state of the art and challenges¹

Abstract

Separation of milk into well-defined fractions will lead to a more optimal use of milk components (milk fat, casein, serum proteins) and their functional properties. In principle, membrane separation technology is well capable of large-scale fractionation of milk. Membrane processes for the isolation of serum proteins from whey, and the reduction of bacteria and spores in skimmed milk have already been adopted by the dairy industry. Other separation steps, such as the separation and/or fractionation of cream and the concentration of casein micelles, could become feasible in the future.

In this paper, we give an overview of the current use of membranes in the fractionation of milk and discuss recent developments in membrane technology. Besides these different separation steps, we focus on the problem of fouling, which is considered the limiting factor in milk filtration. Different strategies to avoid and to decrease fouling are discussed, as well as their suitability in a fractionation process for milk.

Further, new developments on computer modeling are discussed. Both analytical models and Computational Fluid Dynamics (CFD) provide insight in the mechanisms of fouling and can be used to evaluate different methods to control fouling and to optimize process parameters. For the rational design of a milk fractionation process, it is essential that research in various fields, such as new membranes, module design, fouling control and modeling be carried out as part of an integrated approach toward a radical new process.

Introduction

Milk is a constituent of many foods and food products. The functionality of the various components in milk could be utilized more effectively if they were available separately. Fractionated milk components enable a more constant quality of

¹ This chapter is published as: G. Brans, C.G.P.H. Schroën, R.G.M. van der Sman, R.M. Boom, *Journal of Membrane Science* 243 (2004) 263.

consumer products (for example cheese) and the development of new products, such as edible coatings and bio-active peptides. Therefore, milk fractionation will lead to a more efficient and diverse use of milk. Further, working with concentrated streams may reduce the transport of water significantly, having both economical and environmental advantages.

Membrane separation technology seems a logical choice for the fractionation of milk, because many milk components can be separated on size (fig 1.). Membranes are already well established in the processing of whey and are gaining popularity in other dairy applications [1]. However, full membrane fractionation of milk is hardly described in literature; most papers focus on a single stage, such as the separation and fractionation of fat globules for cream, the reduction of bacteria and spores in skim milk, the concentration of casein micelles as pretreatment in cheese manufacturing, and the purification of serum proteins for physico-chemical or nutritional purposes.

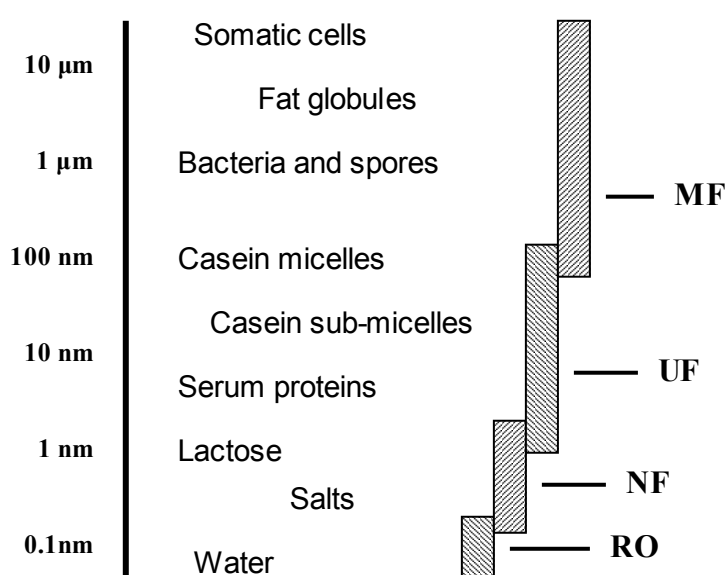


Figure 1: Components in milk: size indication and membrane processes. MF=microfiltration, UF= ultrafiltration, NF=nanofiltration, RO=reverse osmosis.

Milk is a complex feed for membrane based fractionation, because of the broad particle size distribution (1 nm - 20 μm), high concentration of dispersed components (13 w/w %), and natural variation. Current membrane processes for milk have a rather low capacity due to strong flux decline by fouling and processes are energy demanding because of the high cross-flow velocity that is required to control fouling. Additionally, methods to control fouling have increased the complexity in equipment

and operation. In literature, various strategies have been described to reduce fouling. The most relevant methods are discussed later in this paper.

Besides fouling, selectivity is an important issue for membrane fractionation of milk. A number of factors is important in achieving a good combination of retention and transmission of components in the feed. The first is uniformity in membrane pore size. Due to poly-disperse pores, components that should be retained pass the membrane through the larger pores. Smaller pores cause retention of components that should be transmitted. Using traditional polymer membranes, milk fractions could not be obtained in the desired purity, probably because of the wide pore size distribution.

Secondly, it is important that the process conditions are similar over the whole membrane area. This has led to the development of the Uniform Transmembrane Pressure (UTP) concept, and Isoflux and Gradient Porosity (GP) membranes [2]. The introduction of ceramic membranes and the use of the UTP concept enabled the commercial application of membranes for the reduction of bacteria and spores. The UTP concept maintains a constant transmembrane pressure over the length of the module by applying a cross-flow at the permeate side [2]. Isoflux and GP membranes have a spatial change in the membrane resistance to assure uniform process conditions.

Thirdly, fouling affects selectivity. Depth fouling leads to smaller effective pores and to different retention characteristics. Cake layer formation leads to a different retention behavior, as the cake retains small particles that should pass the membrane.

There is an ongoing search for new types of membranes with better properties, and for improved process conditions. The development of membranes with narrow pore size distribution, such as asymmetric ceramic membranes, track etched membranes [3], silicon microsieves [4] and metal microfilters [5] in combination with optimized process conditions, could lead to full fractionation of milk on production scale.

In this paper, we review different membrane processes that are reported for (partial) fractionation of milk (section I). In section II, we discuss different strategies to control fouling and touch briefly upon the use of computer models for process design. In both sections we will focus on large-scale applicability. The paper is concluded with some statements on new developments that are useful or are even required to make fractionation of milk feasible.

Membrane processes for fractionation of milk

Milk can be considered as an emulsion of fat globules in an aqueous phase. The aqueous phase consists of suspended and dissolved components, such as casein micelles, serum proteins, lactose and salts. Besides the major components fat, casein and lactose, milk contains valuable minor components that can be interesting for specific isolation. A typical composition of milk is given in table 1. The composition of milk varies per cow (race, age, stadium of lactation) and depends on the season, climate and feed [6].

Table 1: Average composition of cow milk: concentration and size distribution [6].

	Concentration in whole milk (g/l)	Size range and average (at weight average)
Water	87.1	
Fat globules	4.0	0.1-15 μm , average 3.4 μm
Casein (in micelles)	2.6	20-300 nm, average 110 nm
Serum proteins	0.7	3-6 nm
α lactalbumin	0.12	14 kD
β lactoglobulin	0.32	18 kD
BSA	0.04	66 kD
proteose-pepton	0.08	4-40 kD
immunoglobulins	0.08	150-900 kD
lactoferrin	0.01	86 kD
transferrin	0.01	76 kD
others	0.04	
Lactose	4.6	0.35 kD
Mineral substances	0.7	
Organic acids	0.17	
Other	0.15	

Given the relatively high concentrations and broad particle size distribution, milk is a challenging product for membrane fractionation. Many components are known to cause fouling and therefore, we discuss strategies to control fouling in section II. Because full fractionation of milk with membranes is not known from literature, we focus on single stages that were reported. More specifically, we consider the separation and/or fractionation of fat globules, the reduction of bacteria and spores in skim milk, the concentration of casein micelles, and the purification of serum proteins from cheese whey. In the next section, we will give an overview of the stages that are

already available and which ones need further development for a full fractionation process of milk.

a) Separation and fractionation of milk fat from whole milk

Although separation of fat with membranes is technically possible [7], the industry generally uses centrifugation instead. Cream resulting from centrifugation contains about 40 % fat. Possible advantages of membrane separation are a reduction in energy consumption and less damage to shear sensitive components, such as the fat globule membranes, when relatively low cross flow velocities are used. This can result in enhanced stability of cream and improved sensory properties of consumer products.

The diameter of the fat globules in raw milk is between 0.1 and 15 μm , with an average around 3.4 μm . Milk fat consists of triacyl glycerols and is mainly present in the form of dispersed fat globules. The fatty acid composition is diverse regarding chain length and degree of saturation. This composition gives milk fat its specific flavor and mouth feel. The fat globules are surrounded by a thin membrane, which resembles a cell membrane. At room temperature, the fat is mostly solid. To avoid clumping of milk fat globules, the separation of fat globules usually takes place around 50°C.

Gouedranche and co-workers described the fractionation of milk fat globules with a 2 μm ceramic membrane [8]. They did not report the size distribution of the fat globules in the permeate and the retentate. The two milk fat fractions were evaluated on their effect on texture and sensory properties of different consumer products against the reference cream. Small fat globules gave products with finer texture, which were appreciated more by the taste panel compared to products with large fat globules and the reference cream [8].

The acceptance of membrane separation of milk fat in the future depends on the extra commercial value of the products and the economics of the membrane process. From a technical point of view, the process can be optimized with respect to membrane choice and process parameters.

b) Removal of bacteria and spores from skim milk (cold pasteurization)

Microfiltration (MF) can reduce the amount of bacteria and spores without affecting the taste of the milk (as in UHT) and provides longer shelf life than pasteurization. Decimal reduction factors for MF are higher than for bactofugation, which is the reduction of bacteria and spores by centrifugation [9]. Besides the production of consumption milk with extended shelf life, this method can be used as pretreatment

of skim milk for the production of raw milk cheeses [10] and the reduction of spores in acid cheese milk. The size distribution of bacteria in milk is 0.4-2.0 μm and therewith partly overlapping with the fat globules.

Saboya and Maubois described the use of ceramic membranes with pore size 1.4 μm operated at a uniform transmembrane pressure of 50 kPa and a cross-flow velocity of 7.2 m/s. The flux was around $1.4 \cdot 10^{-4}$ m/s and the decimal reduction factor of bacteria and spores was above 3.5 [2]. Guerra and co-workers could achieve the same flux at lower cross-flow velocities (0.5-1 m/s) with a reversed asymmetric membrane with pore size 0.87 μm and an optimized backpulsing system [11]. In their experiments, the frequency of backpulsing was between 0.2 and 1 s^{-1} and the duration of the pulse was 0.022 s. Bacteria and spores were reduced by a decimal factor between 4 and 5 with 100 % transmission of casein micelles and a flux of $1.4 \cdot 10^{-4}$ m/s. A commercial process for the reduction of bacteria and spores with membranes is available under the name Bactocatch and several hundreds of these systems are operational for the production of consumption milk [1]. It is operated at high cross-flow velocities, typically 6 to 8 m/s and uses ceramic membranes [12].

A recent development is the microsieve, which is made with micro-machining technology. Microsieves have a narrow pore size distribution and a smooth inert silicon nitride surface. Further, their hydrodynamic resistance is very low, allowing extremely low transmembrane pressures. Transmembrane pressure can be two orders of magnitude lower compared to conventional membranes. This lowers the suction force on deposits and reduces the tendency to foul significantly. Using laser interference lithography, it is possible to produce pore sizes as small as 0.1 μm [4]. Van Rijn and Kromkamp [13] described the use of microsieves to reduce the amount of bacteria in milk. Bacterial reduction by a decimal factor of 6.6 could be reached by filtering simulated milk ultra filtrate ('SMUF'), inoculated with *Bacillus subtilis* over a 0.5 μm microsieve in dead-end filtration [13]. With microsieves, a high reduction of bacteria can be achieved at low transmembrane pressure, since these membranes have very high permeabilities. Hence, the use of microsieves seems very promising. In the reduction of bacteria and spores, both fouling control (related to capacity) and selectivity are important. Fouling mechanisms are complete pore blocking by bacteria and spores, partial pore blocking by bridging of casein micelles, adsorption to the membrane surface of serum proteins and in-pore fouling by serum proteins. Selectivity is important, because bacteria and spores must be retained as much as possible, while other milk components should pass the membrane.

c) Concentration of casein micelles from skim milk

Concentrated casein micelles can be recombined with cream for the production of cheese. Other applications include standardization of milk and production of dried native casein for food applications. The permeate of the casein concentration process is a better starting material for the purification of serum proteins than cheese whey.

Whole milk contains 2.6 % w/w casein, but the volume fraction of the micelles can be as much as 10 % of the milk. Besides casein, the micelles consist of calcium, phosphate and water. The voluminosity of the casein micelles is 4.0 ml/g. On the outside, they have a 'hairy' κ -casein surface. These 'hairs' (glycomacropeptide) cause steric hindrance and prevent aggregation of the casein micelles in milk. The diameter of the micelles is between 20 and 300 nm with an average of about 110 nm [6].

The native casein micelles can be concentrated from skim milk by ceramic membranes with pore sizes between 0.05 and 0.2 μm . To minimize fouling, relatively high cross-flow velocities are used, often in combination with the UTP concept.

At a cross-flow velocity of 6.9 m/s, Pouliot and co-workers could achieve a flux of $2.5 \cdot 10^{-5}$ m/s during concentration to a factor 3. They operated a 0.22 μm Ceraflo membrane at a transmembrane pressure of 190 kPa [14]. This is comparable with the results of Vadi and Rizvi who found a flux of $1.9 \cdot 10^{-5}$ m/s for a concentration factor 2, using a 0.2 μm Membralox ceramic membrane with a transmembrane pressure of 193 kPa and a cross-flow velocity of 7.2 m/s. At concentration factor 10, the flux was still $1.3 \cdot 10^{-5}$ m/s [15]. Punidadas and Rizvi reached a somewhat higher flux of $3.1 \cdot 10^{-5}$ m/s for concentration factor 2, at a cross-flow velocity of 5.4 m/s. They used a 0.05 μm asymmetric Ceramem membrane and a transmembrane pressure of 138 kPa [16].

Despite the use of different membranes with different pore sizes and transmembrane pressures, similar fluxes have been reported. This might indicate that experiments were in the pressure independent flux regime and the flux was equal to the critical flux. The critical flux theory is discussed in the section on fouling. Higher fluxes can be obtained by changing the hydrodynamics in the module. Krstic and co-workers describe the use of turbulence promoters in 0.05, 0.1 and 0.2 μm Membralox ceramic membranes. By inserting a Kenics static mixer in the membrane tubes, they reached flux improvements up to 500 % at transient Reynolds numbers. Besides increasing the flux, the insert improved cleaning. The flux increased from $1.7 \cdot 10^{-5}$ to $9.7 \cdot 10^{-5}$ m/s at a cross-flow velocity of 0.45 m/s for the 0.1 μm membrane at a transmembrane pressure of 34 kPa (concentration factor 1). With a transmembrane pressure of 65

kPa, and cross-flow velocity of 12.5 m/s, a flux of $2.5 \cdot 10^{-4}$ m/s was reached, which is a considerable improvement compared to the studies presented previously [17].

To get membrane-based concentration of casein widely accepted in industry, the performance needs to improve. Papadatos and co-workers published an economic study on the feasibility of MF in cheese making for Northern America [18]. Based on prices in the period 1998-2000, they found higher net revenues for both Cheddar and mozzarella cheeses produced by MF in 30 out of the 36 months. There was no difference in revenues between twofold and threefold concentration of casein.

In the concentration of casein micelles, fouling control is more important than selectivity, as compared to the process for the reduction of bacteria and spores. Selectivity is less important, because some whey protein will always be present in the concentrated casein stream and casein that passes the membrane will end up in whey protein concentrate. This affects the economics of the process, because recovery of serum proteins from cheese whey becomes more complicated while the cheese yields decrease. Sometimes, traditional ultrafiltration (UF) is used as pretreatment for cheese. An advantage of UF is the cheaper equipment: a polymer membrane is used instead of a ceramic membrane, and no UTP provisions are required. However, the fact that more whey proteins end up in the cheese manufacturing process is disadvantageous.

d) Recovery of serum proteins from cheese whey

In industry, serum proteins are generally concentrated from whey. Therefore, they are often called whey proteins. There may be small differences in protein composition between cheese whey and permeate of membrane-based casein concentration. For example, glycomacropeptide is present in whey, because it is released from κ -casein during cheese production, but it is hardly found in the milk serum.

Whey is a nutritious protein source, but application in food or feed products without demineralization is limited. Nowadays, whey is concentrated by evaporation or reverse osmosis (RO) and demineralized by electrodialysis or ionexchange resins [19]. An alternative to reduce the amount of salts and to concentrate proteins in one step is nanofiltration (NF). Van der Horst and co-workers [20] give a detailed description of the NF process. NF reduces energy consumption, but only leads to partial demineralization. The concentrated serum proteins can be spray dried and used in food or feed applications. Depending on the protein content, these products are called whey protein concentrate (WPC, 35–80 % protein) or whey protein isolate (WPI, 80–95 % protein).

Often polymer UF membranes are used, but ceramic membranes are gaining more attention, because of better resistance against cleaning and disinfection. Doyen and co-workers [21] carried out a comparative study on whey treatment with polymer (PSF/PVP), ceramic (ZrO_2) and organo-mineral (ZrO_2/PSf) membranes. The molecular weight cut-off values were between 25 and 50 kD. Although the permeability of the membranes was different, the plateau fluxes were comparable, which means experiments were in the pressure independent flux regime. At a cross-flow velocity of 6 m/s, fluxes between $5.6 \cdot 10^{-5}$ and $6.8 \cdot 10^{-5}$ m/s were reached, depending on the concentration factor. Therefore, they concluded that fouling is the limiting factor in whey protein concentration and not the permeability of the membrane.

Besides whey protein concentration, it is attractive to isolate the individual serum proteins. Milk serum proteins consist of: α lactalbumin and β lactoglobulin, bovine serum albumin (BSA), immunoglobulins, lactoferrin, transferrin, traces of enzymes and some minor proteins and peptides (table 1). The β lactoglobulin has interesting physico-chemical properties and can be used in emulsification, foaming and gelling [22]. Lactoferrin and α lactalbumin have pharmaceutical applications [1, 23], and lactoferrin can be used in infant formulas and as a preservative for meat. In addition, there is an increasing interest in bioactive hydrolysates from serum proteins [24]. Reported isolation methods are based on the thermal aggregation of α lactalbumin [25], ion exchange chromatography, precipitation, UF or a combination of these methods [26-30]. Using precipitation and UF, Gesan-Guiziu and co-workers reported a purity of 52-83 % for α lactalbumin and 85-94 % for β lactoglobulin respectively [28]. Konrad and co-workers compared different purification methods for β lactoglobulin and obtained purities between 82.5 and 94.1 % [30]. It is also possible to make use of the specific properties of the protein to enhance the selectivity of the UF process. Adjustment of pH and addition of salt influence the electrostatic and steric interactions between different proteins, and between proteins and the membrane [22, 31].

In the production of WPC or WPI with membranes, fouling control is crucial, because all proteins are retained, and cake formation and gelling take place easily. In the isolation of serum proteins, selectivity is very important, because the purity determines the commercial value of the products, especially for pharmaceutical applications. The higher value allows the use of more expensive modules, types of membrane and methods to control fouling, to obtain a maximum selectivity of the fractionation process. However, alternative technologies could also offer an

economically feasible purification. Therefore, the choice of purification method depends on the application and needs to be studied for each individual application.

It is clear that membranes can be used successfully in several fractionation stages of milk. However, in the current situation, most steps need further development. The separation and fractionation of fat globules with membranes is competitive to centrifugation. Advantages of fat fractionation must be compared on added value with centrifuged cream. The process must be optimized and capacity must be increased by better fouling control and smart choice of the type of membrane and processing conditions.

For the reduction of bacteria and spores in skim milk, the capacity needs to be increased to reduce costs, but the resulting product is superior in quality (longer shelf-life with good taste) compared to UHT and pasteurized milk. Therefore, the process seems feasible in western countries with the current membrane technology. In the concentration of casein micelles, the capacity must also be increased and the added value of the clean permeate as starting material for the purification of serum proteins ('ideal whey', [32]) must be taken into account. In the purification of serum proteins, selectivity is most important and should be increased to obtain purer products or the same purity in fewer steps. The one factor that is limiting in all stages of milk fractionation is fouling. We discuss this aspect in the next section and will also evaluate the possibilities to reduce fouling in milk fractionation.

Methods to decrease fouling and to increase membrane performance

Fouling is the limiting factor in all applications of membrane filtration of milk [33]. The amount of deposits on the membrane must be minimized, because the flux decreases and the selectivity of the separation is affected. Several studies reported on the structure of membrane fouling by milk [34, 35]. Different fouling mechanisms can take place: adsorption, pore blocking, cake layer formation, and depth fouling. Concentration polarization is strictly speaking not fouling, but also decreases the flux and can affect selectivity.

Short-time reversible fouling takes place on a small time scale (seconds, [11]) and can be avoided or removed by the right choice of process conditions, such as high cross-flow velocity or backpulsing. Pore blocking and cake formation are typically considered short-time reversible fouling. Long-time reversible fouling causes a slow flux decrease in time (hours) and can be removed by stopping the production

process and applying a cleaning procedure. Irreversible fouling causes flux decline and cannot be removed by cleaning. Since cleaning is an intrinsic part of safe food manufacturing, and therefore has to be applied regularly, we consider cleaning a mandatory requirement. In this paper we will only consider methods to limit short-time reversible fouling, from now on called 'fouling'. Occurrence of irreversible, non-cleanable fouling decreases membrane performance and determines membrane lifetime.

According to the critical flux theory [36, 37], three regimes can be distinguished for membrane filtration. Each regime has a different flux dependency on the transmembrane pressure (fig. 2, 3). In regime I, the transmembrane pressure is below the critical pressure and there is cake free filtration.

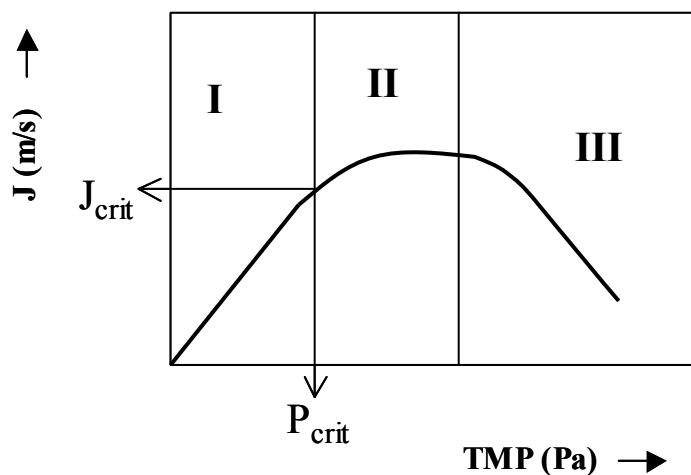


Figure 2: Critical flux regimes: flux dependency on transmembrane pressure. I: Sub-critical operation without flux-dependent fouling, flux is linear with transmembrane pressure. II: Transmembrane pressure is above the critical pressure and flux is described by gel filtration model or backtransport model. III: Transmembrane pressure is far above critical pressure and flux decreases in time.

Two forms of critical flux exist; called the hard form and the weak form. For the hard form, the flux / pressure relation is linear and equal to the clean water flux. For the weak form, the flux / pressure relationship is still linear, but lower than for clean water flux. Filtration in this regime is also known as sub-critical flux operation and is advised to obtain optimal selectivity. Because of the low value of the flux, the capacity is low and a large membrane area is needed. However, higher cross-flow velocity can increase the capacity. In regime II, the transmembrane pressure is above the critical pressure and flux is equal to the limiting flux, which can be

described by the gel filtration model or back-transport models [38], as the transport of materials towards the membrane is in equilibrium with the back transport towards the cross-flow. Hence, a higher cross-flow velocity is advantageous and could even shift the process to regime I.

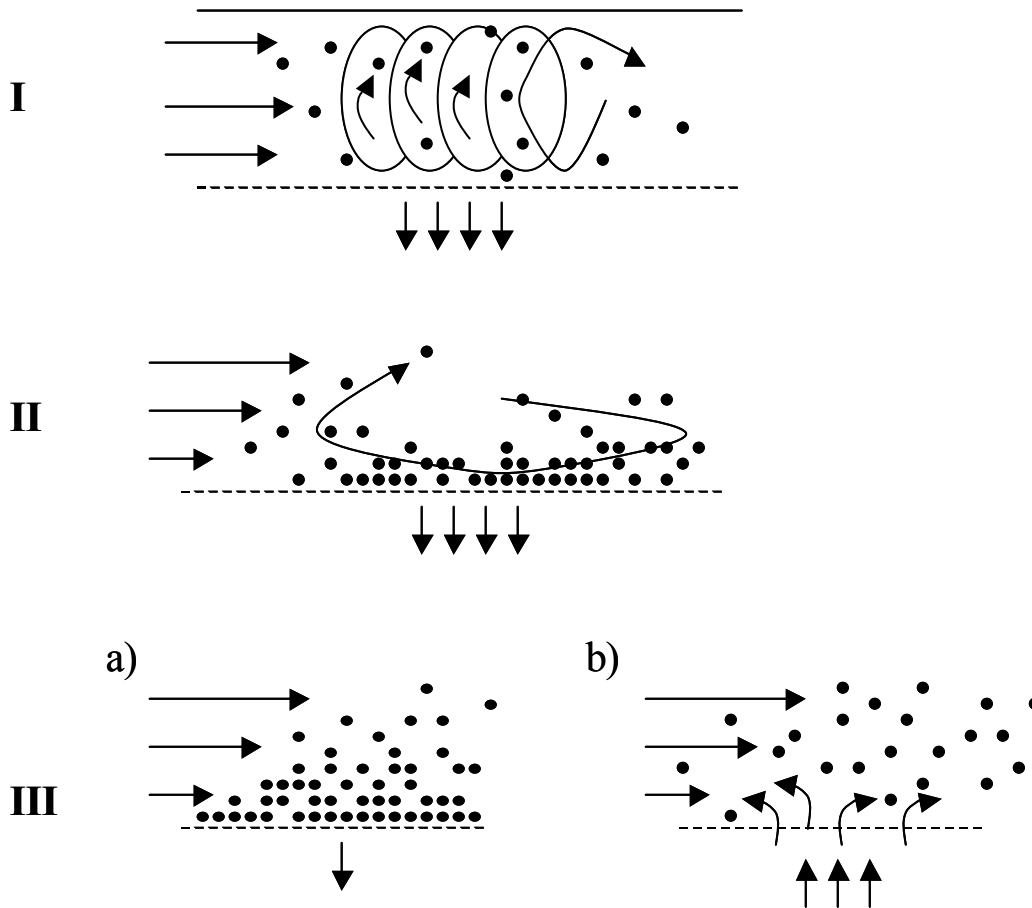


Figure 3: Graphical representation of fouling in different flux regimes. I: Sub-critical operation without fouling, for example by mixing in turbulent flow regime. II: Filtration with a dynamic cake layer, described by backtransport models, such as the shear induced diffusion model. Deposited particles tumble over each other and can be taken up by the cross-flow again. III: Time dependent flux with severe cake formation on small time-scale (a). Backpulsing could be a remedy (b).

Further, the flux is independent of the transmembrane pressure and the pore size of the membrane. However, the ratio between membrane thickness and transmembrane pressure could influence the start of cake formation (pore blocking). Membranes with high permeability in combination with a low transmembrane pressure decrease the suction force on deposits towards the membrane and allow an easier back transport.

When cake formation is minimal, regime II leads to optimal capacity and is chosen for expensive membranes to minimize the membrane area. However, selectivity is not optimal, because of the cake layer formation. This is also true for regime III, where transmembrane pressure is clearly above the critical pressure and results in a time dependent flux, mostly attributed to cake compaction. For longtime stable operation in regime III, it is necessary to remove fouling after short intervals. MF processes for reduction of bacteria and spores, and concentration of casein micelles are operated just above the critical pressure in the lower part of regime II.

Concentration of whey protein takes place in regime II, to have optimum capacity. The isolation of whey proteins is restricted to regime I, for optimal selectivity. Although operated in regime I, some milk components will still cause some fouling due to adsorption, and therewith influence the flux and selectivity more or less. Therefore, adsorption to the membrane surface or in the membrane (depth fouling) still causes flux decline on large time-scale. To minimize particle adsorption, thin membranes with smooth surfaces that have minimal interaction with the feed are recommended.

In the reduction of bacteria and spores, and the concentration of casein micelles with ceramic membranes (regime II), fouling is controlled by the use of a high cross-flow velocity in combination with the uniform low transmembrane pressure (UTP) concept. Basically, the high cross-flow velocity results in a relatively large pressure drop over the cross-flow channel, which causes a decreasing transmembrane pressure over the length of the tube. Therefore, the transmembrane pressure is compensated by a cross-flow at the permeate side [2]. A disadvantage of the UTP concept is the high energy demand as a result of the cross-flow at both sides of the membrane. In spite of that, the UTP is currently the most popular strategy against fouling during the filtration of skim milk to retain bacteria and the concentration of casein micelles. Alternatively, Isoflux and Gradient Porosity membranes can be used. These membranes have a decreasing membrane resistance over length of the tube, which has the same effect as UTP, without the need to control pressure in different sections at the permeate side.

Different strategies to suppress fouling are available in literature. Most methods are discussed in the review of Wakeman and Williams [39]. However, they do not consider the suitability of these methods in specific applications. The method of choice for fouling control must be technically and economically feasible, scalable to production size, and well suited for cleaning in place. In this section both methods to control fouling (table 2) and their applicability in the fractionation of milk are discussed.

Table 2: Summary of methods to enhance membrane performance, principle and possible disadvantages.

Method	Working principle	Possible disadvantage	References
High cross-flow velocity with UTP concept	Enhance backtransport by turbulent flow and low transmembrane pressure	High power consumption, high investment and operating costs	2, 14, 15, 16
Turbulence promoters	Enhance backtransport by micro-turbulences close to the membrane	Difficult cleaning (hygiene), increased power consumption	17, 43
Backpulsing (-washing, -flushing)	Remove cake by reversing the transmembrane pressure	Up scaling, difficult to control pressure in large systems	11, 44, 45
Pulsating cross-flow	Create velocity fluctuations in the feed to promote back transport	Up scaling, difficult to control pressure waves in large systems	46, 47
Air slugs	Increase shear and mixing close to the membrane	Difficult to control bubble size, foaming, denaturation	48, 49
Scouring particles	Increase shear and mixing close to the membrane	Wear of membrane and pumps, denaturation	50
Acoustic/ultrasonic waves, sonication	Promote back transport of deposits by vibrations and cavitations	Power consumption and heating, damage to sensitive compounds	51, 52
Vibrating modules	Increase shear close to the membrane	Up scaling, expensive equipment	40
Rotating disk	Increase shear close to the membrane	Up scaling, aseptic seals	41, 42
Electric fields	Introduce electric forcefield to keep charged particles from the membrane	Electrolysis, gas production, heating, denaturation and power consumption	54, 55

Vibrating modules, such as VSEP [40], and rotating disk modules [41, 42] can be used to prevent particle deposition. Both methods increase the shear rate close to the membrane surface, by either vibrating the membrane or by placing a rotating disk just above the membrane surface. Vibrating membrane equipment is difficult to scale up and expensive. However, some production installations are in use to obtain high concentration factors for bacteria and spores in skim milk. Rotating disks or stirrers could be difficult to implement, because aseptic sealings or bearings are needed between the shaft and the module. A notable feature is that the applied shear is

independent of the cross-flow velocity. Therefore, a low cross-flow velocity can be applied, avoiding a decreasing transmembrane pressure along the membrane and UTP provisions.

Other means of increasing the shear close to the membrane surface are spacers, turbulence promoters, and inserts that create flow instabilities, such as Dean vortices or micro-turbulences [43]. Krstic and co-workers reported high flux improvements in the concentration of casein with a static mixer insert [17]. A possible disadvantage of inserts is cleaning problems, because dead-areas will also be created. Therefore, it is not the method of choice to optimize the flux behavior in the filtration of milk.

Besides modification of the module, different procedures have been developed to remove fouling by non-stationary flow fields (regime III). Backpulsing and comparable techniques, such as backwashing, backflushing and backshocking [44, 45] are effective means to remove fouling. In these procedures, the transmembrane pressure is temporarily inverted and part of the permeate flows back into the cross-flow channel. Deposits on the membrane are lifted and taken up by the cross-flow. Backpulsing needs to be well controlled in large systems. The effectiveness of the pulse depends on the frequency, the duration and the pressure profile, and is highly dependent on the feed composition. Fast reacting valves are available to generate pulses with frequencies indicated by Guerra and co-workers ($0.2-1.0 \text{ s}^{-1}$). They reported good results for the reduction of bacteria in skim milk with the combination of UTP concept and backpulsing. As a result, the cross-flow velocity could be reduced significantly [11].

Further, pulsating or reversed feed flows [46, 47] can be used to control fouling by rapid velocity changes in the cross-flow channel. Pulsating cross-flow is difficult to scale up, because pressure waves are damped in large systems and become less effective over distance.

Other methods to reduce the effect of fouling include air slugs [48, 49], scouring particles [50] and the use of acoustic or ultrasonic waves and sonication [51, 52]. Air slugs and scouring particles improve mixing close to the membrane surface, therewith promoting the up-take of deposits. Air slugs and scouring particles are difficult to control in large membrane systems. The introduction of air could also cause unwanted foaming of milk in the module and denaturation of protein. Scouring particles must be retained and reused (need for cleaning) and cause extra wear in the pumps and damage to the membrane. Therefore, these options do not seem preferable for fractionation of milk.

In the case of acoustic waves and sonication, the energy of the waves is transformed to kinetic energy of the particles. This causes vibrations and cavitations, which

promote the back-transport of deposits into the cross-flow channel. However, ultrasonic and acoustic waves are unfavorable for milk, because the cavitations could cause denaturation of proteins [53]. The membrane rapidly damps ultrasonic waves and standing waves are formed due to the specific module design. Scale-up of ultrasonic assisted membrane filtration is difficult and may prove too expensive for large-scale milk treatment.

Further, constant or pulsed electric fields are reported to enhance membrane filtration [54, 55]. The electric field is used to prevent migration of charged components towards the membrane surface. Electrode reactions may lead to undesired contamination of the milk, such as metal ions and oxidized components. The electric charge of proteins can be influenced by pH. Although pH adjustment of milk is undesirable, this method could be used in the purification of serum proteins from whey.

Models

To choose the appropriate method of fouling control, an experimental approach is often taken. On the other hand, many realistic models for ultrafiltration and microfiltration are available in literature that could be helpful [56-63]. These models can be characterized as macroscopic and are often experimentally validated with model suspensions of clay, latex, silica or yeast cells. They can be used to estimate cake layer formation and concentration polarization as it is affected by the module geometry, feed composition (concentration and particle size), cross-flow velocity and transmembrane pressure. Belfort and co-workers [38], and Bowen and Jenner [64] have written valuable reviews on ultrafiltration and microfiltration models. The application of these models is hampered by the fact that practical systems are usually multi-component systems and the transport of particles through the membrane (transmission) is not taken into account. Different particle sizes interact and cause a more complex fouling pattern than the current models can describe. It is clear that knowledge on these aspects is still lacking.

Because of the broad particle size distribution and fouling characteristics of milk components, the filtration of model suspensions is difficult to translate to the filtration of milk. Samuelsson and co-workers compared the concentration of casein from skim milk with models for different back-transport mechanisms. They found that the shear-induced diffusion model could describe the experiments best [65].

Especially for more complex multi-component systems, Computational Fluid Dynamics (CFD) can provide a better understanding of module performance. CFD

can be used to study fluid flow in complex geometries and to test the influence of process parameters. Single phase CFD is often used to find the optimum configuration of inserts and spacers to decrease particle deposition in membrane modules by micro-turbulences [66, 67]. A new development in CFD is a diffusion-convection approach, in which the dynamic behavior of dissolved components and cake layer formation is taken into account explicitly [68, 69]. Dufreche and co-workers presented a model for particle deposition on a membrane. They studied the change in effective permeability during cake growth [70].

A promising method for suspension flow is the Lattice Boltzmann method, in which the interactions between the fluid and the suspended particles are fully resolved [71, 72]. Casein micelles and fat globules can be approximated as hard spheres [73]. Although current computing power restricts this technique to small-scale simulations, these simulations do give insight into the fundamentals of suspension behavior during MF, such as shear-induced diffusion even for multi-component systems [74]. Fundamental parameters from small-scale simulations can be incorporated in coarser simulations that will provide useful information about the module design and operating conditions in its turn. Although computer models become increasingly powerful, experiments will always be necessary for the fine-tuning of large membrane systems and to study effects that are not included in models. However, the amount of experiments can be reduced considerably, because a realistic 'operating window' can be defined a-priori, based on the modeling results.

Conclusion

Fractionation of milk has clear technological and economical advantages, and could become a key development for the dairy industry. Membrane technology is a realistic option for fractionation on production scale. Some separation steps are already in use, while others need further development.

In general, the capacity of membrane processes needs to increase. Therefore, appropriate fouling control is also important regarding the economics of the process. Although flux enhancement has got a lot of attention in terms of understanding and practical improvements (with inserts, backpulsing), achievement of a high selectivity (full retention of large components and full transmission of small ones) deserves more attention. High selectivity is not only dependent on the membrane, but is just as much dependent on the process conditions and interactions between the components in the feed. New types of membranes with narrow pore-size distribution are currently becoming available.

To enhance capacity and selectivity, both analytical models and CFD are helpful tools that give more fundamental insight in module design, process parameters, and selectivity. It is important that the specific properties of the feed (in this case milk) are considered, and that the complexity of the system is taken into account explicitly. The process needs to be simple and reliable, and absolutely food safe.

In this paper, we show that fractionation of milk with membranes is feasible from a technological point of view. In the near future, we expect that process conditions and methods to control fouling will be optimized for existing membranes. Eventually, more drastic changes will take place, such as new types of membranes and unconventional module and/or process designs. The role of computer modeling will become more pronounced. An integrated approach of these disciplines is expected to bring fractionation of milk within reach, even on commercial scale.

Acknowledgements

We would like to acknowledge the support of the Dutch foundation of Economy, Ecology and Technology (EET), Friesland Coberco Dairy Foods, Aquamarijn Micro Filtration BV, and J. Kromkamp for carefully reading the manuscript.

References

- [1] G. Daufin, J.P. Escudier, H. Carrere, S. Berot, L. Fillaudeau and M. Decloux, Recent and emerging applications of membrane processes in the food and dairy industry, *Trans IChemE*, 79 (2001) 89.
- [2] L.V. Saboya and J.L. Maubois, Current developments of microfiltration technology in the dairy industry, *Lait*, 80 (2000) 541.
- [3] P. Apel, Track etching technique in membrane technology, *Radiation Measurements*, 34 (2001) 559.
- [4] S. Kuiper, Development and application of microsieves, PhD thesis University of Twente, Enschede, The Netherlands (2000).
- [5] R.G. Holdich, I.W. Cumming, S. Kosvintsev, A.J. Bromley and G. Stefanini, Clarification by slotted surface microfilters, *Minerals Engineering*, 16 (2003) 121.
- [6] P. Walstra, T.J. Geurts, A. Noomen, A. Jellema and M.A.J.S. van Boekel, *Dairy Technology: principles of milk properties and processes*, Marcel Dekker, New York, 1999.
- [7] Alfa-Laval A.B., Separation of skim milk from milk or cream by filtering, GB Patent 1451747, 1976.

- [8] H. Goudedranche, J. Fauquant and J.L. Maubois, Fractionation of globular milk fat by membrane microfiltration, *Lait*, 80 (2000) 93.
- [9] A. Stack and G. Sillen, Bactofugation of liquid milks, *Nutrition and Food Sci.*, 98 (1998) 280.
- [10] P. Zoon and G. Hup, Process for the preparation of raw milk cheese, Eur. Patent 0546641A1, 1991.
- [11] A. Guerra, G. Jonsson, A. Rasmussen, E. Waagner Nielsen and D. Edelsten, Low cross flow velocity microfiltration of skim milk for removal of bacterial spores, *Int. Dairy Journal*, 7 (1997) 849.
- [12] S. Holm, R. Malmberg and K. Svensson, Method and plant producing milk with low bacterial content, WO Patent 8601687, 1989.
- [13] C.J. van Rijn and J. Kromkamp, Method for filtering milk, WO Patent 0209527, (2001).
- [14] M. Pouliot, Y. Pouliot and M. Britten, On the conventional cross-flow microfiltration of skim milk for the production of native phosphocaseinate, *Int. Dairy Journal*, 6 (1996) 105.
- [15] P.K. Vadi and S.S.H. Rizvi, Experimental evaluation of a uniform transmembrane pressure crossflow microfiltration unit for the concentration of micellar casein from skim milk, *J. Membrane Sci.*, 189 (2001) 69.
- [16] P. Punidadas and S.S.H. Rizvi, Separation of milk proteins into fractions rich in casein or whey proteins by cross flow filtration, *Food Research International*, 31 (1998) 265.
- [17] D.M. Krstic, M.N. Tekic, M.D. Caric and D.S. Milanovic, The effect of turbulence promoter on cross-flow microfiltration of skim milk, *J. Membrane Sci.*, 208 (2002) 303.
- [18] A. Papadatos, M. Neocleous, A.M. Berger and D.M. Barbano, Economic feasibility evaluation of microfiltration of milk prior to cheesemaking, *J. Dairy Sci.*, 86 (2003) 1564.
- [19] M. Greiter, S. Novalin, M. Wendland, K.D. Kulbe and J. Fischer, Desalination of whey by electro dialysis and ion exchange resins: analysis of both processes with regard to sustainability by calculating their cumulative energy demand, *J. Membrane Sci.*, 210 (2002) 91.
- [20] H.C. van der Horst, J.M.K. Timmer, T. Robbertsen, J. Leenders, Use of nanofiltration for concentration and demineralization in the dairy industry: Model for mass transport, *J. Membrane Sci.*, 104 (1995) 205.
- [21] W. Doyen, W. Adriansens, B. Molenberghs and R. Leysen, A comparison between polysulfone, zirconia and organo-mineral membranes for use in ultrafiltration, *J. Membrane Sci.*, 113 (1996) 247.
- [22] A.L. Zydney, Protein separations using membrane filtration: new opportunities for whey fractionation, *Int. Dairy Journal*, 8 (1998) 243.

-
- [23] R. Ulber, K. Plate, T. Demmer, W. Buchholz, H. Scheper, Downstream processing of bovine lactoferrin from sweet whey, *Acta Biotechnologica*, 21 (2001) 27.
- [24] H. Korhonen, Technology options for new nutritional concepts, *Int. J. Dairy Technology*, 55 (2002) 79.
- [25] R. Pearce, Thermal separation of beta-lactoglobulin and alpha-lactalbumin in bovine cheddar cheese whey, *Australian J. Dairy Technology*, 38 (1983) 144.
- [26] K.R. Kristiansen, J. Otte, R. Ipsen and K.B. Qvist, Large-scale preparation of β -lactoglobulin A and B by ultrafiltration and ion-exchange chromatography, *Int. Dairy Journal*, 8 (1998) 113.
- [27] A. Muller, A. Daufin and B. Chaufer, Ultrafiltration modes of operation for the separation of alpha-lactalbumin from acid casein whey, *J. Membrane Sci.*, 153 (1999) 9.
- [28] G. Gesan-Guiziu, G. Daufin, M. Timmer, D. Allersma and C. van der Horst, Process steps for the preparation of purified fractions of alpha-lactalbumin and beta-lactoglobulin from whey protein concentrates, *J. Dairy Research*, 66 (1999) 225.
- [29] J. Maté and J.M. Krochta, β -lactoglobulin separation from whey protein isolate on a large-scale, *J. Food Sci.*, 59 (1994) 1111.
- [30] G. Konrad, B. Lieske and W. Faber, A large-scale isolation of native β -lactoglobulin: characterization of physicochemical properties and comparison with other methods, *Int. Dairy Journal*, 10 (2000) 713.
- [31] B. Cheang and A.L. Zydney, Separation of α -Lactalbumin and β -Lactoglobulin using membrane ultrafiltration, *Biotechnology and Bioengineering*, 83 (2003) 201.
- [32] J.L. Maubois, New applications of membrane technology in the dairy industry, *Australian J. Dairy Technology*, 46 (1991) 91.
- [33] A. Makardij, X.D. Chen and M.M. Farid, Microfiltration and ultrafiltration of milk: some aspects of fouling and cleaning, *Trans IChemE*, 77 (1999) 107.
- [34] B.J. James, Y. Jing, X.D. Chen, Membrane fouling during filtration of milk – a microstructural study, *J. Food Eng.*, 60 (2003) 431.
- [35] W.R. Bowen, T.A. Doneva, J.A.G. Stoton, Protein deposition during cross-flow membrane filtration: AFM studies and flux loss, *Colloids and Surfaces B: Biointerfaces*, 27 (2002) 103.
- [36] R.W. Field, D. Wu, J.A. Howell and B.B. Gupta, Critical flux concept for microfiltration fouling, *J. Membrane Sci.*, 100 (1995) 259.
- [37] J.A. Howell, Sub-critical flux operation of microfiltration, *J. Membrane Sci.*, 107 (1995) 165.

- [38] G. Belfort, R.H. Davis and A.L. Zydney, The behavior of suspensions and macromolecular solutions in cross flow microfiltration, *J. Membrane Sci.*, 96 (1994) 1.
- [39] R.J. Wakeman and C.J. Williams, Additional techniques to improve microfiltration, *Separation and Purification Technology*, 26 (2002) 3.
- [40] O. Al-Akoun, L. Ding, R. Chotard-Ghodsnia, M.Y. Jaffrin and G. Gesan-Guiziou, Casein micelles separation from skimmed milk using a VSEP dynamic filtration module, *Desalination*, 144 (2002) 325.
- [41] J. Engler and M.R. Wiesner, Particle fouling of a rotating membrane disk, *Water Research*, 34 (2000) 557.
- [42] L. Ding, O. Al-Akoun, A. Abraham and M.Y. Jaffrin, Milk protein concentration by ultrafiltration with rotating disk modules, *Desalination*, 144 (2002) 307.
- [43] H.B. Winzeler and G. Belfort, Enhanced performance for pressure-driven membrane processes: the argument for fluid instabilities, *J. Membrane Sci.*, 80 (1993) 35.
- [44] W.D. Mores and R.H. Davis, Yeast-fouling effects in cross-flow microfiltration with periodic reverse filtration, *Industrial Eng. Chem. Research*, 42 (2003) 130.
- [45] S. Redkar, V. Kuberkar and R.H. Davis, Modeling of concentration polarization and depolarization with high-frequency backpulsing, *J. Membrane Sci.*, 121 (1996) 229.
- [46] S. Curcio, V. Calabro and G. Iorio, Monitoring and control of TMP and feed flow rate pulsatile operations during ultrafiltration in a membrane module, *Desalination*, 145 (1-3) (2002) 217.
- [47] M.Y. Jaffrin, B.B. Gupta and P. Paullier, Energy saving pulsatile mode cross flow filtration, *J. Membrane Sci.*, 86 (1994) 281.
- [48] Z.F. Cui and K.I.T. Wright, Flux enhancements with gas sparging in downwards cross flow ultrafiltration: performance and mechanism, *J. Membrane Sci.*, 117 (1996) 109.
- [49] Z.F. Cui and T. Taha, Enhancement of ultrafiltration using gas sparging: a comparison of different membrane modules, *J. Chem. Technology and Biotechnology*, 78 (2003) 249.
- [50] T.R. Noordman, A. de Jonge, J.A. Wesselingh, W. Bel, M. Dekker, E. ter Voorde and S.D. Grijpma, Application of fluidised particles as turbulence promoters in ultrafiltration Improvement of flux and rejection, *J. Membrane Sci.*, 208 (2002) 157.
- [51] R.J. Wakeman and E.S. Tarleton, An experimental study of electroacoustic cross flow microfiltration, *Trans IChemE*, 69 (1991) 286 Part A.
- [52] H. Duriyabunleng, J. Petmune and C. Muangnapoh, Effects of the ultrasonic waves on microfiltration in plate and frame module, *J. Chem. Eng. Japan*, 34 (2001) 985.

-
- [53] M. Villamiel and P. de Jong, Influence of high-intensity ultrasound and heat treatment in continuous flow on fat, proteins and native enzymes of milk, *J. Agric. Food Chem.*, 48 (2000) 472.
- [54] C. Visvanathan and R. Ben Aim, Application of an electric field for the reduction of particle and colloidal fouling in cross flow microfiltration, *Separation Science and Technology*, 24 (1989) 383.
- [55] R.J. Wakeman, Electrically enhanced microfiltration of albumin suspensions, *Trans IChemE*, 76 (1998) 53 Part C.
- [56] C.A. Romero and R.H. Davis, Global model of cross flow microfiltration based on hydrodynamic particle diffusion, *J. Membrane Sci.*, 39 (1988) 157.
- [57] C.A. Romero and R.H. Davis, Experimental verification of the shear-induced hydrodynamic diffusion model of cross flow microfiltration, *J. Membrane Sci.*, 62 (1991) 249.
- [58] Y. Lee and M.M. Clark, Modeling of flux decline during cross flow ultrafiltration of colloidal suspensions, *J. Membrane Sci.*, 149 (1998) 181.
- [59] I.H. Huisman and C. Tragardh, Particle transport in cross flow microfiltration – I. Effects of hydrodynamics and diffusion, *Chem. Eng. Sci.*, 54 (1999) 271.
- [60] A. Ould-Dris, M.Y. Jaffrin, D. Si-Hassen and Y. Neggaz, Effect of cake thickness and particle polydispersity on prediction of permeate flux in microfiltration of particulate suspensions by a hydrodynamic diffusion model, *J. Membrane Sci.*, 164 (2000) 211.
- [61] W.R. Bowen and P.M. Williams, Prediction of the rate of cross-flow ultrafiltration of colloids with concentration-dependent diffusion coefficient and viscosity – theory and experiment, *Chem. Eng. Sci.*, 56 (2001) 3083.
- [62] G. Gesan-Guiziu, R.J. Wakeman and G. Daufin, Stability of latex cross flow filtration: cake properties and critical conditions of deposition, *Chem. Eng. J.*, 85 (2002) 27.
- [63] N.N. Kramadhathi, M. Mondor and C. Moresoli, Evaluation of the shear-induced diffusion model for the microfiltration of polydisperse feed suspension, *Separation and Purification Technology*, 27 (2002) 11.
- [64] W.R. Bowen and F. Jenner, Theoretical descriptions of membrane filtration of colloids and fine particles: an assessment and review, *Advances in Colloid and Interface Sci.*, 56 (1995) 141.
- [65] G. Samuelsson, I.H. Huisman, G. Tragardh and M. Paulsson, Predicting limiting flux of skim milk in cross flow microfiltration, *J. Membrane Sci.*, 129 (1997) 277.
- [66] S.K. Karode and A. Kumar, Flow visualization through spacer filled channels by computational fluid dynamics I. Pressure drop and shear rate calculations for flat sheet geometry, *J. Membrane Sci.*, 193 (2001) 69.

- [67] J. Schwinge, D.E. Wiley and D.F. Fletcher, A CFD study of unsteady flow in narrow spacer-filled channels for spiral-wound membrane modules, *Desalination*, 146 (1-3) (2002) 195.
- [68] D.E. Wiley and D.F. Fletcher, Techniques for computational fluid dynamics modelling of flow in membrane channels, *J. Membrane Sci.*, 211 (2003) 127.
- [69] C.J. Richardson and V. Nassehi, Finite element modeling of concentration profiles in flow domains with curved porous boundaries, *Chem. Eng. Sci.*, 58 (2003) 2491.
- [70] J. Dufreche, M. Prat, P. Schmitz and J.D. Sherwood, On the apparent permeability of a porous layer backed by a perforated plate, *Chem. Eng. Sci.*, 57 (2002) 2933
- [71] A.J.C. Ladd, Numerical simulations of particulate suspensions via a discretized Boltzmann equation Part 1 Theoretical foundation, *J. Fluid Mechanics*, 271 (1994) 285.
- [72] A.J.C. Ladd, Numerical simulations of particulate suspensions via a discretized Boltzmann equation Part 2 Numerical results, *J. Fluid Mechanics*, 271 (1994) 311.
- [73] M. Alexander, L.F. Rojas-Ochoa, M. Leser and P. Schurtenberger, Structure, dynamics, and optical properties of concentrated milk suspensions: an analogy to hard-sphere liquids, *J. Colloid and Interface Sci.*, 253 (2002) 35.
- [74] J. Kromkamp, D. van den Ende, D. Kandai, R.G.M. van der Sman and R.M. Boom, Shear-induced self-diffusion in non-Brownian suspensions by lattice Boltzmann simulation, Submitted *J. fluid mechanics*.



Chapter 3: Optimization of the pore geometry and membrane design for micro-machined membranes¹

Abstract

For micro-machined membranes, it is possible to choose pore size, pore geometry and membrane porosity, within certain limits. Different pore geometries (circular, square, slit shaped and triangular pores), particle size to pore size ratios, pore edges and membrane porosities were evaluated with lattice Boltzmann computer simulations and torque balance considerations for various modes of operation. We focused on hydrodynamic interactions and assumed uncharged neutral surfaces of the particle and the pore. However, the model can easily be extended with additional relations for such interactions in practical systems with defined properties.

It was concluded that pore geometry can have a large effect on the flux (up to 60%). Further, the effect of shielding could be quantified. Above a surface coverage of 0.05, the particles effectively shield each other from the flow field, therewith necessitating either a higher cross flow velocity or a lower transmembrane pressure for particle removal.

Based on the simulations, an extended criterion for the critical flux was developed, which includes the effects of pore geometry, particle to pore size ratio and membrane porosity. Different optimal membrane choices follow for processes aimed at retention of all particles, and for processes aimed at fractionation of particles into different fractions.

Introduction

New types of microfiltration membranes, such as silicon or silicon nitride microsieves [1] and metal microfilters [2] have become available. These are made by photolithographic treatment of a silicon wafer and subsequent etching, or electrochemical metal deposition on a skeleton in an electrolysis bath, respectively.

¹ This chapter is accepted for publication in Journal of Membrane Science: G. Brans, R.G.M. van der Sman, C.G.P.H. Schroën, A. van der Padt, R.M. Boom, Optimization of the membrane and pore design for micro-machined membranes.

Compared to conventional ceramic and polymer membranes, these membranes have exemplary properties, such as a smooth and flat surface, a very low membrane resistance and narrow pore size distribution. The porosity and pore shape can be chosen almost freely, and therewith these membranes open areas for membrane filtration that have not been possible before. The pores are usually placed in a regular pattern and the porosity can be much higher compared to conventional membranes, up to 0.8 for rectangular shapes [3], fig. 1. By realizing separations that were not possible before, these membranes could truly create a revolution in microfiltration.

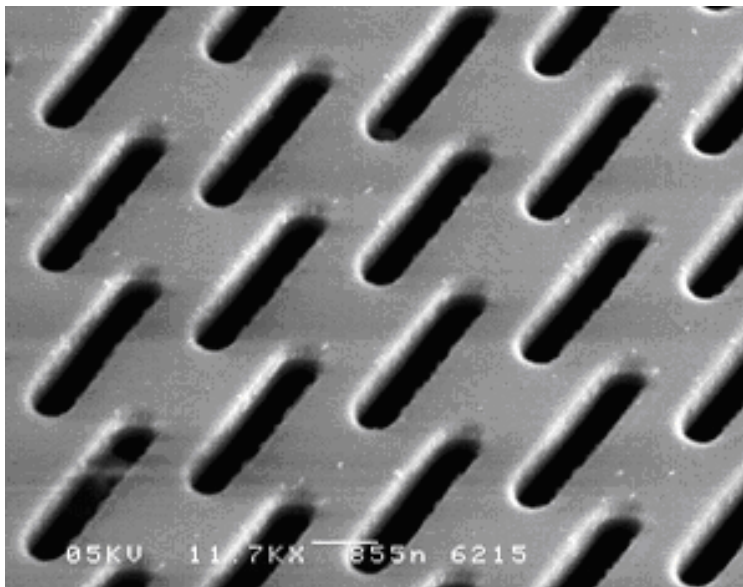


Figure 1: Microsieve with slit shaped pores. Courtesy Aquamarijn Micro Filtration BV.

Although the membranes themselves have almost ideal properties, common membrane filtration phenomena, such as concentration polarization, pore blocking, and cake formation still affect membrane performance [4]. In fact, due to the very high permeabilities of these membranes, these phenomena will be even more important than with conventional membranes. Depending on the degree of “fouling”, three filtration regimes can be identified [5]:

1) In the sub-critical flux regime, the membrane surface is still free of particles. Due to the removal of fluid at the membrane, concentration polarization takes place, as in any filtration regime. In this regime, the back-transport of particles away from the membrane can easily keep up with the convective transport of particles towards the membrane. Thus, concentration polarization hardly influences the flux (linear relation

between transmembrane pressure and flux), because permanent particle deposition or layer formation is absent.

II) At higher fluxes than the critical flux, an equilibrium is reached between the particle transport towards the membrane and the back-transport, after the formation of a steady (cake) layer on the membrane. Steady state fluxes are reached with either Brownian diffusion, shear induced diffusion or inertial lift as the relevant back-transport mechanism, depending on the size of the retained component. [6].

III) At even higher fluxes or particle concentrations, the transport of particles towards the membrane is larger than the back-transport. This leads to a continuously growing cake layer with a continuous flux decline. Regime III can only be applied when the cake layer is removed periodically, for example by pulsed cross flow or backpulsing. Otherwise, the cross flow channel will become blocked.

The type of filtration regime is determined by the hydrodynamic conditions in the system and is influenced by the membrane resistance, the transmembrane pressure, cross flow velocity, module geometry and the feed composition. In literature, the transition from regime I to II is often referred to as the critical flux or critical pressure, whereas the transition from regime II to III is called the limiting flux or limiting pressure [5].

In the sub-critical flux regime (I), particles may deposit on a pore, but will be released again. Kuiper *et al.* developed a model for the release of a single deposited particle from a circular pore in regime I [7]. For the actual design and optimization of micro-machined membranes, the effect of different pore shapes and membrane porosities should be investigated together with hydrodynamic effects for multiple particle situations. Computational Fluid Dynamics (CFD) have been applied successfully in membrane technology for the optimization of inserts and spacers in membrane channels [8, 9], and in the investigation of concentration polarization and cake formation [10, 11]. However, CFD has not often been used to study the process of particle deposition and pore blocking on the scale of individual pores. This scale, however, is now of utmost important, due to the availability of micro-machined membranes.

In this paper, we used a lattice Boltzmann CFD model to find optimal pore shape and porosity of microsieves. After validation of the model with analytical solutions for orifice flow and the drag force on a stationary sphere, we considered the permeability of different pore geometries and evaluated the forces acting on a deposited particle for the different pore geometries in cross flow. Focus was on the transition of filtration regime I to II to obtain the maximum flux, in the absence of particle deposition. Furthermore, the effect of membrane porosity and sharpness of the pore edge on the

drag force was studied on neutral surfaces with no charge interactions between the particle and the pore.

Finally, the simulation results are compiled into an overall criterion for the critical flux. The practical relevance and the consequences for membrane design are discussed for filtration processes aiming at concentration or fractionation of particle suspensions in the different filtration regimes.

Theory

a) Single particle release model

Kuiper *et al.* developed a model that predicts the required cross flow velocity to release a spherical particle from a membrane with circular pores [7]. The model provides guidelines for the module design and operating conditions for the transition from filtration regime I to II. The model is based on a torque balance over the particle under laminar flow conditions and gives a first impression of the effects that play a role. For particles with size in the order of 1 μm , the pressure suction force and the particle drag force are dominant, while lift forces can be neglected.

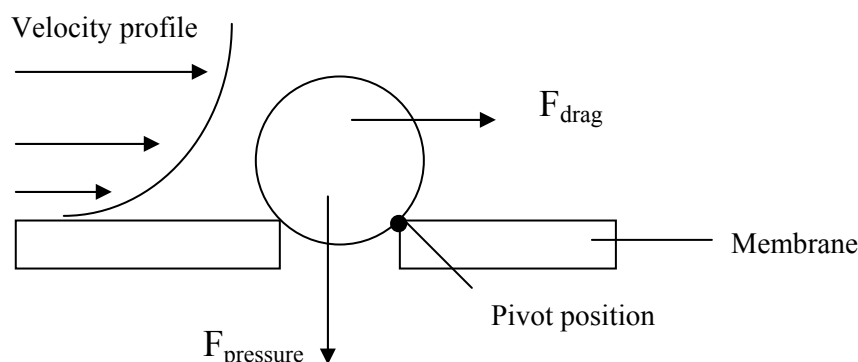


Figure 2: Forces acting on a deposited particle, after Kuiper *et al.* [7].

The pressure force and the drag force were calculated with analytical equations. These forces were converted to torques by multiplying with the distance between the point of impact of the force and the pivot position. The particle will be released from the pore if the torque of the particle drag force exceeds the torque of the pressure force towards the pivot position. In that situation, the particle will roll out of the pore and will be taken up by the flow field again (fig. 2).

Hence, the torque caused by the drag force must be larger than the torque of the pressure force to avoid pore blockage. When combined with the assumption of fully

developed Poiseuille flow in the cross flow channel, the following particle release criterion was obtained for a flat membrane [7]:

$$\frac{\Delta P_{inlet}}{\Delta P_{chan}} < 7.0 \frac{h_{chan}}{l_{mem}} \left(\frac{d}{d_p} \right)^3 \quad [1]$$

With ΔP_{inlet} the transmembrane pressure at the inlet, ΔP_{chan} the pressure drop over the cross flow channel and the average transmembrane pressure defined as $\Delta P_{inlet} - 0.5\Delta P_{chan}$. h_{chan} is the height of the cross flow channel, l_{mem} the length of the membrane, d the particle diameter and d_p the pore diameter. The model is only valid for circular pores, low particle concentration, low membrane porosity, and assumes that the particle does not penetrate into the pore. It is further assumed that a circular pore is completely blocked by a spherical particle and there is no interaction between particles on neighboring pores.

Hence the model cannot be used when one of these criteria is not met. Since the current micro-machined membranes have options beyond these criteria, extension of the model towards broader applicability is required.

b) Lattice Boltzmann CFD model

Lattice Boltzmann is a relatively new modeling technique that has been successful in the simulation of fluid flow in complicated geometries, such as porous media and suspension flow [12, 13]. It has been proven that the lattice Boltzmann equation is equivalent to a discretized version of the Navier-Stokes equation [14].

For a detailed description of the lattice Boltzmann method we refer to the books of Wolf-Gladrow [14] and Succi [15]; we will outline the method only briefly. In the lattice Boltzmann approach, imaginary fluid parcels move on a regular lattice by subsequent collision and propagation steps.

During a collision, parcels exchange impulse, and change their velocities and directions. The parcels have the tendency to relax towards an equilibrium distribution. In the collision step, a new equilibrium distribution $f_{i,eq}$ is calculated from the hydrodynamic moments of the actual local distribution f_i . The collision operator ω , also known as the inverse of the time relaxation parameter τ , is correlated to the viscosity. In the propagation step, the fluid parcels are propagated into the direction of their corresponding velocity c (fig. 3).

The collision and propagation steps are described by:

$$f_i(x + \bar{c}_i \Delta t, t + \Delta t) = f_i(x, t) - \omega(f_i(x, t) - f_{i,eq}(x, t)) \quad [2]$$

in which t and x are the discretized time and place, $c = \Delta x / \Delta t$ is the velocity. Viscosity is defined as:

$$\nu = c_s^2 \left(\frac{1}{\omega} - 0.5 \right) \Delta t \quad [3]$$

with ν the kinematic viscosity and c_s the (numerical) speed of sound, chosen as $c/\sqrt{3}$. The equilibrium distribution function is as follows:

$$f_{i,eq} = w_i \rho \left(1 + \frac{\bar{c}_i \cdot \bar{u}}{c_s^2} + \frac{(\bar{c}_i \cdot \bar{u})^2}{2c_s^4} - \frac{\bar{u}^2}{2c_s^2} \right) \quad [4]$$

in which ρ is the density of the fluid, c_i is the velocity in direction i and u is the fluid velocity. For a model with three dimensions and 19 velocities (D3Q19), the weight factors w_i are defined as $w_i = 1/3$ for $i=0$, $w_i = 1/18$ for $i=1, \dots, 6$ and $w_i = 1/36$ for $i=7, \dots, 18$. The set of 19 velocities has been proven to be sufficient for simulating fluid flow phenomena with high accuracy in 3D [14].

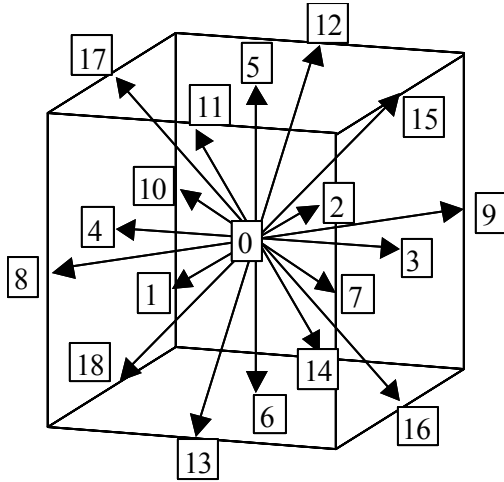


Figure 3: Lattice Boltzmann D3Q19 scheme [15]. The arrows with numbers 1-18 indicate the velocities c_i in the lattice Boltzmann model; 0 is the rest parcel, of which the velocity equals zero.

Simulations were performed in a three-dimensional cubic lattice with dimensions (L) 100x100x100 and a gridsize Δx of 0.1 μm . For problems where the effect of the

periodic walls was supposed to be absent, the dimensions of the lattice were enlarged. In all cases, the dimensions proved large enough. To check if the resolution was sufficient, the effect of grid refinement was evaluated, but this did not affect the results. The membrane was placed in the middle of the lattice. The flow was driven by pressure periodic boundary conditions [16], and in the other dimensions regular periodic boundaries were applied. In cross flow simulations, boundary conditions for velocity and pressure were used according to Zou and He [17]. No-slip boundary conditions were applied for rigid walls and the particle [18]. The force acting on the particle was calculated numerically by the summation of local forces over all the solid-fluid boundaries of the particle. The force on a boundary node can be calculated from the local distribution f_i [19]:

$$F_d = \sum_{n=1}^m \sum_{i=1}^{18} F_i,$$

$$F_i(r + 0.5c_i\Delta t, t + 0.5\Delta t) = 2(f_i(r, t) - f_{i'}(r + c_i\Delta t, t))c_i \frac{\Delta x^3}{\Delta t} \quad [5]$$

where F_i is the force acting on the solid-fluid boundary r of the lattice node n in direction i ; $f_{i'}$ is the distribution in the opposite direction of i . The total force on the object, F_d , is calculated by summation of the forces over the total amount of boundary nodes m .

c) Benchmark studies

The lattice Boltzmann code was benchmarked with analytical solutions for orifice flow and the drag force coefficient of a stationary sphere. If the thickness l_o of the orifice plate is smaller than the orifice diameter d_p , the flow through the orifice is described by Sampson's equation [3]:

$$Q = \frac{d_p^3}{24\eta} \Delta P \quad \text{if } l_o < \frac{1}{2}d_p \quad [6]$$

and for flow through a short channel with thickness l_o as [3]:

$$Q = \frac{\Delta P}{\left(\frac{128l_o\eta}{\pi d_p^4} + \frac{24\eta}{d_p^3} \right)} \quad \text{if } l_o > 2d_p \quad [7]$$

where Q is the volumetric flow rate, ΔP is the pressure difference, η is the viscosity of the fluid.

In the orifice benchmark simulations, the maximal porosity considered was 0.03. Thus, equations 6 and 7 can be used directly (correction for porosity $\sim 0.1\%$) [1]. Simulations of orifice flow were compared with the analytical solutions for orifices with negligible length and short channels with lengths of three times the orifice diameter. The volumetric flow rate was determined for various diameters with a pressure difference of 3.33 kPa.

Another benchmark was performed by simulating the drag force on a stationary sphere. The drag force coefficient C_d (Nm^{-1}s) of a periodic packing of spheres was compared with the asymptotic expression by Hasimoto [20]. This formula accounts for the periodic boundaries in all dimensions.

$$F_d = C_d \bar{u} = C_d \frac{Q}{L^2} \quad [8]$$

with

$$\frac{6\pi\eta}{C_d} = \frac{1}{r} - \frac{2.837}{L} + \frac{4.19}{L^3} r^2 - \frac{27.4}{L^6} r^5 \quad [9]$$

F_d is the drag force exerted on a sphere with radius r , and L is the length of the periodic cubic unit cell in which the sphere has been placed. Again, the volumetric flow rate was determined for various particle diameters with a constant pressure difference of 3.33 kPa. The drag force F_d was calculated with equation 5.

d) Simulations

After the benchmarks were successfully concluded, we evaluated various aspects of the design of micro-machined membranes, namely the pore geometry, the particle size to pore size ratio, the sharpness of the pore edge and the membrane surface coverage.

The different pore geometries in this study were circular, square, slit shaped ($l=2d_p$, $l=3d_p$), and equilaterally triangular, as shown in figure 4. The characteristic pore size d_p was 1.0 μm (based on size for particle transmission), and the membrane thickness was also 1.0 μm .

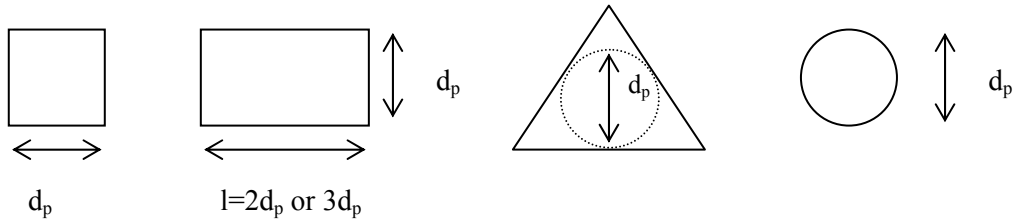


Figure 4: Topview of square, slit ($l=2d_p$), triangular and circular pore geometry.

To compare the same membrane porosity for all pore geometries, the permeability per open membrane area k' (m) of each pore geometry was calculated as:

$$k' = \frac{\eta Q}{\Delta P A_p} \quad [10]$$

where Q is the volumetric flow rate, ΔP the pressure difference, η the viscosity of the fluid, and A_p is the open pore area. This corrected permeability can be interpreted as the permeability of a hypothetical membrane normalized to a porosity of 1, and the indicated pore geometry.

We considered pore blocking by one deposited particle, placed exactly on the pore. The height of the particle h above the membrane was calculated with Pythagoras' theorem (fig. 5). For slits with perpendicular orientation, the particle was placed half way the largest dimension.

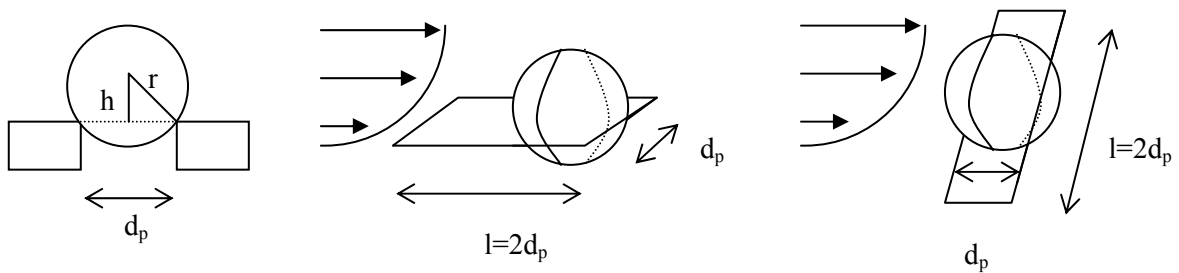


Figure 5: Position of a particle on a pore. The height of the particle above the membrane (h) was calculated with Pythagoras' theorem. For slits oriented parallel to the cross flow, the particle was located at the end of the slit; for perpendicular slits the particle was located in the middle.

For slits oriented in the cross flow direction, the particle was placed at the end of the slit (fig. 5), because the cross flow will transport the particle towards this position. We studied aspect ratios of particle diameter to pore size of 1.2, 1.6, 2.0 and 3.0

respectively, based on the particle size that would just fit inside the pore. The transmembrane pressure was 3.33 kPa and the cross flow velocity 0.16 ms^{-1} . The forces exerted on the particle by the cross flow and the transmembrane pressure were calculated as described in the section discussing the theoretical background of the lattice Boltzmann model (eq. 5).

To study the effect of a deposited particle that partially penetrates the pore, simulations were performed for the drag force on the particle as a function of the three-dimensional shape of the pore opening; with a perfectly circular pore, with a wedge shaped pore and with a pore with rounded edges (fig. 6). Further, the influence of the membrane porosity and surface coverage was studied by decreasing the size of a periodic box, in which a particle had been placed on a circular pore with constant cross flow velocity.

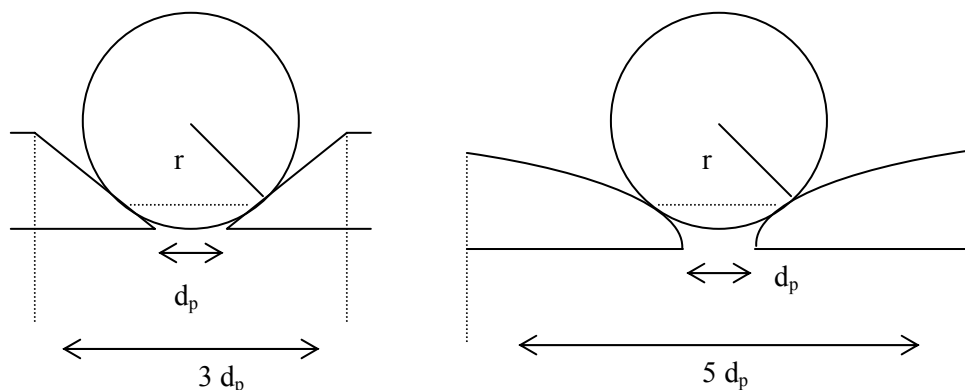


Figure 6: Rounded pore throats: geometry of circular pores. Left: throat with constant angle (wedge), Right: parabolic throat.

Results

a) Benchmarks with analytical solutions

Both the analytical results and the simulation results for orifice flow and flow through a short channel are depicted in figure 7. Results are in good agreement with the analytical solution. Small deviations were expected due to the fact that a circular orifice cannot be exactly defined on the square lattice (for small orifices $\sim 4\%$). The orifice is constructed by discretization of grid cells, which results in a stair case geometry. For larger diameters of the orifice and the short channels investigated here, the deviations from the analytical solution become around 0.1%.

Another benchmark was the simulation of the drag force coefficient on a spherical particle placed in a uniform flow field with periodic boundaries. The drag force

coefficient was calculated for different particle sizes and compared with the Hasimoto expression (fig. 8). Overall, there is a good agreement between our model and the expression, although there were some small deviations. This can be explained again by the discretization of the sphere, similar to the orifice benchmark. The relative deviations were 4% for the smallest particle diameter, and 1% for the largest particle diameter. This is in agreement with Ladd, who showed that the lattice Boltzmann method describes this case accurately [21].

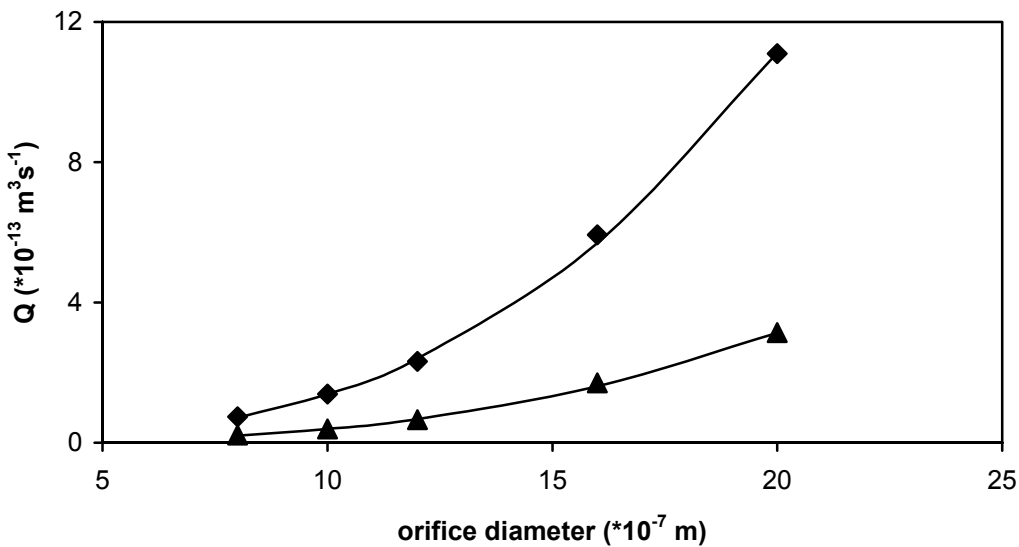


Figure 7: Flow simulations of orifices (diamonds) and short channels with length three times the diameter, (triangles) and the analytical solutions (lines).

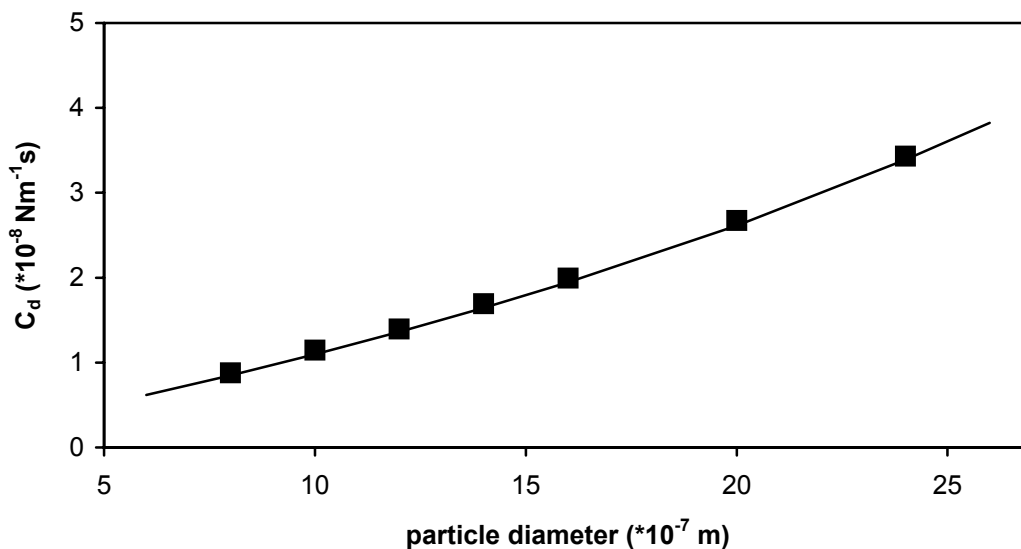


Figure 8: Simulation results (squares) and the analytical solution of Hasimoto [20] (line) of the drag force coefficient on a periodic array of spheres.

b) Different pore geometries and influence of pore blocking

Subsequently, the effects of different pore geometries (circular, square, slit shaped and triangular) were investigated. We evaluated the membrane permeability in open (unblocked) situation and the torque balance of a deposited particle in case of pore blocking.

The permeabilities of the different pore geometries per open membrane area are depicted in figure 9.

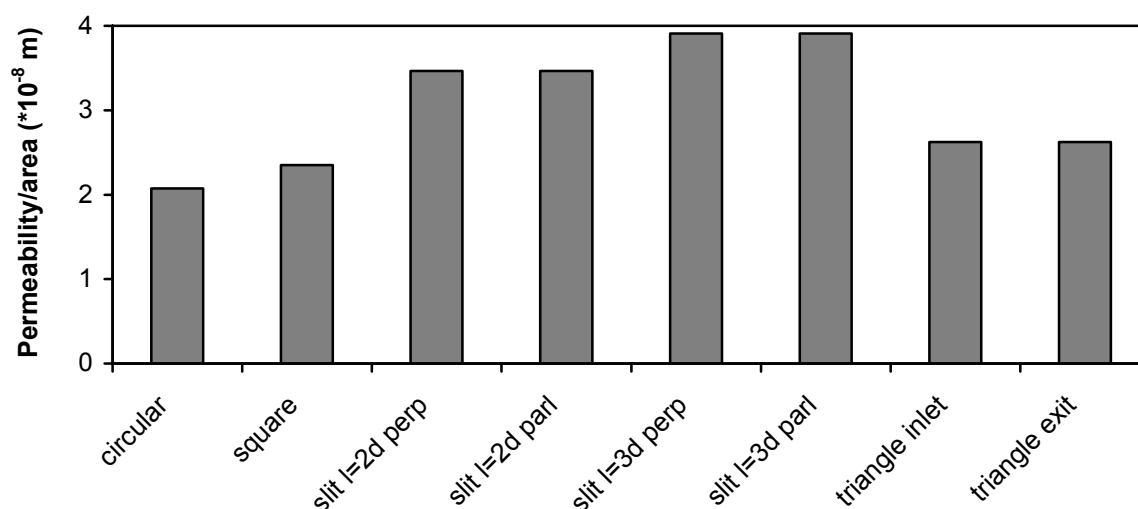


Figure 9: Permeability of different pore geometries in open condition, corrected for the open pore area (k). Slits and triangular pores were evaluated in different orientations: slits parallel (parl) and perpendicular (perp) to the cross flow direction, triangular pores pointing towards the inlet of the feed and the outlet (exit). The nominal pore size was $1.0 \mu\text{m}$, cross flow velocity 0.16 ms^{-1} and transmembrane pressure 3.33 kPa .

Compared to circular pores, slits with dimension $l=3d_p$ have almost a double permeability per area, meaning almost twice the flux at the same membrane porosity and transmembrane pressure. The orientation of the slits did not influence the permeability; the same is true for the triangular pores. This was expected, because for open pores the cross flow does not affect the pressure profile around the pore. From a permeability point of view, long slit shaped pores are thus preferred.

The simulations for blocked pores are most relevant in the sub-critical flux regime (I); particles that deposit on the pores by chance can be removed by the force of the cross flow. The influence of the transmembrane pressure on the particle is twofold: first, there is a direct pressure difference over the particle and second, there is a flow around the particle towards the permeate side, when the particle does not completely

block the pore. This results in an additional drag force. To combine the two effects, we may use as a relevant parameter the total (pressure and drag) force exerted by the transmembrane pressure and transmembrane flow on the particle. To compare different pore geometries, we define a pore shape force factor S as the force exerted on the particle, divided by the force that the particle would experience on a circular pore of the same size (d_p).

In figure 10, the pore shape force factor is depicted for different pore geometries as function of the aspect ratio between the particle and the pore (d/d_p). The orientation of the triangular and slit shaped pores toward the feed flow field is important.

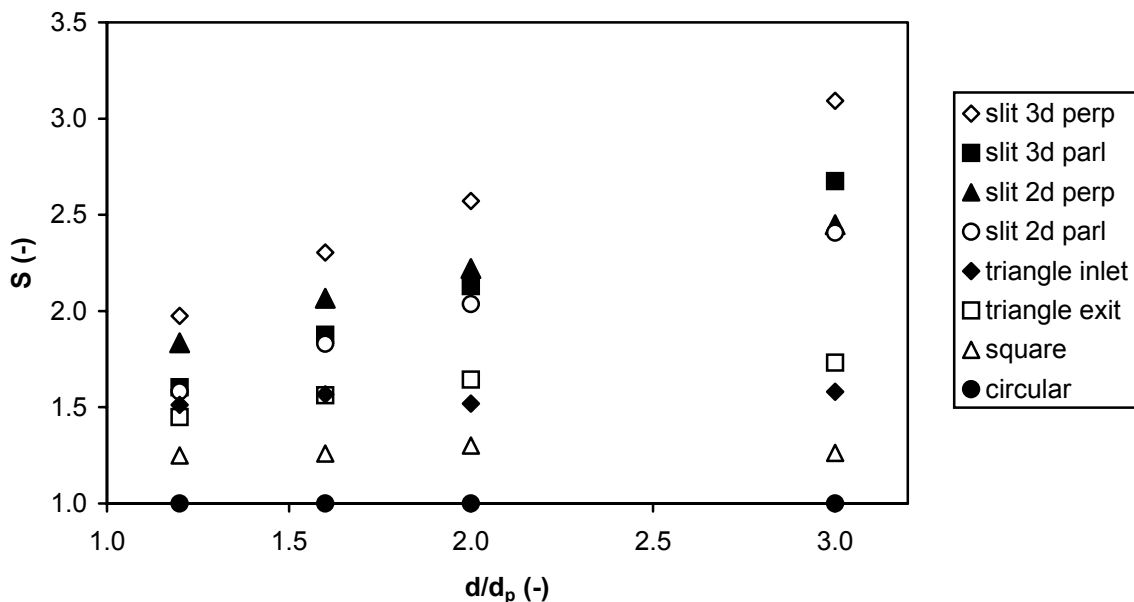


Figure 10: Pore shape force factor S for different pore geometries and particle diameter to pore size ratios of 1.2, 1.6, 2.0 and 3.0. S is normalized to the pressure force of a particle on round pore ($2.0 \cdot 10^{-9}$ N). Process parameters similar to figure 9.

The drag force exerted on a particle positioned on a triangular pore pointing to the inlet of the feed is larger than for pores pointing to the feed outlet. This can be explained by the different local pressures around the corners of the triangular pore, depending on the orientation towards the cross flow. Therewith S is also influenced.

A similar phenomenon was found for slit-shaped pores. A slit orientation parallel to the cross flow direction is beneficial because of the resulting position of the particle. For slit-shaped pores oriented perpendicular to the cross flow direction, it was assumed that particles would deposit in the middle of the pore. The velocity of the fluid through the pore is highest there and the flow field converges near the ends of the slit, leading to a force directed towards the center of the slit. For slit pores parallel

to the cross flow direction, the particle is placed at the end of the slit. We assumed the particle to be deposited there, because of the drag force. In this position, the pressure force is lower, because most of the fluid flows along one side of the particle. Particles in the middle of a slit oriented perpendicularly to the cross flow direction had fluid flowing on both sides of the particle, therewith causing a higher pressure force on the particle, and a higher S .

The shape force factor S for a particle deposited on the square and triangular pore were very similar to those found for circular pores; however for slit shaped pores S increased much faster with increasing d/d_p (fig. 10). This is caused by the larger pore area that is covered by the particle. For slit shaped pores, the sphere covers the pores better with increasing particle size, therewith effectively increasing the force on the particle. For triangular and square pores, this area does not vary too much with increasing particle diameter, because most of the pore is already covered by the particle at the lowest aspect ratio of 1.2.

For the smallest particles, the pressure force with a triangular pore pointing to the feed outlet was larger compared to that with circular pores ($S = 1.5$). The torque of the pressure force on a deposited particle with these triangular pores, however, is 33% lower compared to circular pores, because of the different location of the pivot point yielding only half the arm length compared to other pore geometries (eq. 14). Further, the membrane permeability was 20% larger in open situation (fig. 9). Thus when these effects are combined, the critical flux with triangular pores pointing towards the feed outlet could be 60% higher than with circular pores (assuming a negligible amount of pores is actually blocked). In practice, this can be accomplished by changing the pore geometry and increasing the transmembrane pressure, while the membrane porosity and cross flow velocity are kept constant.

Since the simulations were performed in the creeping flow regime, the drag force and the pressure force scale linearly with the cross flow velocity and the transmembrane pressure. The current results can be used for any combination of cross flow velocity and transmembrane pressure by linear scaling, provided that particle size, pore size and membrane porosity do not change. Based on this, we can find the conditions that correspond to the criterion for critical flux, where the torque of the drag force exceeds the torque of the pressure force and particles are released (table 1).

c) Pore edge design

The previous simulations were carried out with pores having sharp (90°) edges. In that case, particles do not deposit too deeply into the pores and the calculated drag force exerted by the cross flow was relatively independent on the pore geometry. In

practice however, any pore will be at least somewhat rounded, and it may be that production, cleaning and membrane usage cause further smoothing of the pore edges. Thus, particles deposit deeper into the membrane and are less exposed to the cross flow than the simulations of the ideal situation, therewith effectively reducing both the drag force and the arm length.

Table 1: Required cross flow velocity for particle release of 1.2 μm particles from various pore geometries with nominal pore size 1.0 μm at transmembrane pressure of 3.33 kPa, assuming linear relation with simulations (cross flow velocity 0.16 ms^{-1}).

Geometry ¹⁾	F_{pressure} (10^{-9} N)	F_{drag} (10^{-9} N)	M_{pressure} (10^{-15} Nm)	M_{drag} (10^{-15} Nm)	Required cross flow (ms^{-1})
circular	1.94	1.40	0.97	0.90	0.172
square	2.42	1.41	1.21	0.91	0.214
slit $l=2d$	3.56	1.46	1.78	0.94	0.303
perpendicular					
slit $l=2d$ parallel	3.07	1.45	1.54	0.93	0.263
slit $l=3d$	3.83	1.47	1.92	0.95	0.323
perpendicular					
slit $l=3d$ parallel	3.11	1.40	1.56	0.90	0.276
triangle inlet	2.44	1.41	1.22	0.91	0.215
triangle outlet	2.81	1.41	7.03	0.91	0.124

¹⁾ Slits and triangular pores were evaluated in different orientations: slits parallel and perpendicular to the cross flow direction, triangular pores pointing towards the feed inlet and the retentate outlet.

The effect that small particles penetrate the pore was investigated with circular pores with sharp edge, a wedge-shaped pore, and a pore with rounded edges. The latter was assumed to have a parabolic profile (fig. 6). The pressure force on the particle was for both rounded pores identical to a regular circular pore with sharp edges (i.e. $S = 1$).

The wedge shaped pore yielded a drag force on the deposited particle that was significantly lower than that of a sharp edged pore (fig. 11). For the wedge shaped pore, the drag force on a particle varied from 21% for $d/d_p = 1.2$ to 71% for $d/d_p = 3.0$ compared to the particle on the sharp pore. The effect of the rounded pore was slightly smaller than the wedge shaped pore, because the flow field can better develop in the pore mouth. The smaller drag force for these geometries was expected, since especially particles with small aspect ratio penetrated relatively deep into the pore. These simulation show that sharp pore edges are essential. Smoother

pore geometries, as present in polymer and ceramic membranes, require either a higher cross flow velocity or lower transmembrane pressure for a clean membrane surface. A similar effect is expected for deformable particles. Because they penetrate deeper in the pore, they become less exposed to the cross flow and experience a lower drag force.

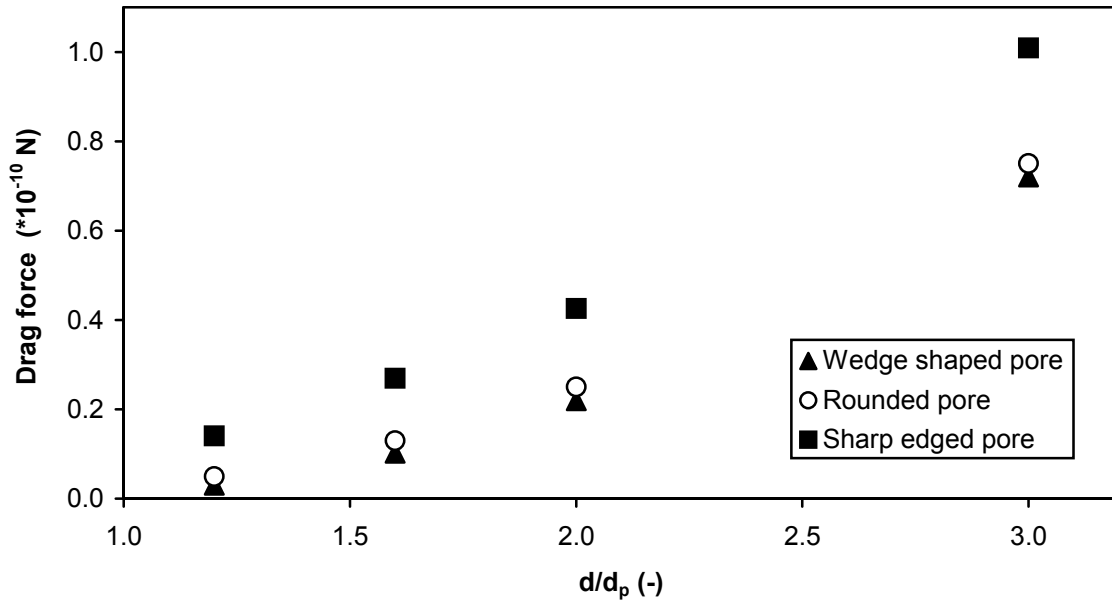


Figure 11: Rounded pore edges: comparison of drag force in cross flow direction on particle with circular pore for different ratios of particle diameter to pore size. Pore geometries of fig. 6 and pore size was 1 μm . The cross flow velocity was 0.16 ms^{-1} and transmembrane pressure 3.33 kPa.

d) Membrane porosity and surface coverage

Especially for micro-machined membranes with high porosity, it can be expected that the flow field around a particle is influenced by the presence of other pores, and of deposited particles nearby. The former is an effect of the overall porosity of the membrane; the latter is due to disturbance of the cross flow field around particles. The fraction of pores on the membrane surface that is blocked by particles is an important parameter here. This surface coverage θ was defined as the cross sectional area of spherical particles divided by the membrane area:

$$\theta = \frac{\frac{1}{4} \pi d^2 \varepsilon}{A_p} \quad [11]$$

with A_p the total open pore area and ε the membrane porosity. For circular pores, this becomes:

$$\theta = \varepsilon \left(\frac{d}{d_p} \right)^2 \quad [12]$$

The effect of the surface coverage θ was studied with the lattice Boltzmann model by decreasing the size of a periodic box, in which a particle was placed on a circular pore. This simulates a decrease of the interpore (interparticle) distance and hence an increase of the porosity ε . In this system we applied complete blocking of pores in square arrangement with a constant cross flow velocity.

The drag force on the particle starts to decrease when the surface coverage becomes higher than 0.05 (fig. 12), which implies that once a particle has deposited, the downstream pores are more likely to become blocked too, due to the shielding effect. At the maximum surface coverage of 0.78 for squarely arranged pores, the drag force exerted by the cross flow was only 25% of the drag force at coverage 0.02. For particles on hexagonal arranged pores (surface coverage 0.93), the relative drag force was 24%, which was very similar to that of squarely arranged pores. Consequently, the cross flow velocity should be four times higher to create the same torque of drag to remove the particle from the membrane.

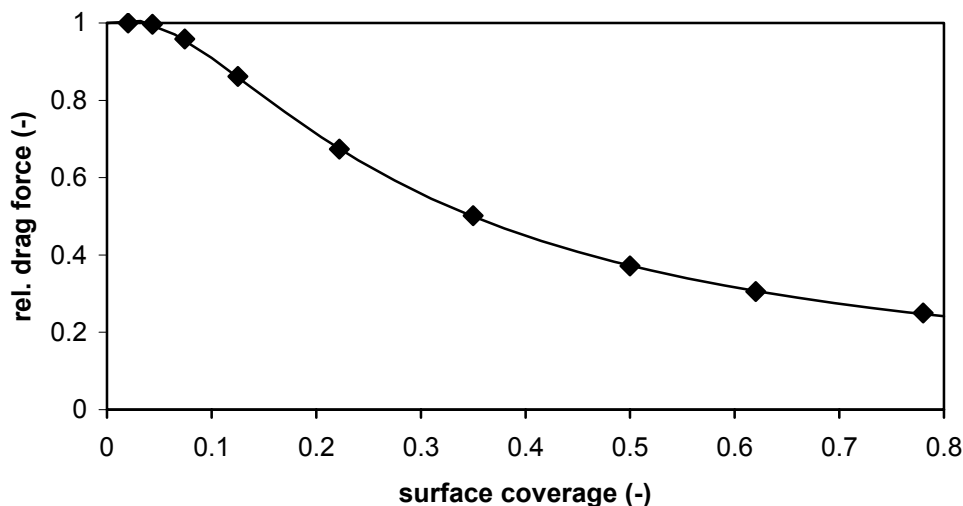


Figure 12: Influence of surface coverage on drag force in the cross flow direction for 1.6 μm particle on circular pore in square arrangement according to the simulations and according to the correlation $f_r(\theta)$ given by equation 16 (line).

Thus a hysteresis effect can be expected: when the transmembrane pressure is slowly increased, the first particle will deposit at the critical transmembrane pressure related to $\theta = 0$. Since the critical transmembrane pressure for deposition at higher θ is smaller, this will trigger fast deposition of other particles, due to the surface coverage effect, and the complete membrane surface will become blocked suddenly (θ high). Resuspension of particles will only take place at a transmembrane pressure that is lower than the original pressure at which the first particle deposited (related to $\theta = 0$). Evidently, instead of a lower transmembrane pressure, one may also read a higher cross flow velocity.

For circular pores, the pressure force is not affected by the surface coverage, because pores are completely blocked. For partially blocked pores, there is still a remaining flux through the pores, which contributes to the pressure force. At higher surface coverage, the flux and the pressure force could be affected and was checked in simulations. Simulations with slit pores (perpendicular, $l=3d$) and surface coverage of 0.25 gave almost identical pressure force compared to surface coverage of 0.02, and thus we may assume that the effect of surface coverage on the pressure force could be neglected.

The simulations show that surface coverage and membrane porosity do affect particle release. Therefore, these factors must be considered in the design of micro-machined membranes and the choice of process conditions. In the following section, we will quantify these effects and incorporate them into an extended torque balance model.

e) Criterion for critical flux

Based on simulations presented in this article and the model of Kuiper *et al.* an extended criterion can be defined for the critical flux with 90° pore edges. Starting from the torque balance:

$$M_{drag} > M_{pressure} \quad [13]$$

For the torque caused by the drag force we first consider the Stokes drag force (F_{st}) on a spherical particle close to a wall ($F_{st}=1.7 \cdot 3 \cdot \pi \eta v_c d$, with 1.7 the wall correction) and multiply with the height of the point of impact. This height is above the center of the particle and equals 0.685 times the particle diameter [7]. The torque of the pressure force is calculated by multiplying the pressure force with the arm, given in most pore geometries by half the diameter of the pore size ($\frac{1}{2} d_p$) [7]. The effects of

surface coverage and the particle to pore size ratio on the drag force are included in the torque balance.

$$\left. \begin{aligned}
 M_{drag} &> M_{pressure} \\
 M_{drag} &= F_{drag} \cdot \text{arm} = M_{drag}(\text{single particle on wall}) \cdot f_1(\theta) \cdot f_2\left(\frac{d_p}{d}\right) \\
 M_{pressure} &= F_{pressure} \cdot \text{arm} = \text{area} \cdot \Delta P_{inlet} \cdot \text{arm}
 \end{aligned} \right\} \rightarrow$$

$$3.5\pi\eta v_c d^2 f_1(\theta) f_2\left(\frac{d_p}{d}\right) > \begin{cases} \frac{1}{4}\pi d_p^2 S \Delta P_{inlet} \frac{1}{4}d & \text{triangular pores pointing to the exit} \\ \frac{1}{4}\pi d_p^2 S \Delta P_{inlet} \frac{1}{2}d & \text{for all other pore geometries} \end{cases}$$

S is the pore shape force factor for the pressure force and v_c the local fluid velocity in the membrane module at the height of the centre of the particle. ΔP_{inlet} is the transmembrane pressure at the inlet of the cross flow channel, where the particles experience the largest pressure force.

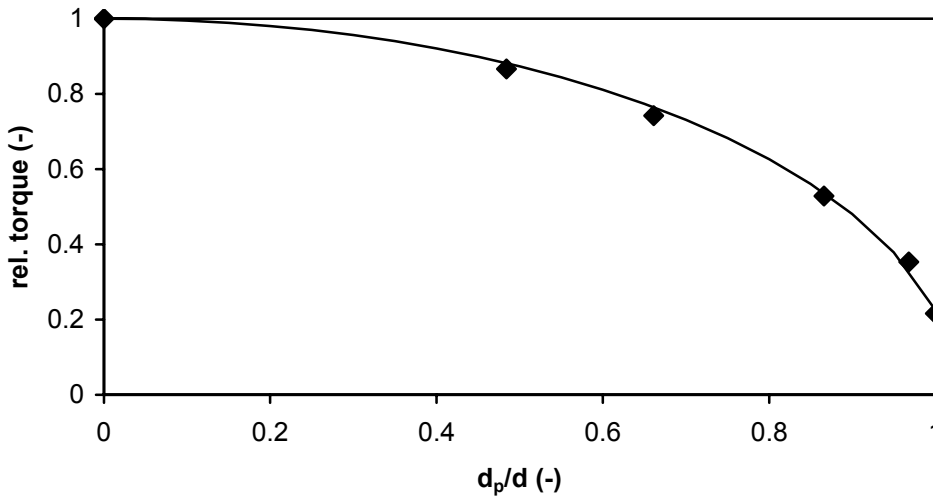


Figure 13: Influence of the particle height above the pore, as determined by d_p/d (fig. 5), on the torque exerted by the cross flow towards the pivot position (1.6 μm particle on circular pore) according to the simulations (symbols) and according to the correlation $f_2(d_p/d)$ given by equation 15 (line).

$f_1(\theta)$ is the drag correction factor as function of the surface coverage with spherical particles in square arrangement and $f_2(d_p/d)$ is the torque correction for the height of the particle above the pore (determined by d_p/d). We assume that functions $f_1(\theta)$ and

$f_2(d_p/d)$ act independently. Please note that for triangular pores pointing towards the exit of the feed flow, the arm length is a quarter of the particle diameter, because of a different location of the pivot position.

For circular pores, the pore shape force factor S is defined to be 1 and is independent of the particle diameter to pore size ratio. For the other pore geometries, S depends also on the particle diameter to pore size ratio (fig. 9). The functions $f_1(\theta)$ and $f_2(d_p/d)$ were determined by least squares fitting of the simulation results (fig. 12 and 13) and can be expressed as:

$$f_1(\theta) = \frac{1 + a_0\theta}{1 + a_1\theta + a_2\theta^2} \quad [15]$$

$$f_2\left(\frac{d_p}{d}\right) = \sqrt{1 + b_0\left(\frac{d_p}{d}\right)^2} \quad [16]$$

with fit parameters $a_0=4.506$, $a_1=3.571$, $a_2=23.778$ and $b_0=-0.949$.

Further, it is common to use wall shear stress instead of local velocity, which in the laminar flow regime is defined for the cross flow velocity relevant for the particle $v_c = \frac{1}{2}d \tau_w / \eta$. Together with some rearrangement this leads to:

$$\frac{\tau_w}{S\Delta P_{inlet}} \left(\frac{d}{d_p}\right)^3 f_1(\theta) f_2\left(\frac{d_p}{d}\right) > 0.0714 \quad [17]$$

Note that the wall shear stress is determined by the flow profile through the feed channel. Therefore, the module geometry affects the wall shear stress via the cross flow velocity and the height of the cross flow channel.

The dimensionless term $\tau_w/\Delta P_{inlet}$ is related to an Euler number describing the transported energy compared to the dissipated energy $Eu = \rho u^2/\Delta P$ and $\tau_w = 0.5 \rho u^2 f$ with f the friction factor [22]. In our case, the energy transport and dissipation are not defined in the same direction, but perpendicular. The ratio of wall shear stress to the flux or transmembrane pressure has indeed been recognized as an important factor in experimental research [23]. For the present work, one might define an effective Euler number as $\tau_w/S\Delta P_{inlet}$ which is the determining dimensionless number for the system.

The criterion can be simplified for two special situations. The first situation applies to the filtration of large particles (compared to the pore size) with a low porosity membrane and circular pores.

For this process, S equals 1 and because pores are much smaller than the particle diameter (d/d_p large) and porosity is low (surface coverage < 0.05), $f_1(\theta)$ and $f_2(d_p/d)$ are both unity. Thus, the particle release criterion can be simplified to:

$$\frac{\tau_w}{\Delta P_{inlet}} \left(\frac{d}{d_p} \right)^3 > 0.0714 \quad [18]$$

The second situation is the filtration of a suspension with a highly porous membrane, where the smallest particle diameter in the feed is close to the pore size, for example 10% larger in case of particle fractionation. Therefore $f_1(\theta=1)$ is 0.25 and $f_2(d_p/d=0.9)$ is 0.48. This can be considered the worst-case scenario for the critical flux:

$$\frac{\tau_w}{S \Delta P_{inlet}} > 0.45 \quad [19]$$

This worst-case scenario can be used for membrane module design and selection of appropriate process conditions. In a rectangular membrane channel, the wall shear can be calculated from the average cross flow velocity (assuming Poiseuille flow) $\langle v \rangle$: $\tau_w = 6 \langle v \rangle \eta / h_{chan}$, with h_{chan} the channel height. The average cross flow velocity can be calculated with $\langle v \rangle = \Delta P_{chan} h_{chan}^2 / (12 l_{mem} \eta)$, where ΔP_{chan} is the pressure drop over the cross flow channel and l_{mem} the length of the membrane. In realistic membrane processes $\Delta P_{chan} / \Delta P_{inlet}$ can be 1 at maximum. With an average transmembrane pressure in the channel equal to $0.5 \Delta P_{inlet}$ ($\Delta P_{inlet} - 0.5 \Delta P_{chan}$). Substitution in equation 19 yields:

$$\frac{h_{chan}}{S l_{mem}} > 0.225 \quad [20]$$

This implies that the channel height needs to be at least 0.225 times the membrane length. The effect of the criterion on the module design and appropriate process conditions is more elaborated in figure 14 for circular and triangular pores. The extended criterion tells us that depending on the channel dimension, a minimum pressure gradient over the cross flow channel should be applied. For very thin

channels, for example $h_{chan}/2l_{mem} = 0.001$, this pressure gradient is very large, even when the pore size is much smaller than the particle diameter.

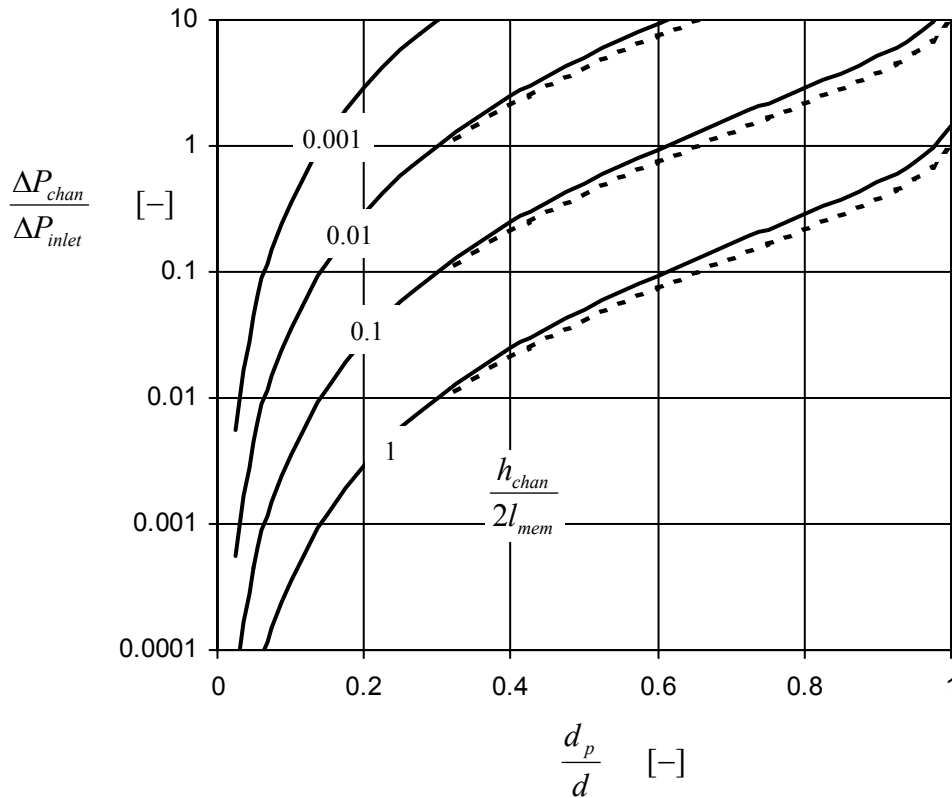


Figure 14: Transition from regime I to II for different module designs with $h_{chan}/2l_{mem}$ between 0.001 and 1.0 and membrane porosity $\varepsilon = 0.5$. Above the curves, pore blocking will not occur, of circular pores (solid lines) and triangular pores pointing towards the feed exit (dashed lines). For triangular pores, the pore shape force factors S were taken from fig. 10 (S was only available when $d_p/d > 0.33$).

This is not realistic because the pressure drop over the cross flow channel would easily exceed the transmembrane pressure, causing permeate back flow at the end of the module. For wider channels, such as $h_{chan}/2l_{mem} = 0.1$, one can see that as long as the pore size is small compared to the particle diameter, the pressure gradient that has to be applied over the feed channel is not too high.

For fractionation of particles close to the membrane pore size ($d/d_p < 1.1$), this implies that the use of the Uniform Transmembrane Pressure (UTP) concept is essential to overcome unpractical module designs. With UTP, the permeate is recycled along the backside of the membrane to maintain a uniform transmembrane pressure over the length of the membrane [24]. Otherwise, the process will end up in filtration regime II or III, were periodic removal of the cake is required for a stable fractionation process.

Discussion

a) Optimal membrane and process design

Based on the simulation results presented earlier, recommendations can be given for application of micro-machined membranes (table 2). The optimal membrane design and choice of process parameters depend on the filtration goal (retention of all particles or fractionation of a poly-disperse particle suspension) and the filtration regime.

Table 2: Recommendations for membrane design, depending on the aim of the filtration and the filtration regime.

		Filtration (retention/concentration) high flux, low energy consumption	Fractionation high selectivity (full retention and full transmission)
Regime I	Pore shape Pore size Porosity	Triangular $d/d_p = 3$ to 5 low to average porosity	Triangular Depends on required product size low porosity (coverage < 0.05)
Regime II	Pore shape Pore size Porosity	Not circular ¹⁾ $d/d_p = 3$ to 5 average	²⁾
Regime III	Pore shape Pore size Porosity	Slit shaped ³⁾ $d/d_p > 1$ high porosity	Pore blocking by one particle ⁴⁾ Circular Depends on required product size high porosity

¹⁾ The membrane design is not so important, because the cake layer predominantly determines the filtration behavior. However, complete pore blocking may not occur.

²⁾ This process is not applicable. When a steady cake has developed, small particles will be captured in the cake (selectivity is lost). When the cake is removed periodically, it resembles fractionation in regime III.

³⁾ Selected because of the possibility of highest porosity and lowest membrane permeability. (The particle release criterion is not valid in regime III.)

⁴⁾ Only possible with periodic removal of the cake.

For retention, the objective is maximum flux, while for fractionation it can be either maximum flux or maximum selectivity.

- 1) Retention of all particles: For retention of particles in regime I, a relatively small pore size ($d/d_p = 3$ to 5) is needed, next to high surface porosity. Our simulations indicate that triangular pores pointing to the feed outlet are optimal. A pore size that is clearly smaller than the smallest particle size

enables a high enough drag force on particles, because particles cannot penetrate into the pore. The combination of cross flow velocity and transmembrane pressure must be such that the backtransport of particles to the cross flow channel is sufficient to keep the membrane clean (single particle release criterion, eq. 17). In regime II, a steady cake layer is developed, which determines the flux. The membrane properties are less important, albeit it is still recommended to use a high aspect ratio to prevent particles getting stuck in the membrane pores. For retention in regime III (limiting flux regime), a high porosity and small pore size are recommended ($d/d_p = 3$ to 5). A high porosity avoids local focusing of the flow around a pore, which could effectively increase the resistance of the first blocking layer. As in the previous case, the problem of particles getting stuck into the pores is reduced at high d/d_p . The pore geometry is not so important. Filtration may continue until the flux has become too low due to the cake formation, and then the cake layer needs to be removed by for example a backpulsing technique.

- 2) Fractionation: We assume here that the optimization criterion is optimal selectivity (i.e. high retention of large particles and high transmission of small particles), and not necessarily achieving highest flux. In fractionation processes, the pore size is determined by the required selectivity. Large particles must be rejected, while smaller particles must be able to pass the membrane. Therefore, regime II and III are not suitable, because the cake layer will determine the selectivity, instead of the membrane. For fractionation in the sub-critical flux regime, the cross flow velocity and transmembrane pressure must correspond with the membrane pore size, such that rejected particles are removed from the pore (eq. 17) and transported back to the cross flow channel, while small particles can still pass the membrane. As shown by the simulations, triangular pores with the side towards the inlet of the feed may be a good choice. However, fractionation in regime I can be unstable, when particles with diameters close to the pore size are present (d/d_p close to 1). These particles then become embedded in the pore ($f_2(d_p/d)$ low) and very high cross flow velocities are required to remove them. Gradually more pores will become blocked, leading to a decreasing flux.

Fractionation in regime III as such is not possible, unless the cake is removed periodically. One might consider two options here. When a pore geometry is chosen such that a particle cannot completely block the pore (such as slit shaped or triangular pores), blockage will still allow the permeation of fluid through the pore. However, the available space will probably be too small to allow transmission of

small particles. These small particles are therefore retained (for the greater part), and the permeate will contain hardly any of the smaller particles. Alternatively, one might consider using membranes with circular pores that can be blocked completely without affecting other pores. The flux is reduced more quickly, but the permeate that is obtained will have a high concentration of small particles. Combining this with a frequent backpulsing strategy to periodically lift off the particles and allow further permeation will then result in optimal transmission of the small particles and retention of the large particles, at a reasonable flux level.

Besides an optimal design from hydrodynamic point of view, micro-machined membranes must meet additional requirements, such as sufficient mechanical strength [3]. The manufacturing of robust micro-machined membranes with exact pore geometry, high porosity and a thin active layer is still a challenge. However, given the fast developments in this area we do expect that progress will be made here.

b) Influence of particle-pore interactions

In this paper, the critical flux criterion was developed from a hydrodynamic point of view, while neutral interaction between the particle and the pore was assumed. However, in reality always additional interactions will be present, such as electrostatic (Van der Waals) or double layer interactions. Depending on the system and distance between the particle and the pore, these interactions have an attractive or repulsive nature.

When the properties of the system (membrane, particle, medium) are defined, the interaction between the particle and the pore can be quantified with the DLVO theory [25]. The resulting force can be added to the pressure force on the right hand side of equation 14. Bowen and Sharif showed that electrostatic forces can indeed play a crucial role in the filtration of 0.1 μm particles [26]. Though hydrodynamic forces become more significant for larger particles, surface properties could be an important aspect in the design of micro-machined membranes for microfiltration purposes as well [27].

Conclusion

CFD simulations were used to evaluate the influence of pore geometry and process conditions on deposition or release of particles. The simulations indicated that triangular pores pointing towards the outlet of the feed result in an optimal balance

between the torque of drag, the torque of pressure force, and the permeability of the pore. Further, sharp (90°) pore edges enhance particle release, while wear and particle deformation (both causing a deeper penetration of the particle into the pore) have a negative influence.

An extended particle release criterion was presented for membranes with uniform straight pores, various pore geometries, and membrane surface coverage. This criterion yields a critical value for the wall shear stress (and thus the required cross flow velocity) for a given transmembrane pressure. It also shows that the smallest particles in the suspension are determining the critical flux. Especially for particle fractionation, this implies a strict membrane and module design.

Although the model was developed for hydrodynamic interactions under neutral conditions, the model can be extended with a DLVO term to include interactions between the particle and the pore for practical systems.

Based on our findings, recommendations on membrane and process design were given for processes aimed at retention of all particles, and processes aimed at fractionation of particles into different fractions.

Acknowledgements

The authors would like to acknowledge the support of the Dutch ministries of Economic Affairs, Education, Culture and Sciences, and of Housing, Spatial Planning and Environment through a grant of the Dutch program Economy, Ecology and Technology (EETK20033). Dr. Rolf Bos of Friesland Foods BV, and Dr. Cees van Rijn and ir. Wietze Nijdam of Aquamarijn Micro Filtration BV are greatly acknowledged for the stimulating discussions.

Nomenclature

A_p	open pore area	$[m^2]$
c	Lattice Boltzmann velocity	$[ms^{-1}]$
c_i	Lattice Boltzmann velocity in direction i	$[ms^{-1}]$
c_s	Lattice Boltzmann speed of sound	$[ms^{-1}]$
C_d	drag force coefficient	$[Nm^{-1}s]$
d	particle diameter	$[m]$
d_p	characteristic pore size or diameter	$[m]$
Eu	Euler number	$[-]$
F_d	particle drag force	$[N]$

F_i	force on boundary in direction i	[N]
f	friction factor	[-]
f_i	density of direction i	[kgm ⁻³]
$f_{i,eq}$	equilibrium of direction i	[kgm ⁻³]
f_i	density of direction opposite of i	[kgm ⁻³]
F_{st}	Stokes drag force	[N]
h	height of particle above the membrane	[m]
h_{chan}	height of cross flow channel	[m]
k'	permeability per open pore area	[m]
l	slit length	[m]
l_{mem}	membrane length	[m]
l_o	orifice thickness / small channel length	[m]
L	periodic box size	[m]
M	torque	[Nm]
ΔP	pressure drop	[Pa]
ΔP_{chan}	pressure drop over cross flow channel	[Pa]
ΔP_{inlet}	transmembrane pressure at inlet	[Pa]
Q	flow rate	[m ³ s ⁻¹]
r	particle radius	[m]
S	pore shape force factor	[-]
t	discretized time	[s]
Δt	integration time step	[s]
u	fluid velocity	[ms ⁻¹]
v_c	local fluid velocity	[ms ⁻¹]
$\langle v \rangle$	average cross flow velocity	[ms ⁻¹]
w_i	Lattice Boltzmann weight factor for direction i	[-]
x	discretized position	[m]
Δx	grid size	[m]
ε	membrane porosity	[-]
η	viscosity	[Pas]
θ	membrane surface coverage	[-]
ν	kinematic viscosity	[m ² s ⁻¹]
ρ	density	[kgm ⁻³]
τ_w	wall shear stress	[Pa]
ω	Lattice Boltzmann collision operator	[-]

References

- [1] C.J.M. van Rijn, M.C. Elwenspoek, Micro filtration membrane sieve with silicon micro machining for industrial and biomedical applications, *Micro Electro Mechanical Systems (MEMS)* (1995) 83, Amsterdam, the Netherlands.
- [2] A.J. Bromley, R.G. Holdich, I.W. Cumming, Particulate fouling of surface microfilters with slotted and circular pore geometry. *J. Membrane Sci.*, 196 (2002) 27.
- [3] C.J.M. van Rijn (ed.), *Nano and micro engineered membrane technology*. Elsevier Science (2004) Amsterdam, the Netherlands.
- [4] G. Brans, J. Kromkamp, N. Pek, J. Gielen, J. Heck, C.G.P.H. Schroën, R.G.M. van der Sman, R.M. Boom, Modeling and evaluation of microsieve design for latex particle filtration. To be submitted to *J. Membrane Sci.* (2005).
- [5] R.W. Field, D. Wu, J.A. Howell and B.B. Gupta, Critical flux concept for microfiltration fouling. *J. Membrane Sci.*, 100 (1995) 259.
- [6] G. Belfort, R.H. Davis, A.L. Zydney, The behavior of suspensions and macromolecular solutions in cross flow microfiltration. *J. Membrane Sci.*, 96 (1994) 1.
- [7] S. Kuiper, C.J.M. van Rijn, W. Nijdam, G.J.M. Krijnen, M.C. Elwenspoek, Determination of particle-release conditions in microfiltration: a simple single-particle model tested on a model membrane. *J. Membrane Sci.*, 180 (2000) 15.
- [8] S.K. Karode, A. Kumar, Flow visualization through spacer filled channels by computational fluid dynamics I. Pressure drop and shear rate calculations for flat sheet geometry. *J. Membrane Sci.*, 193 (2001) 69.
- [9] J. Schwinge, D.E. Wiley, D.F. Fletcher, A CFD study of unsteady flow in narrow spacer-filled channels for spiral-wound membrane modules. *Desalination*, 146 (1-3) (2002) 195.
- [10] D.E. Wiley, D.F. Fletcher, Techniques for computational fluid dynamics modelling of flow in membrane channels, *J. Membrane Sci.*, 211 (2003) 127.
- [11] C.J. Richardson, V. Nassehi, Finite element modeling of concentration profiles in flow domains with curved porous boundaries, *Chem. Eng. Sci.*, 58 (2003) 2491.
- [12] R.J. Hill, D.L. Koch, A.J.C. Ladd, The first effects of fluid inertia on flows in ordered and random arrays of spheres. *J. Fluid Mech.*, 448 (2001) 213.
- [13] A.J.C. Ladd, R. Verberg, Lattice Boltzmann simulations of particle fluid suspensions. *J. Stat. Physics*, 104 (2001) 1191.

- [14] D.A. Wolf-Gladrow, Lattice-Gas cellular automata and lattice Boltzmann models. Springer Verlag (2000), Berlin, Germany.
- [15] S. Succi, The lattice Boltzmann equation for fluid dynamics and beyond. Oxford University Press, (2001) Oxford, England.
- [16] T. Inamuro, M. Yoshino, F. Ogino, Lattice boltzmann simulation of flows in a three-dimensional porous structure, *Int. J. Numer. Meth. Fluids* 29 (1999) 737.
- [17] Q. Zou, X. He, On pressure and velocity boundary conditions for the lattice Boltzmann BGK model. *Phys. Fluids*, 9 (1997) 6 1591.
- [18] D. Kandhai, A. Koponen, A. Hoekstra, M. Kataja, J. Timonen, P.M.A. Slood, Implementation aspects of 3D Lattice-BGK: boundaries, accuracy and a new fast relaxation method. *J. Comp. Physics* 150 (1999) 482.
- [19] A.J.C. Ladd, Numerical simulations of particulate suspensions via a discretized Boltzmann equation Part 1 Theoretical foundation. *J. Fluid Mech.* 271 (1994) 285
- [20] H. Hasimoto, On the periodic fundamental solutions of the Stokes equations and application to viscous flow past a cubic array of spheres. *J. Fluid Mech.*, 5 (1959) 317.
- [21] A.J.C. Ladd, Numerical simulations of particulate suspensions via a discretized Boltzmann equation Part 2 Numerical results. *J. Fluid Mech.* 271 (1994) 311
- [22] S. Elmaleh, L. Vera, R. Villarroel-Lopez, L. Abdelmoumni, N. Ghaffor, S. Delgado, Dimensional analysis of steady state flux for microfiltration and ultrafiltration membranes. *J. membrane Sci.* 139 (1998) 37.
- [23] O. LeBerre, G. Daufin, Skimmilk cross flow microfiltration performance versus permeation flux to wall shear stress ratio. *J. Membrane Sci.* 117 (1996) 261.
- [24] P.K. Vadi, S.S.H. Rizvi, Experimental evaluation of a uniform transmembrane pressure crossflow microfiltration unit for the concentration of micellar casein from skim milk. *J. membrane Sci.* 189 (2001) 69.
- [25] P.C. Hiemenz (ed), Principles of colloid and surface chemistry, second edition. Marcel Dekker (1986) New York, United States.
- [26] W.R. Bowen, A.O. Sharif, Hydrodynamic and colloidal interactions effects on the rejection of a particle larger than a pore in microfiltration and ultrafiltration membranes. *Chem. Eng. Sci.* 53 (1998) 879.
- [27] A. Arafat, K. Schroën, L.C.P.M. de Smet, E.J.R. Sudhölter, H. Zuilhof, Tailor-made functionalization of silicon nitride surfaces. *JACS* 126 (2004) 8600.



Chapter 4: Evaluation of microsieve membrane design¹

Abstract

In principle, microsieve membranes have high fluxes, due to their extremely low flow resistance and their uniform pore size. However, it was found experimentally, that the design of the support structure, even though its flow resistance is negligible, had great effect on the flux and the evolution of pore blocking. This finding was quantified using Computational Fluid Dynamics (CFD) simulations of the flow through the microsieve.

From the CFD calculations, we could conclude that the design of a microsieve should necessarily encompass the design of the top layer and the support structure together. The first design of the microsieve only had 30% of the maximum possible flux. It was shown that the channel height between the pore field and the support structure should be at least 150 μm for optimal use of the microsieve.

Introduction

Microsieves (fig. 1) are special microfiltration membranes manufactured with photolithographic techniques developed in the semi-conductor industry [1]. Currently, microsieves are mostly used for analytical purposes; large-scale applications, such as the clarification of beer and filtration of milk are under investigation [2, 3]. Due to their extremely thin active top layer, their relatively large porosity, and their open support structure the fluxes can be two or three orders of magnitude larger than for conventional membranes, even when using very low transmembrane pressures. Because of the large fluxes through the membrane, the outlet of the microsieve should be constructed in such a way that it accommodates these high fluxes. Besides this, also accumulation of particles on the membrane will take place faster than for regular membranes and this has to be taken into account for optimal use of the microsieve. Thus, it is important to quantify these effects, which are inherent to any microfiltration process, but not always as important as for microsieves.

¹ This chapter is accepted for publication in Journal of Membrane Science: G. Brans, J. Kromkamp, N. Pek, J. Gielen, J. Heck, C.J.M. van Rijn, R.G.M. van der Sman, C.G.P.H. Schroën, R.M. Boom, Evaluation of microsieve membrane design.

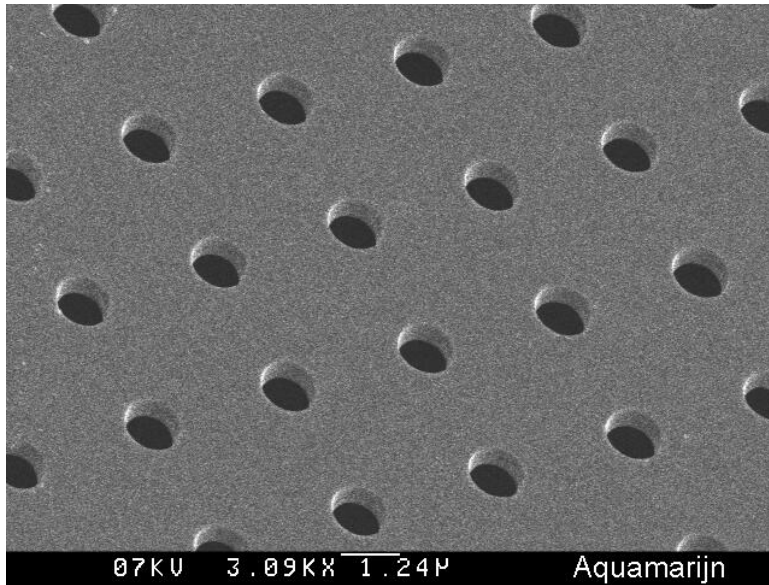


Figure 1: SEM photo of a microsieve (Courtesy of Aquamarijn Micro Filtration BV).

Kuiper *et al.* [4] studied the blocking of individual pores in a microsieve by a particle in the feed. They were able to relate the occurrence of pore blocking to the force balance on the particle, resulting from the suction force by the transmembrane pressure, and the drag force exerted by the crossflow over the membrane. The pore blocking behavior of microsieves on a larger scale is, however, not yet clear, also because the study of Kuiper *et al.* 'only' included a force balance for one pore without considering effects of the design of the microsieve as such i.e. multiple pores, and surface interaction.

In this paper, we therefore focus on the design of the microsieve and relate this to the flux and deposition of particles from the feed onto the membrane. The flux was related to the exact microsieve design, consisting of the top layer and support structure. This was done with simulation of the fluid flow through the support structure of the microsieve with lattice Boltzmann CFD simulations. These results were used to explain particle deposition during filtration of latex solutions, and ultimately, come to guidelines for a better design of the microsieve.

Pore blocking model

The flux decrease during the filtration of particle suspensions with microsieves was compared to a theoretical pore-blocking model, in which it is assumed that all open pores contribute equally to the total flux. We used a slightly modified version of the

model of Ho and Zydney [5]. The flux through a membrane $J_{membrane}$ (ms^{-1}) with n pores per area (m^{-2}) can be expressed as the sum of the flow rates through the open and blocked pores:

$$J_{membrane} = a \cdot n \cdot Q_{open} + (1-a) \cdot n \cdot Q_{blocked} \quad [1]$$

with a (-) the fraction of open pores. Q_{open} (m^3s^{-1}) is the average flux per open pore and $Q_{blocked}$ (m^3s^{-1}) is the average flow rate per (partially) blocked pore. In principle, Q_{open} can be calculated for microsieves with round pores of diameter D according:

$$Q_{open} = \Delta P / \left(\left(\frac{128h\eta}{\pi D^4} + \frac{24\eta}{D^3} \right) f_c(\varepsilon) \right) \quad [2]$$

and for slits with dimensions length l and width D [1]:

$$Q_{open} = \Delta P / \left(\left(\frac{12h\eta}{lD^3} + \frac{32\eta}{\pi lD^2} \right) f_s(\varepsilon) \right) \quad [3]$$

where ΔP (Pa) is the transmembrane pressure, h (m) the membrane thickness and η (Pas) is the viscosity of the fluid. $f_c(\varepsilon)$ and $f_s(\varepsilon)$ are correction factors for the cooperative effect of neighboring pores, for circular pores and slit pores respectively. Their values are taken from literature [1]. This correction becomes significant above a membrane porosity ε of 0.2, as is the case for the microsieves used in this study.

When the particle diameter is smaller than the distance between the pores, circular pores can be completely blocked by spherical particles and $Q_{blocked}$ can thus be assumed equal to zero, this is the case for design A of the microsieve. When the particle diameter is larger than the distance between the pores or the pores have a different geometry, filtration continues after the formation of the first layer and a thicker cake can develop. This was the case for design B of the microsieve.

For dead-end filtration, the flux during the formation of the first layer of particles can be described with:

$$\frac{dJ_{membrane}}{dt} = -C_b \frac{J_{membrane}}{n} (J_{open} - J_{blocked}) n_{block} \quad [4]$$

Where C_b (m^{-3}) is the bulk particle concentration in number per volume, and n_{block} (-) the number of pores that is blocked by one single particle. J_{open} , J_{block} and n_{block} were calculated from the flux curve against the number of particles on the microsieve.

Materials and methods

Different microsieve designs were used in this research. Microsieve A has round pores with a diameter of $1.2 \mu\text{m}$; the porosity of the pore fields is 0.49, and in total, the sieve has $8 \cdot 10^6$ pores. Microsieve B has an improved design with negligible resistance of the support structure (channel height $> 350 \mu\text{m}$). Because of limited freedom in microsieve design, the microsieve has slit-shaped pores of $0.8 \times 2.5 \mu\text{m}$ and pore field porosity 0.4. The size of the microsieve samples was 1 cm^2 , and they were provided by the D-force project.

The flow through microsieves was analyzed with CFD computer simulations, in which the channel height was varied between 35 and $350 \mu\text{m}$ (in practice it is possible to increase the channel height over $350 \mu\text{m}$ and still have a mechanically stable microsieve). The CFD simulations were performed with the lattice Boltzmann (LB) method [6], which has been successfully applied for fluid flow in complex geometries, porous media, and suspensions [7].

Because the height of the channel between the support structure and the membrane top layer is much smaller than the width of the pore field in the third dimension, this can be considered a 2D problem. A 2D LB model with 9 discrete velocities (D2Q9) was used to determine the influence of the sieve support structure.

No-slip boundary conditions were used for rigid walls. At the inlet and outlet, pressure and velocity boundary conditions were used according to Zou and He [8]. A fully developed parabolic velocity profile was defined at the inlet of the cross flow channel, and fixed pressures at the retentate outlet and permeate outlet. The membrane pore field was implemented as a continuous layer with a hydraulic resistance. This resistance was calculated from equation 2 and the membrane porosity [9].

White sulfate latex particles with diameters of 1.6 and $9.6 \mu\text{m}$ were obtained from Interfacial Dynamics Corporation (Portland, Oregon). Feed solutions were prepared by diluting the 8% stock solution with MilliQ water from a Millipore Academic filter unit (Billerica, Massachusetts). Before use, microsieves were hydrophilized by ozon plasma treatment (Harrick PDC-32G plasma cleaner, Ossining, New York; used at its highest level for 2 minutes). Microsieves were, either glued into a polysulfone holder (GE-Bayer TSE 399C, Japan), or melted into the holder by microwave heating. Subsequently, the holder was placed into the module. The filtration experiments were

carried out in dead-end mode. The transmembrane pressure (± 0.1 kPa) was set by a static water column and recorded by pressure sensors (Keller Druckmesstechnik, Winterthur, Switzerland). The amount of permeate was registered on a balance (Sartorius 4200, Göttingen, Germany) that was connected to a computer. After usage, the system was cleaned for at least 1 h with 1% Ultrasil 11 solution (Ecolab, St. Paul, Minnesota) at slightly elevated temperature (around 40°C) and rinsed with MilliQ water.

For the analysis of particle deposition, a 3D lattice Boltzmann model with 19 velocities (D3Q19) was used to simulate the resistance of the first and second layer of particles. The position of the particles was determined by assuming hexagonal close packing. For a more extensive description of the LB models and its validation, the reader is referred to Brans and coworkers [10].

Results and discussion

a) Microsieve design

The flow through a type A microsieve was studied with the 2D LB CFD model. Simulation results are depicted in figure 2 and 3. We found that the support structure has a large influence on the flow through the microsieve.

At a transmembrane pressure of 4.0 kPa, the presence of the support structure limits the capacity to about 30 % of the clean water flux that could be achieved with a sieve without support structure (calculated from the velocity profile, figure 3).

Although the flow resistance of the support structure itself is negligible, the configuration of the membrane layer together with the support structure has a large influence on the flow pattern and the total resistance. Most of the flux permeates through the middle of the pore field. The channel between the support structure and the membrane layer is 35 μm , and a small pressure difference arises to drive the water from the edges of the pore fields towards the middle. Hence, the transmembrane pressure at the edges of the pore field is lower than in the middle of the pore field. This is directly reflected in the local flux as can be seen in figure 3.

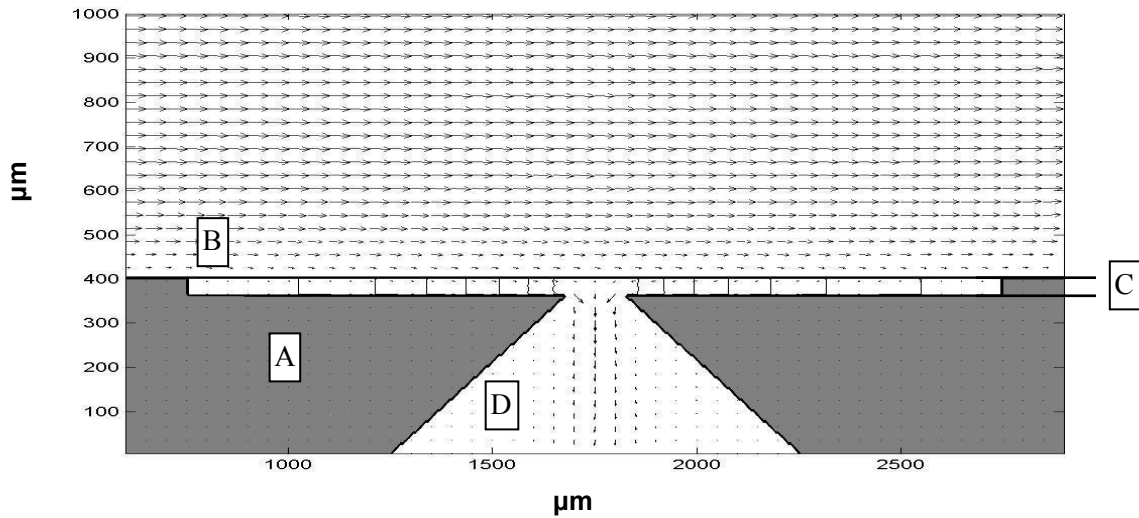


Figure 2: 2D lattice Boltzmann simulation of flow through a type A microsieve; grid dimensions 700*260 and grid size 5 μm . A is the support structure and B the membrane top layer (length 2500 μm , depth 60 μm). The permeate outlet width D was 140 μm between the support structure just underneath the membrane and 1000 μm at the bottom. In the simulations, the channel height C was varied between 35 (as is shown in the figure for design A) and 350 μm . Additional information on e.g. the pore size can be found in the materials and methods section. Arrows indicate flow direction and local fluid velocity; transmembrane pressure was 4.0 kPa.

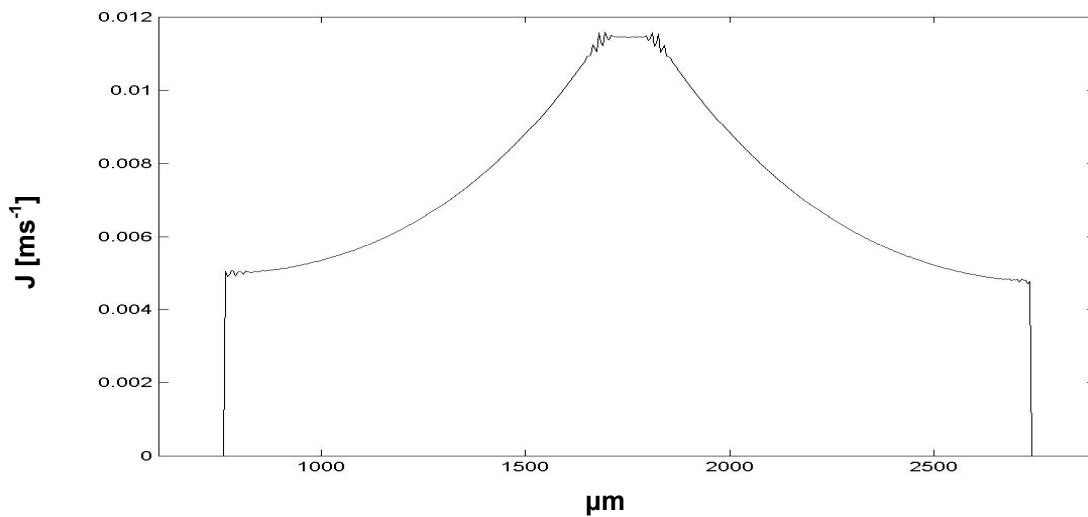


Figure 3: Flux through the membrane layer as a function of the horizontal position (derived from fig. 2). The flux is a direct function of the local pressure difference across the membrane.

A solution to this is to increase the channel height between the support structure and membrane layer. The effect thereof is investigated with lattice Boltzmann simulations. In table 1, the calculated relative flux is shown for microsieves with different channel heights. The main conclusion is that the channels have to be as high as 150

micrometer to reach fluxes above 90 % of the flux of a support layer-free microsieve, therewith stressing the importance of this design parameter.

Table 1: The effect of changing the channel height between the support structure and the membrane top layer (sieve design A has a channel height of 35 μm). The relative flux was calculated from a simulation of a sieve without support structure.

Channel height (μm)	Relative flux (-)
35	0.30
60	0.63
150	0.92
350	0.99

b) Filtration of latex particle suspensions: design A with channel height 35 μm

From the simulations, it is clear that microsieve design influences the flux largely, now we investigate how this influences particles deposition during filtration. Latex particles of diameter 1.6 μm were filtered with type A microsieves in dead-end mode.

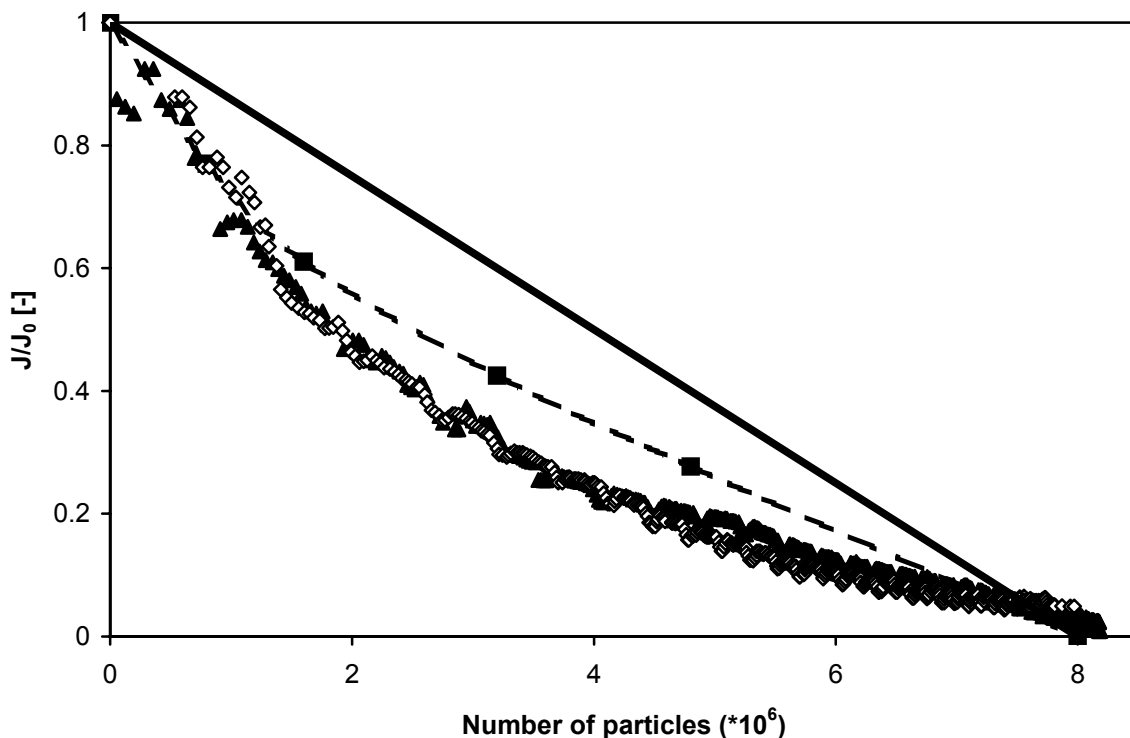


Figure 4: Normalized flux during dead-end filtration of 1.6 μm particle suspensions with type A microsieves). The latex concentrations were 1.6 mg l^{-1} (diamonds) and 0.82 mg l^{-1} (triangles); the transmembrane pressure was 4.0 kPa. Further, the results of the regular pore blocking model (solid line) and a model that includes the effect of support structure (squares) are shown.

The normalized flux is shown for two concentrations (0.82 and 1.6 mg l⁻¹) in figure 4 as function of the number of particles retained by the microsieve, together with the prediction of the regular pore-blocking model. The two suspension concentrations gave almost identical curves for the relative flux against the number of particles. As can be seen, the experimental curves do not agree with the pore-blocking model. In the initial stage, the flux decreased faster than the model prediction, while at the end the flux decreased slower. This indicates that fluxes are not the same for each pore, as was expected from the simulations on the channel height.

During the latex filtration experiments, it was observed that particles preferably deposited in the middle of the pore field. This is in agreement with our simulation results, which also indicated that most of the flux goes through the centre of the microsieve, and therefore will have a higher chance to be blocked. Simulations of a type A microsieve that gradually becomes blocked, starting in the middle of the membrane field with the pores that carry most of the flux (based on experimental observations), show a similar behavior as the experimental fluxes (fig. 4), although the experimental fluxes seem to decrease slightly faster than the flux simulations.

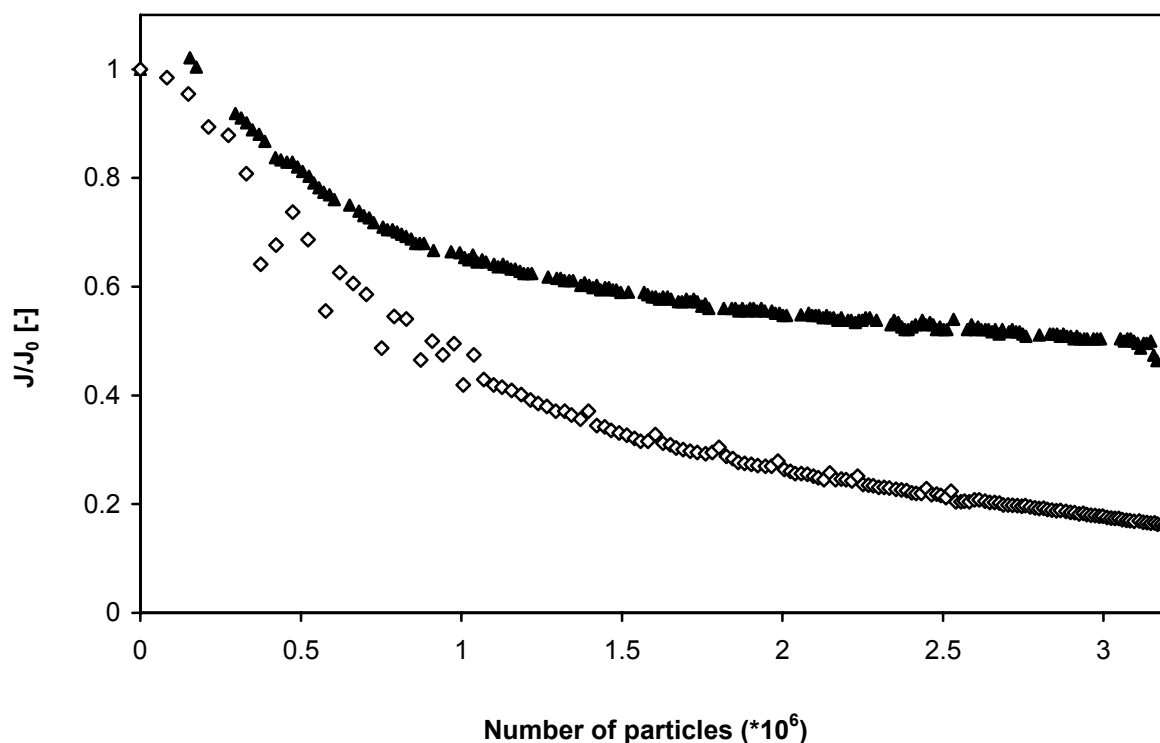


Figure 5: Normalized flux curves during dead-end filtration of 9.6 µm particle suspensions with type A (diamonds) and B (triangles) microsieves at a latex concentration of 17 mg l⁻¹. The transmembrane pressure was 4.0 kPa.

Filtration of 9.6 μm latex particles with type A microsieves leads to incomplete pore blocking, since one particle covers multiple pores. Thus multiple particle layers are formed. The build-up of multilayer started in the middle of the pore fields even before the whole pore field was covered with a monolayer of particles. The flux curve showed a gradual flux decrease (fig. 5), because of the factors mentioned earlier. Because of the multiple layers, the flux behavior could not be analyzed with the simple pore-blocking model.

c) Filtration of latex particle suspensions: design B with channel height > 350 μm

A new microsieve design with negligible resistance of the support structure was tested together with the old design. Flux curves for 9.6 μm latex particles at concentration 17 mg l^{-1} are shown in figure 5. Only for microsieve B, the flux against the number of particles gave a straight line with different slopes for the first two layers of 9.6 μm particles. The slopes were determined with linear regression and the reliabilities were estimated (fig. 6). After $4.1 \cdot 10^5$ particles, the slope of the flux curve seems to change, which corresponds to the completion of the first layer.

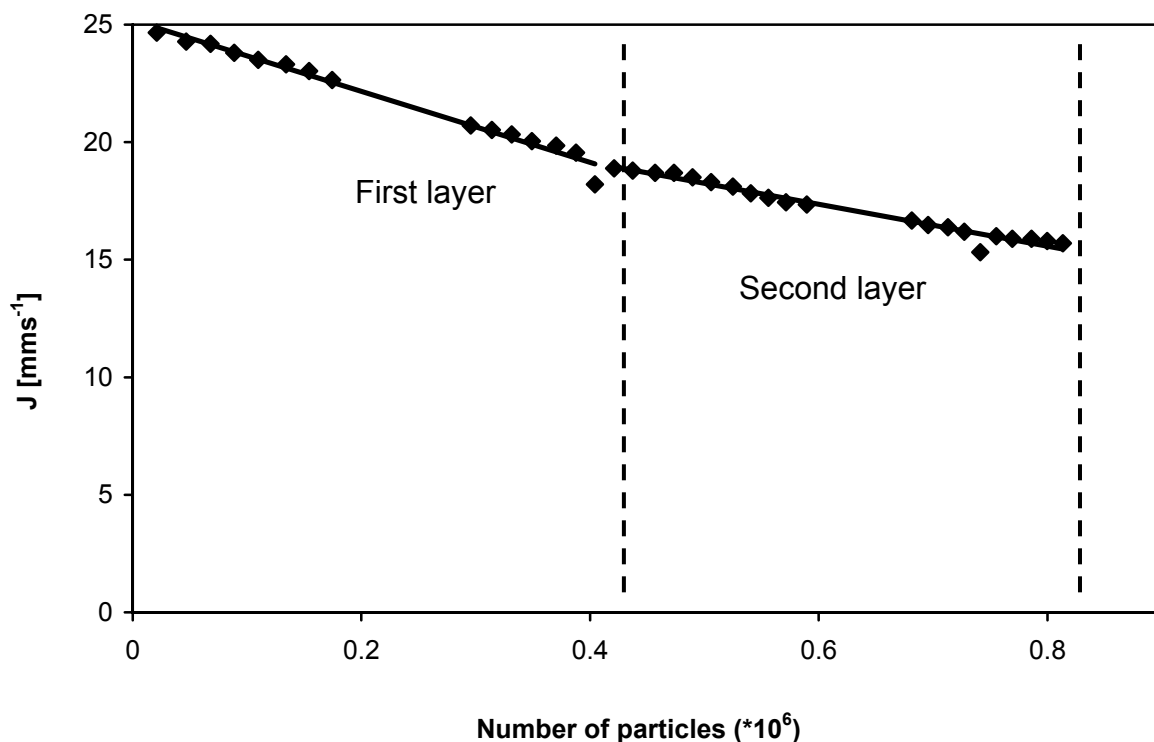


Figure 6: Flux decrease during filtration of 9.6 μm particles with type B microsieve: the formation of the first and second particle layers. Latex concentration was 17 mg l^{-1} and transmembrane pressure 4.0 kPa. The slope of the first layer was $-15.1 \cdot 10^{-6} \pm 0.59 \cdot 10^{-6} \text{ ms}^{-1} \text{ particle}^{-1}$ (95% conf. int.). The slope of the second layer, was $-9.08 \cdot 10^{-6} \pm 3.69 \cdot 10^{-6} \text{ ms}^{-1} \text{ particle}^{-1}$ (95% conf. int.).

One particle covers approximately 22 pores, based on the porosity of the pore fields and surface coverage of 0.5 by a closely packed 2D monolayer of spheres. The parameters of the pore-blocking model, J_{open} and $J_{blocked}$, were calculated for the first blocking layer and were 0.026 ms^{-1} and 0.019 ms^{-1} respectively. After $8.1 \cdot 10^5$ particles, in principle the second layer was completed. $J_{blocked2}$, the average flux through one pore with two particle layers was equal to 0.016 ms^{-1} . For the subsequent layers, the difference in the slope was less pronounced. The straight lines in the initial phase are in agreement with the pore-blocking model of Ho and Zydney [5]. They could only distinguish the first deposition layer on a track-etched membrane and assumed random cake formation afterwards.

Further, the resistances of the first and second layer of particles on the membrane were determined (table 2). Notice that these resistances must be interpreted as the additional resistance in combination with the membrane (first layer), and additional resistance in combination with the membrane and the first layer (second layer). The first blocking layer caused the largest flux decline, 73 % of the original flux.

Table 2: Experimentally determined resistances and computer simulations of dead end filtration of $9.6 \mu\text{m}$ latex particles with microsieve design B at transmembrane pressure 4.0 kPa. The membrane resistance according to eq. 3 was $7.8 \cdot 10^7 \text{ m}^{-1}$, with $f_s(\varepsilon)$ 0.93.

	Experiment	Simulation
Resistance first layer [m^{-1}]	$3.7 \cdot 10^7$ ¹⁾	$3.6 \cdot 10^7$ ¹⁾
Resistance second layer [m^{-1}]	$2.2 \cdot 10^7$ ²⁾	$2.9 \cdot 10^7$ ²⁾
J_{open} [ms^{-1}]	0.026	0.045
$J_{blocked}$ [ms^{-1}]	0.019	0.030
$J_{blocked2}$ [ms^{-1}]	0.016	0.023

¹⁾ note that resistance must be interpreted as additional resistance to the membrane resistance.

²⁾ note that resistance must be interpreted as additional resistance to the membrane and first particle layer.

Numerical simulation of the first layer on the membrane with the 3D lattice Boltzmann model gave a resistance of $3.6 \cdot 10^8 \text{ m}^{-1}$, which is in agreement with the experimental data ($3.7 \cdot 10^8 \text{ m}^{-1}$; some experimental and numerical data are shown in more detail in table 2). The experimental resistance of the second layer was $2.2 \cdot 10^8 \text{ m}^{-1}$, while numerical simulation gave a resistance of $2.9 \cdot 10^8 \text{ m}^{-1}$, which is still in relative good agreement. The resistance of the first layer is higher than the second layer, due to the specific configuration of the particles near the pores. Dufreche and coworkers

also reported a higher resistance for particles on a perforated plate, than for particles slightly further away from the plate [11].

To round off, the importance of a correct design of the total membrane became eminently clear from the particle filtration experiments and the computer simulations. Both, the top layer and support layer should be considered together in the design in order to make best use of microsieves. We expect that the microsieve design can be further optimized, for example, pore field design and porosity are still to be investigated in detail.

Conclusion

The support structure of the sieve has a large influence on flux and particle deposition, as shown by computer simulations and particle filtration. For microsieve design A, only 30 % of the sieve area was used effectively during filtration. CFD simulations showed that the height of the channel between the pore field and the support structure had a large effect on the flow resistance, and caused non-uniform flow through the pore field, which limits the application of the current design of the microsieve.

Acknowledgements

We would like to acknowledge the support of the Dutch Economy, Ecology and Technology program (EETK20033), and the D-force project (Friesland Foods BV, Aquamarijn Micro Filtration BV, Membrane technology group University of Twente and Food and Bioprocess engineering group Wageningen University) for providing the microsieve samples and interesting discussions. Furthermore, we like to thank Remco Fokkink of the Department Physical Chemistry and Colloid Science for the ozone plasma treatment.

References

[1] C.J.M. van Rijn, M.C. Elwenspoek, Micro filtration membrane sieve with silicon micro machining for industrial and biomedical applications, Micro Electro Mechanical Systems (MEMS) proceedings (29 jan – 2 feb 1995) 83, Amsterdam, the Netherlands.

-
- [2] C.J.M. van Rijn, W. Nijdam, L.A.V.G. van der Stappen, O.J.A. Raspe, L. Broens, S. Hoof, Innovation in yeast cell filtration: cost saving technology with high flux membranes, Proceedings of European Brewery Conference (23 may 1997) 501, Maastricht, the Netherlands.
- [3] C.J.M. van Rijn and J. Kromkamp, Method for filtering milk, WO0209527, 2001.
- [4] S. Kuiper, C.J.M. van Rijn, W. Nijdam, G.J.M Krijnen, M.C. Elwenspoek, Determination of particle-release conditions in microfiltration: a simple single-particle model tested on a model membrane. J. Membrane Sci. 180 (2000) 15.
- [5] C. Ho and A. Zydney, A combined pore blockage and cake filtration model for protein fouling during microfiltration. J. Colloid Interface Sci. 232 (2000) 389.
- [6] S. Succi The Lattice Boltzmann equation for fluid dynamics and beyond. Oxford University Press, (2001) Oxford, England.
- [7] R. Hill, D. Koch, A. Ladd, The first effects of fluid inertia on flows in ordered and random arrays of spheres. J. Fluid Mechanics 448 (2001) 213.
- [8] Q. Zou, X. He, On pressure and velocity boundary conditions for the lattice Boltzmann BGK model. Phys. Fluids 9 (1997) 1591.
- [9] J. Kromkamp, A. Bastiaanse, J. Swarts, G. Brans, R. van der Sman, R. Boom A suspension flow model for hydrodynamics and concentration polarization in crossflow microfiltration. J. Membrane Sci. 253 (2005) 67.
- [10] G. Brans, R.G.M. van der Sman, C.G.P.H. Schroën, R.M. Boom Optimization of membrane geometry for micro-machined membranes. In press J. Membrane Sci. (2005)
- [11] J. Dufreche, M. Prat, P. Schmitz, J. Sherwood On the apparent permeability of a porous layer backed by a perforated plate. Chem. Eng. Sci., 27 (2002) 2933.

Chapter 5: Transmission and fractionation of micro-sized particle suspensions¹

Abstract

In processes aimed at the fractionation of a multi-component feed stream, transmission of small particles through the membrane is just as important as retention of larger particles. In this paper, we describe the mechanisms of transmission of mono-disperse latex particles through a polymer membrane. The effects of process parameters, such as transmembrane pressure, cross flow velocity and feed concentration were investigated. In dead end filtration mode, we found that, depending on the transmembrane pressure, four particle transmission regimes could be distinguished.

Particle deposition on polymer membranes and polymer microsieves was investigated in-line with Confocal Scanning Laser Microscopy (CSLM). It was observed that with the polymer membrane random depth fouling took place, while the microsieve exhibited in-pore fouling.

In addition, bi- and tri-disperse particle suspensions were fractionated with cross flow membrane filtration. Based on the phenomena observed, it is concluded that the design of a fractionation process starts with defining a stable transmission regime for small particles, and subsequently choosing process conditions for minimal deposition of the larger particles.

Introduction

The separation of micro-sized particle suspensions is an important topic in the chemical, food, and pharmaceutical industry. Product purity and particle size distribution are important factors determining the functionality and the economic value of these products.

As a rule of thumb, membranes are capable of separating particles that differ in size by a factor of ten. Particles are transmitted through a membrane with a nominal pore size of three to five times the particle size. For the retention of large particles,

¹ This chapter is in preparation for publication: G. Brans, A. van Dinther, B. Odum, C.G.P.H. Schroën, R.M. Boom, Transmission and fractionation of micro-sized particle suspensions.

particles must be at least twice as large as the nominal pore size. In these numbers, the effects of particle size distribution and membrane pore size distribution are taken into account.

For efficient use of natural feed streams, components need to be separated more precisely and into various well-defined fractions. Such a fractionation system can consist of e.g. multiple membrane stages, which should combine high retention of the larger species with high transmission of the smaller species through the membrane. Because the components often differ only slightly in size and they may be rather poly-disperse, these separations are not trivial.

As an example, in the membrane pasteurization of skim milk, the smallest bacteria can be 0.7 μm , while these have to be separated from casein micelles as large as 0.5 μm [1]. For these types of separations, membranes with narrow pore size distributions such as track-etched membranes [2], microsieves [3] or metal microfilters [4] are of essence.

Ramachandran and Fogler investigated particle transmission during dead end filtration with track-etched Nuclepore filters that have uniform pores [5]. Various phenomena were found to play a role. Low flow velocities caused particle adsorption to the pore walls (in-pore fouling), while higher flow velocities resulted in better particle transmission. When the flow velocity was increased further, the pores blocked because of bridging. All these aspects need to be understood for the successful design of fractionation processes.

Besides the effects of in-pore fouling and bridging, a cake layer may build up on the membrane, therewith further reducing productivity and selectivity. Cake formation usually starts with deposition of large particles, which results in flux decline and reduced transmission of small particles, as the cake retains them. Although cake formation can be reduced to some extent by charge interactions, as described by Iritani *et al.* [6], mostly this is not an option and cake formation should be prevented completely for fractionation purposes.

In this paper, we first report the transmission behavior of particles through a polymer membrane in dead end and in cross-flow mode. Ideally, the particles should be transmitted completely for fractionation. However, we also studied the location of particles that block the membrane under different process conditions. Deposition of particles on top of the membrane is generally reversible. Particles deposited inside pores however, cannot be removed. Particle transmission was investigated with mono-disperse latex particles using polymer membranes and polymer microsieves, and was visualized with Confocal Scanning Laser Microscopy (CSLM) for both types of membrane. Based on the knowledge gained for mono-disperse suspensions,

fractionation experiments were performed with bi- and tri-disperse suspensions. From this, general rules were derived for fractionation processes.

Theory

The transmission of particles through the membrane T is defined as:

$$T = \frac{C_f}{C_p} \quad [1]$$

Where C_f is the concentration in the feed and C_p the permeate concentration. Transmission is related to the retention R via $T=1-R$.

The flux curves were analyzed with a standard blocking model and pore blocking model [7]. The standard blocking model assumes that deposition takes place on the pore walls, causing the pore diameter to decrease, while the number of active pores per unit area remains the same. This model gives for the flux J through the membrane:

$$J = \frac{\Delta P}{\eta \cdot R_0 (1 + k_1 t)^2} \quad [2]$$

With ΔP the transmembrane pressure, η the viscosity and R_0 the initial membrane resistance. k_1 is a constant, related to deposition rate, and t the time.

For the pore-blocking model, it is assumed that the number of active pores decreases proportionally with the cumulative permeate volume due to pore blocking while the pore diameter remains constant. The flux through the membrane is described by:

$$J = \frac{\Delta P}{\eta \cdot R_0 e^{k_2 t}} \quad [3]$$

with k_2 a constant, related to the blocking rate.

Materials and methods

a) Conventional membrane experiments

Transmission and fractionation experiments were performed with 0.2 μm cellulose acetate membranes (Sartorius 11107-293, Goettingen, Germany). The pore size distribution of the membrane was determined with coulter porometry, which yielded an average pore size of 0.33 μm . In the fractionation of the tri-disperse suspension also a 3.0 μm cellulose acetate-nitrate polymer membrane (Millipore SSWP304F0 Billerica, Massachusetts) was used. The membranes were pre-conditioned and cleaned by recirculating 0.1% Ultracil 11 (Henkel) in demineralized water for 30 minutes. After that, the membranes were rinsed twice with milli-Q water for 20 minutes.

The membranes were placed in a flat plate module with a channel height of 1 mm. In the dead end experiments, a static water column supplied the transmembrane pressure. In the cross flow experiments, a 5003U Watson & Marlow gear pump (Cornwall, England) or a TS011 Heukelom gear pump (Achterveld, the Netherlands) was used, and a valve in the retentate tubing controlled the transmembrane pressure. The flux was measured by a balance (Sartorius CP4202S, Goettingen, Germany) and the transmembrane pressure was recorded with electronic sensors (Keller Druckmesstechnik, Winterthur, Switzerland). A computer logged all data.

Surfactant free polystyrene latex was obtained in various sizes from Interfacial Dynamics Corporation (Portland, Oregon); the 0.1 μm particles were synthesized in our lab using the method of Goodwin *et al.* [8]. The size of the latex particles was verified with light diffraction (Malvern Mastersizer 2000, Malvern England). The initial concentration of the latex suspensions was determined from the dry weight (80°C, 24 h); the concentration of the latex particles was measured with a Spectronic 20 Genesys spectrophotometer (Spectronic Instruments, USA) at 550 nm, using a calibration curve. Latex suspensions were diluted with milli-Q water to the desired concentration.

Dead end transmission experiments were carried out with 0.1% 0.1 μm particles at transmembrane pressures between 0.9 and 5.0 kPa. In cross flow experiments, 0.5 to 0.9% of 0.1 μm particles were filtered at a transmembrane pressure of 3.0 kPa. For fractionation of bi-disperse suspensions, 0.1 μm particles were separated from larger co-particles with diameters between 0.3 and 1.4 μm , in dead end and cross flow. The transmembrane pressure was 0.7 kPa and the particle concentration 0.041% (0.082% in total). The tri-disperse suspension consisted of 0.1, 1.0, and 10 μm latex particles in equal volume fractions (1:1:1 w/w, concentration 0.041% each), and was fractionated with two membranes of 0.2 μm and 3.0 μm at transmembrane

pressures of 2.0 kPa and 0.7 kPa, respectively. Most particle filtration experiments were repeated and showed good reproducibility.

b) CSLM experiments

For the Confocal Scanning Laser Microscopy (CSLM) experiments we used 3.0 μm cellulose acetate-nitrate polymer membranes (Millipore SSWP304F0 Billerica, Massachusetts) and 5.0 μm polymer PES microsieves that were kindly provided by Membrane Technology Group, University of Twente (Enschede, the Netherlands). Polymer microsieves are a novel type of membranes that are produced by polymer casting in a silicon mold consisting of pillars [9]. The resulting membrane has very uniform pores in a regular pattern (fig. 1). Because of its pore size distribution, the 3.0 μm regular polymer membrane was expected to have similar retention characteristics for larger particles as the 5.0 μm polymer microsieve.

The membranes were glued in a 1 cm^2 polysulfone holder with silicone glue (GE-Bayer TSE 399C, Japan). Steel netting supported both the polymer membranes and microsieves to withstand the transmembrane pressure. The holders were placed into a different flat plate module (specially made for CSLM) with a microscopy glass above the membrane and a channel height of 0.2 mm. The cross flow was driven by a gear pump; flux and transmembrane pressure were logged by a personal computer.

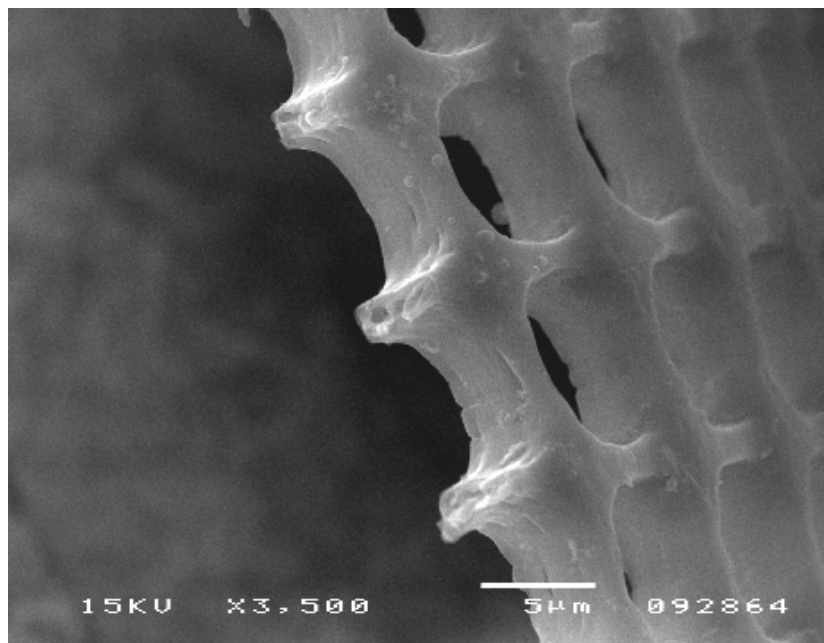


Figure 1: SEM photo of a polymer microsieve (Membrane Technology Group, University of Twente) [9].

Friesland Foods (Deventer, the Netherlands) kindly let us use their CSLM facilities (Leica TCS SP2, Heidelberg, Germany). Images were made with a lens of magnification 20 and working distance of 3.2 mm. Images of the membrane surface were taken (for each particle size separately) and combined into an overlay with the Leica CSLM software. The acquisition time per image was about 1 s and images were made once per minute. Fluorescent latex particles were obtained from Molecular Probes Europe BV (Leiden, the Netherlands). We used F8834 9.7 μm red FluoSpheres polystyrene microspheres (ex/em 580/605) and F8852 1.0 μm yellow-green FluoSpheres sulfate microspheres (ex/em 505/515). In transmission experiments, $5.3 \cdot 10^{-7}$ % 1.0 μm yellow-green particles were filtered with increasing transmembrane pressure in steps of 0.5 kPa; in fractionation experiments $5.3 \cdot 10^{-7}$ % 1.0 μm particles and $2.3 \cdot 10^{-5}$ % 9.7 μm red particles with transmembrane pressure of 0.55 kPa.

Results and Discussion

a) Effect of pressure on transmission of mono-disperse particles in dead end

To study the influence of transmembrane pressure on the transmission, 0.1 μm particle suspensions (0.1%) were filtered through the 0.2 μm cellulose acetate membrane in dead end mode with pressures between 0.9 and 5.0 kPa. In figure 2a, transmission is shown for various transmembrane pressures. Particle transmission can be divided in four regimes, depending on the transmembrane pressure:

- 1) At 0.9 and 1.0 kPa, there was full particle transmission during the entire experiment. Because the flow velocity through the membrane pores was low, particles were thought to follow the major streamlines, resulting in minimal adsorption and blocking, and therewith in a stable flux and full transmission.
- 2) At higher transmembrane pressure, particles were expected to come into contact with the pore walls. This happened between 1.2 and 2.2 kPa, when the flow velocity through the membrane was higher and particles started to deviate from the major streamlines. The particles could be adsorbed to the pore walls, therewith reducing the flux and the transmission.
- 3) Between 2.5 and 4.0 kPa, the hydrodynamic forces become larger than the adsorptive forces, resulting in a higher initial transmission. However, because of the higher fluxes, the chance that particles meet and block the pore becomes larger, therewith decreasing the flux in time.
- 4) At even higher transmembrane pressure (4.5 and 5.0 kPa), bridging occurred. When multiple particles arrived at a pore entrance at the same time, the pore

could be plugged instantly and consequently the transmission decreased to zero.

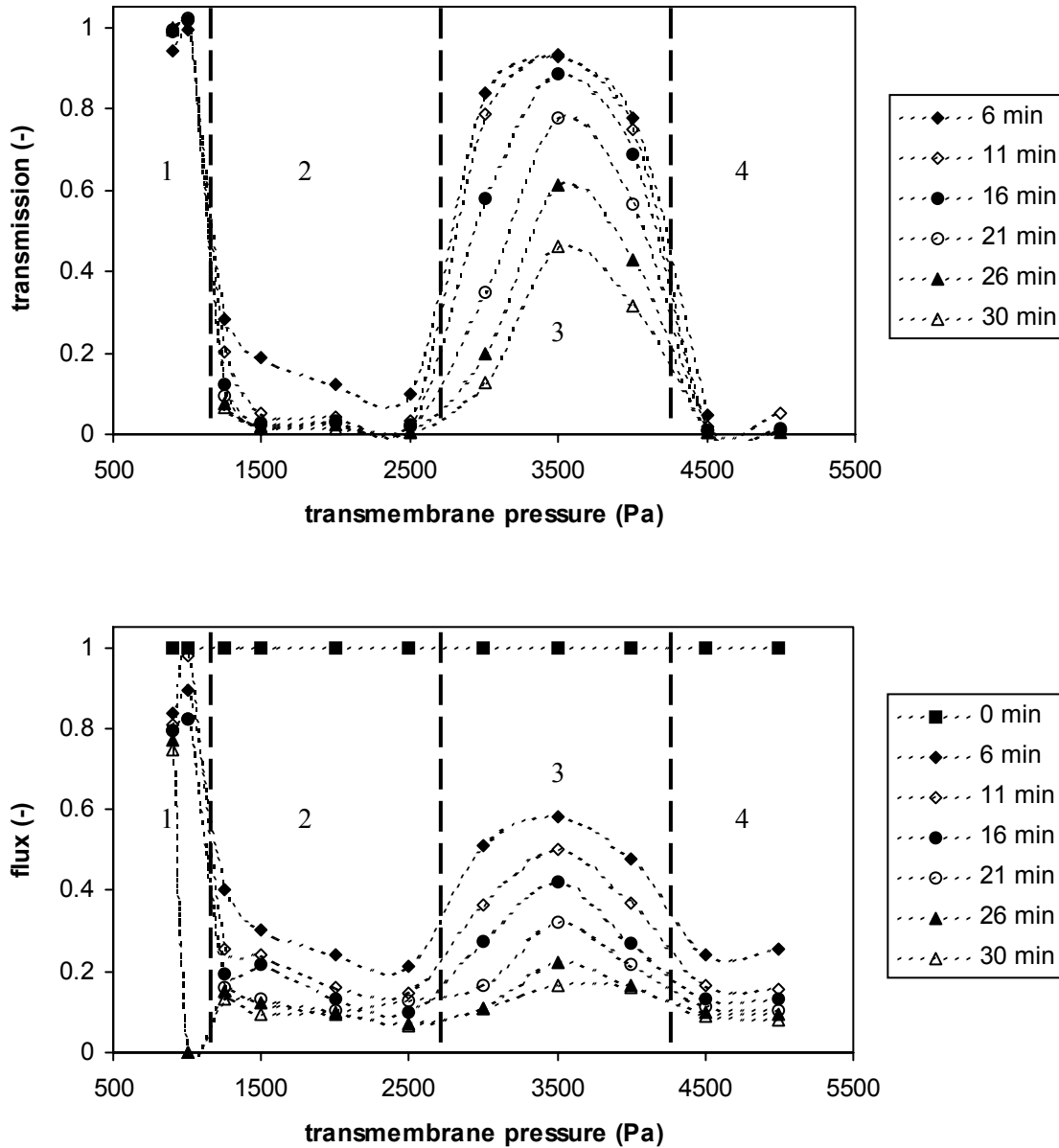


Figure 2a and 2b: The influence of the transmembrane pressure on the relative flux and transmission of 0.1 μm latex particle suspension (0.1 %) with a 0.2 μm cellulose acetate membrane in dead end filtration. Transmission regimes are indicated by numbers. Dashed lines are given to guide the eye.

Our observations are in line with the results of Ramachandran and Fogler, who studied the transport of particles through Nuclepore track-etched membranes, which lack interconnected pores [5]. They measured the required pressure drop over the membrane for a constant flow of the suspension through the membrane and found

that the efficiency of particle retention by hydrodynamic bridging increased with increasing flow. In a subsequent paper, Ramachandran *et al.* discussed the influence of colloidal forces on particle adsorption and pore blocking [10]. With their model, based on the combination of hydrodynamic and colloidal (DLVO based) forces, they predicted the existence of different transmission regimes for particles flowing through a membrane pore.

The main difference between the work by Ramachandran and Fogler and the current paper is that we used a tortuous path polymer membrane with a pore size distribution and therefore, bridging is more likely to take place inside the membrane as well. This could explain the time dependency of regime 3.

In figure 2b, the relative fluxes are depicted. Flux decrease and reduced particle transmission are strongly correlated, although flux decrease is often observed somewhat earlier than transmission decrease. At 0.9 and 1.0 kPa, there is a constant flux and full transmission, while flux and transmission both decrease sharply at 1.2 kPa. The initial fluxes (first 5 minutes) were analyzed with the standard blocking model and the pore blocking model, by fitting the initial resistances and the time constants (results not shown). The flux decrease in regimes 2 and 3 coincided best with the standard blocking model, while fluxes in regime 4 were in better agreement with the pore blocking model. This suggests that particle deposition predominantly starts with in-pore fouling in regimes 2 and 3 (depth filtration throughout the membrane), and pore blocking in regime 4 (blocking by bridging, membrane surface related). Eventually, the system is expected to show dead end cake filtration, with no significant particle transmission.

The combination of decreased particle transmission and increased flow resistance was also seen by Biggs *et al.*, who investigated particle deposition in a constriction with numerical simulations of 2D suspension flow [11]. The deposition and detachment of particles was implemented with a so-called sticking probability, for both the deposition on the pore wall and the adhesion to already deposited particles. Particle deposition affected the flow pattern around the particles and increased the rate of subsequent deposition, which is in line with our observation that as soon as the flux decrease sets in, the transmission follows in a much more pronounced fashion.

b) Particle deposition in cross flow transmission experiments

To investigate the interaction of particles with the membrane, the transmission process was followed in-line with CSLM. In transmission experiments, a $5.3 \cdot 10^{-7}$ %

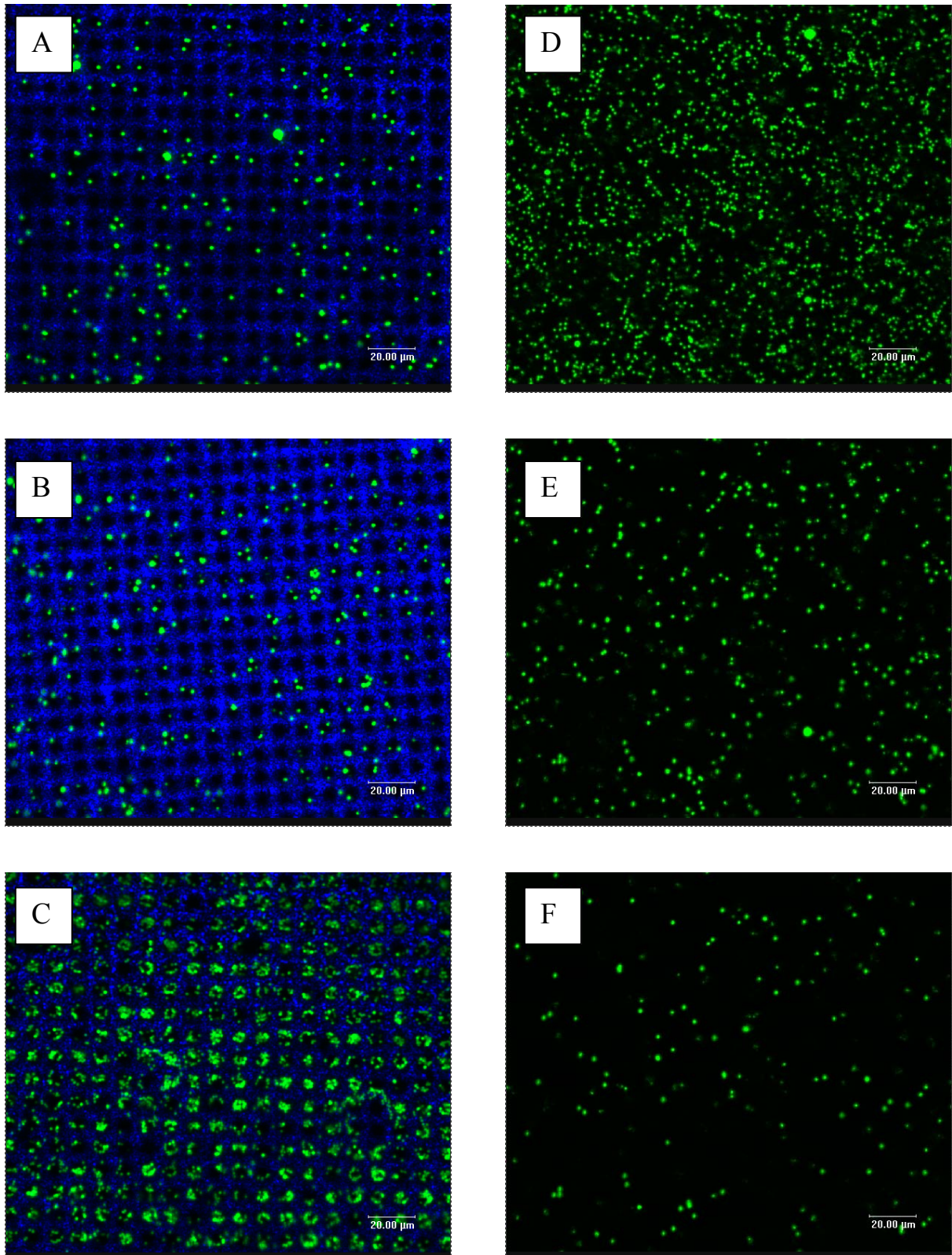


Figure 3: CSLM images of transmission of mono-disperse suspension with $5.3 \cdot 10^{-7} \%$ $1.0 \mu\text{m}$ particles. Snapshots A, B, C: $5.0 \mu\text{m}$ polymer microsieve on $t = 5, 15$ and 25 min at transmembrane pressure of $0.4, 1.0$ and 1.5 kPa. Snapshots D, E, F: $3.0 \mu\text{m}$ polymer membrane on $t = 5, 20$ and 34 min at $0.5, 1.5$ and 2.5 Pa. The cross flow velocity was 0.047 ms^{-1} .

suspension of 1.0 μm green particles was filtered through a 3.0 μm regular polymer membrane and a 5.0 μm polymer microsieve (fig. 3). To study the effect of the pressure on particle deposition, the transmembrane pressure was increased in steps of 0.5 kPa (fig. 4a and 4b).

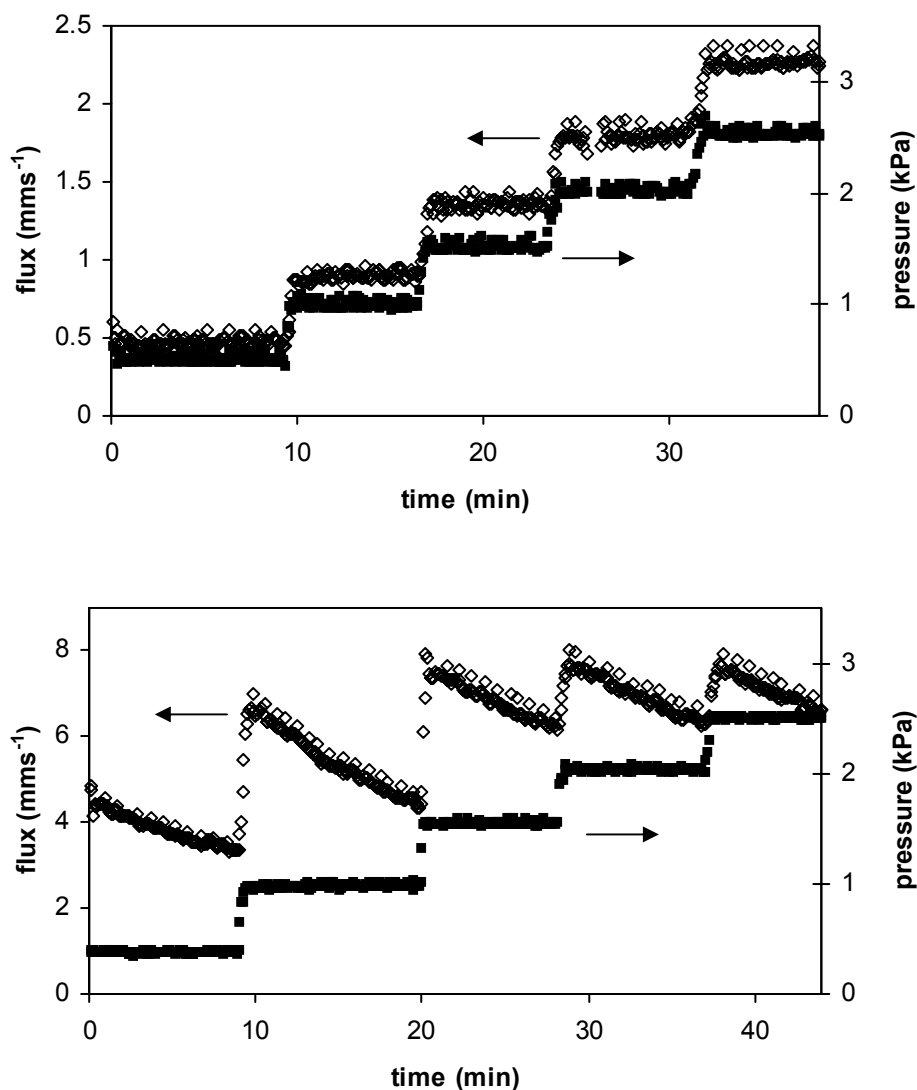


Figure 4a and 4b: Flux curves and transmembrane pressure in time during particle transmission experiments with 3.0 μm polymer membrane (top) and 5.0 μm polymer microsieve (down) under CSLM.

The microsieve showed a different fouling behavior compared to the polymer membrane (fig. 3). With the polymer membrane, small particles were adsorbed at random places in the tortuous structure of the membrane or became trapped in the pores (see also fig. 5). Blocking by bridging was not observed, probably due to the low particle concentration. The microsieves showed in-pore fouling and adhesion to

the membrane pore edges. This indicates that membrane-particle interactions are crucial in particle transmission processes.

In figure 5, a SEM photo of the cellulose acetate membrane with particles is shown after cross flow filtration in regime 2. The particles were indeed adsorbed randomly to the membrane surface and inside the membrane, as observed with CSLM (fig. 3).

The flux of the polymer membrane increased linearly with the transmembrane pressure. Please note that only the first flux level of the polymer membrane (fig. 4b) was below the critical flux of shear-induced diffusion (0.93 mms^{-1} , [12]), but this could not prevent particle adsorption to the membrane. Because of the open tortuous membrane structure, the fluid can easily flow around a deposited particle and therefore the flux was not affected. The microsieve, however, showed decreasing fluxes after each pressure step, due to particle deposition inside the pores, leading to significant reduction of the membrane permeability. It has to be noted, however, that the initial flux through the microsieve was approximately one order of magnitude higher compared to the conventional polymer membrane.

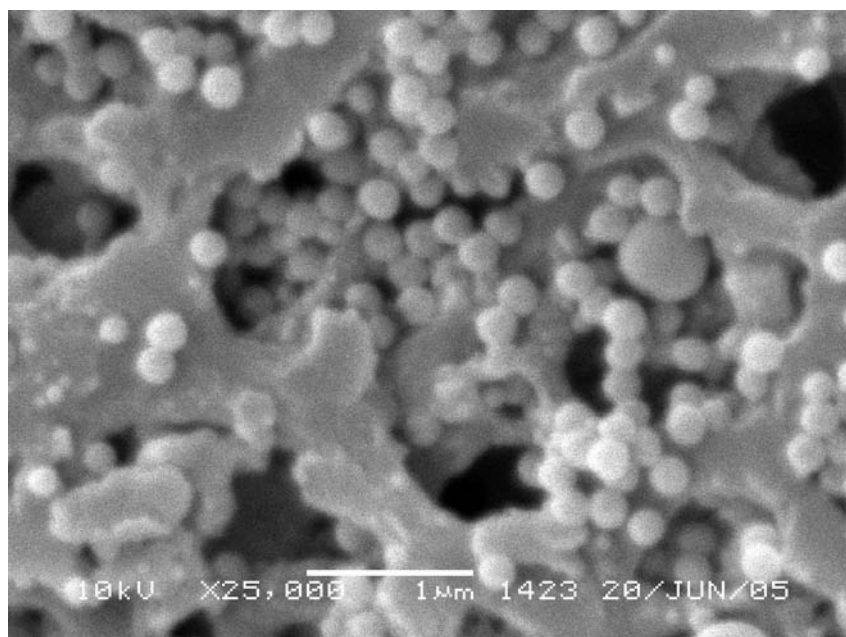


Figure 5: SEM photo after 30 minutes filtration of 0.1% 0.1 μm latex particles with 0.2 μm cellulose acetate membrane (top view). Cross flow velocity was 0.044 ms^{-1} and transmembrane pressure 2.0 kPa (Membrane Technology Group, University of Twente).

The coverage of the membrane surface by particles was quantified from the relative area that the colored particles occupy with image analysis software (fig. 6). Initially, the curves show a linear increase of deposited particles with the cumulative permeate-volume, indicating that a constant fraction of the convected particles

adsorbed to the membrane. At the third pressure step (1.5 kPa, 20 min), the polymer microsieve reached a maximum particle coverage that was 10 % of the total area. Further increase of the pressure did not increase the colored area, which probably means that particle deposition stopped and that still considerable area was available for permeation of particles (microsieve porosity 20 %). For the conventional polymer membrane, particle deposition continued to increase linearly with the cumulative permeate volume and a surface coverage of 13 % was reached at the end of the experiment but we expect that it would have gone higher if the experiment would have been continued.

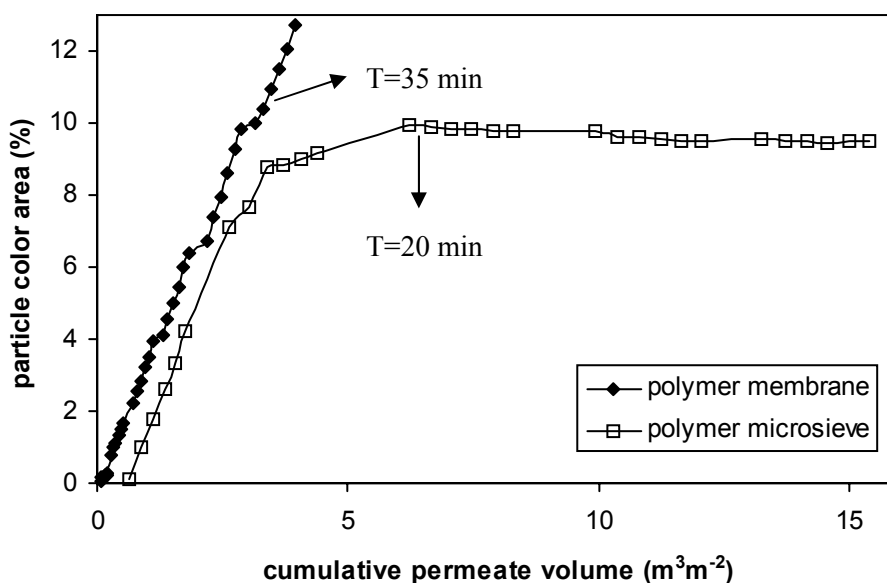


Figure 6: Relative colored area of 1.0 μm particles against the cumulative permeate volume during transmission experiments with 5.0 μm polymer microsieve and 3.0 μm polymer membrane under CSLM. Note that after every six points, the transmembrane pressure was increased according to figure 4.

Based on calculations, almost all particles were captured with the conventional membrane, which had very low particle transmission. At the end of the microsieve experiment, however, the presence of particles in the permeate was confirmed qualitatively by filtering a small amount of permeate through a 0.2 μm disposable filter and visual inspection with CSLM.

c) Effect of concentration on particle transmission in cross flow

Cross flow experiments with 0.1 % particle suspensions also showed four transmission regimes, as was the case in dead end filtration. However, the cross flow velocity affected the transmembrane pressures at which these transmission regimes

occurred. Depending on the cross flow velocity, regime 3 (see fig. 2) now showed time dependent or independent particle transmission (fig. 7a and 7b). At the right cross flow velocity, full transmission could be observed over time.

Clearly, transmission is governed by hydrodynamic and colloidal interaction forces. To obtain more insight in the deposition mechanism, the effect of higher particle concentrations was investigated.

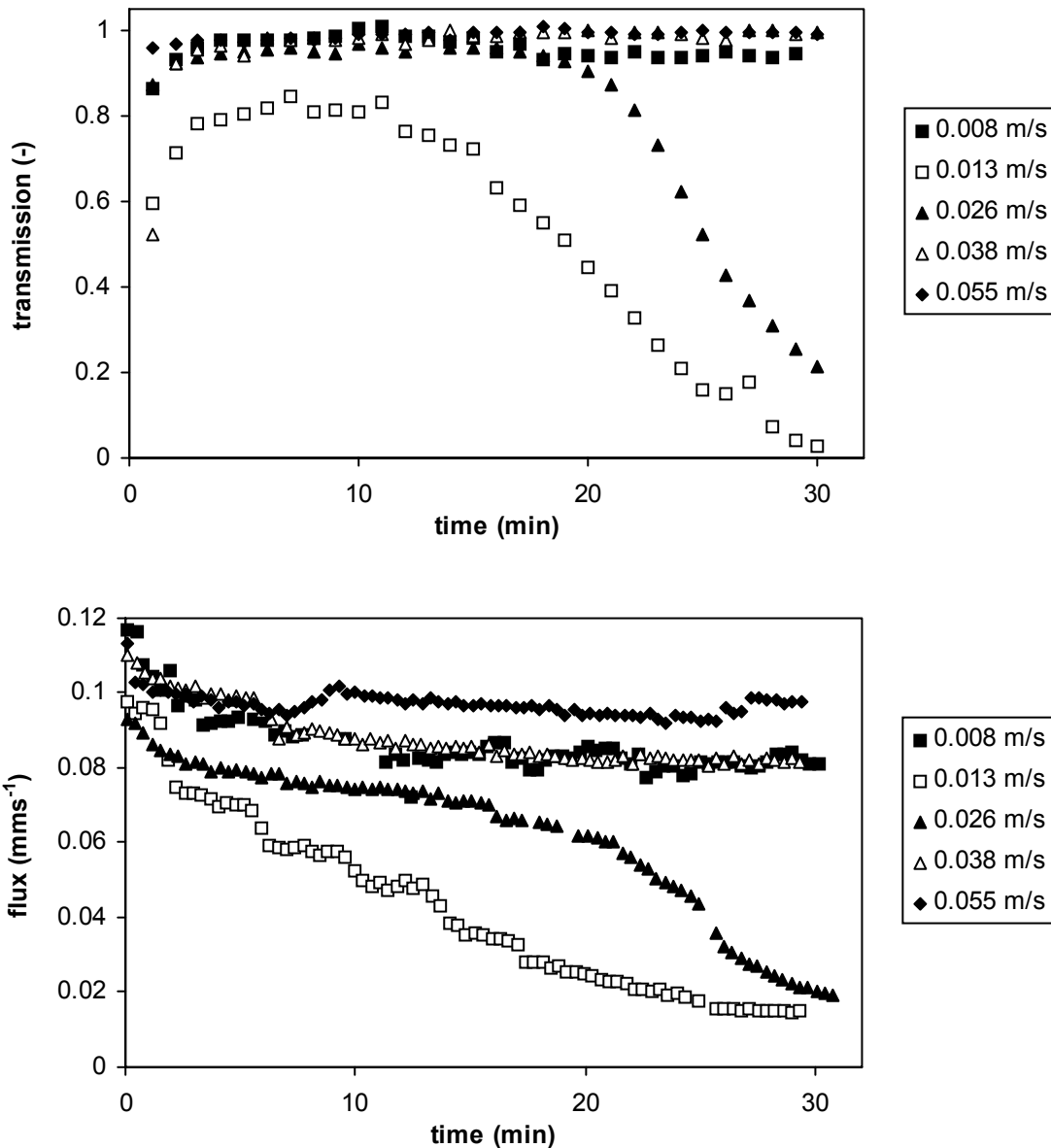


Figure 7a and 7b: The influence of the cross flow velocity on the flux and transmission of 0.1 µm latex particle suspension (0.1 %) with a 0.2 µm cellulose acetate membrane, at transmembrane pressure of 3.5 kPa.

The concentration of the 0.1 μm latex suspension was varied between 0.5 and 0.9 %. The transmembrane pressure and cross flow velocity were chosen such, that a 0.1 % particle suspension showed full transmission (3.0 kPa, 0.026 ms^{-1}).

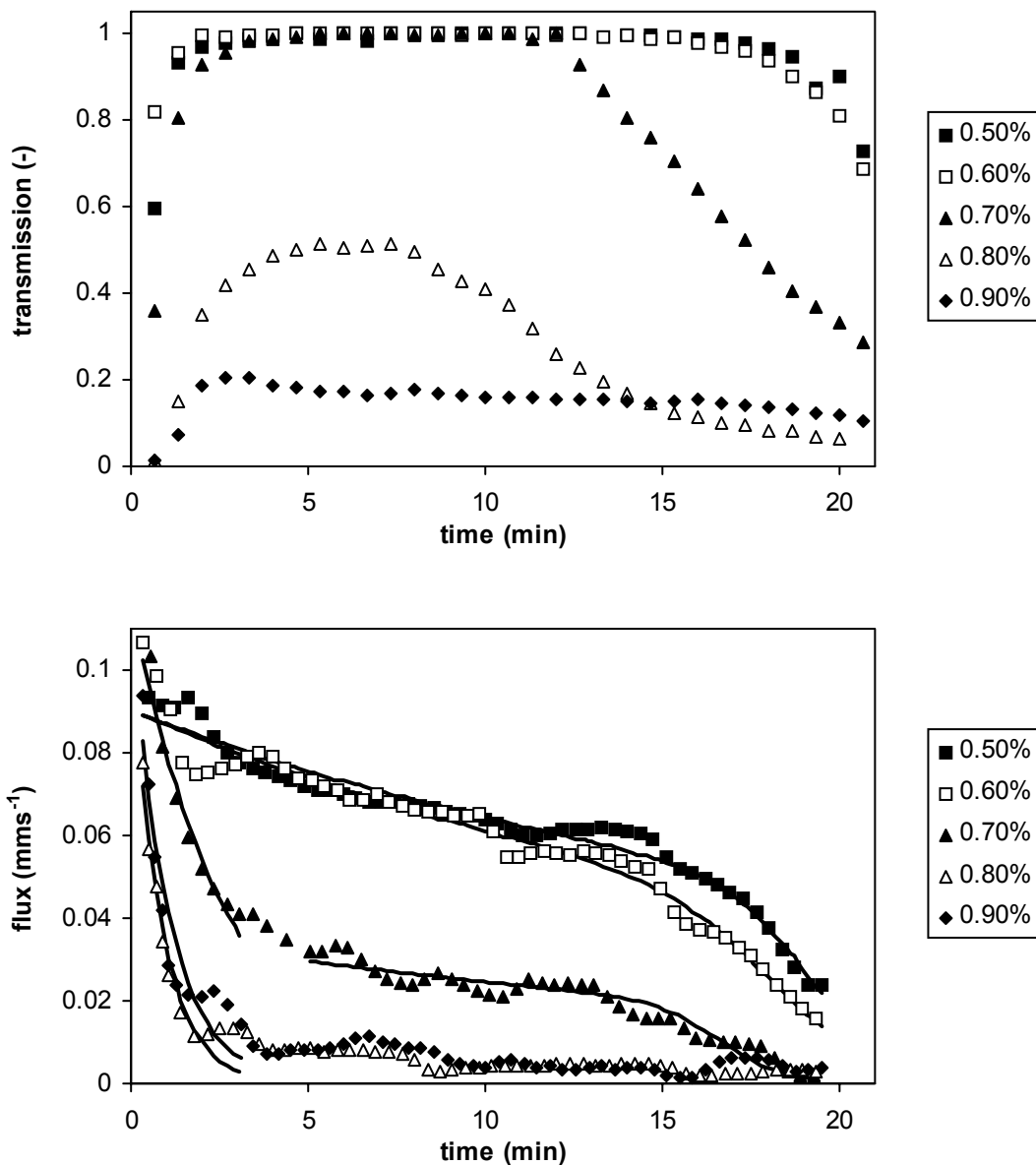


Figure 8a and 8b: The effect of particle concentration on the flux and transmission of particles in cross flow filtration of 0.1 μm latex particles with 0.2 μm polymer membrane. Cross flow velocity was 0.026 ms^{-1} and transmembrane pressure 3.0 kPa. Solid lines are fits with pore blocking model (first part 0.7 % and 0.8, 0.9 %) and combination of the pore blocking and standard filtration model in series (second part 0.7 % and 0.5, 0.6 %), after Tracey and Davis [7].

The feed suspension was recirculated and we took care that particle concentration in the feed never increased more than 10 %. Particle transmission and fluxes with

different concentrations are shown in figure 8a and 8b. The 0.8 and 0.9 % latex suspensions had low fluxes and transmission from the start, while the particle transmission of the 0.7 % suspension decreased after 11 minutes, and after 17 minutes for both 0.5 and 0.6 %. These observations are in line with Pandya *et al.* who described a similar concentration dependency for plugging of porous media [13]. They found that suspensions with low concentration had stable flux and full transmission. Above a critical concentration, blocking occurred after a lag time, which was shorter for higher concentrations.

Unlike the pressure regimes 2 to 4 in dead end filtration, where particle transmission decreased to zero, the transmission in cross flow reached a “steady state” value of around 0.1. Apparently, the cross flow makes particle deposition “dynamic” and induces backtransport, therewith allowing particles to pass the membrane to some extent.

The original flux curves were fitted with the models of Tracey and Davis (fig. 8b) [7]. The first three minutes of the 0.7, 0.8 and 0.9 % suspensions could be described well with the pore blocking model. After three minutes, the fluxes of the 0.8 and 0.9 % became constant. A combination of the pore blocking model and standard filtration model in series could describe the flux of the 0.7 % suspension after three minutes, and the flux of the 0.5 and 0.6 % suspensions during the whole filtration. The fluxes of the 0.5 and 0.6 % suspensions decreased gradually until 15 minutes. After that, a sharp decrease was observed, where the pore restrictions became effective (in-pore fouling). This indicates that for low concentrations the flux decrease is governed by particle deposition in the membrane, and for higher particle concentrations deposition takes place on the membrane surface (pore blocking by bridging).

To investigate the effect of particle concentration further, the flux is plotted against the number of accumulated particles (fig. 9). If the flux decrease would have been independent of the particle concentration, the initial slopes would coincide, therewith indicating a complete blocking mechanism. This is clearly not the case and the blocking rate increases more than proportional with the concentration, which indicates bridging. The 0.9 % suspension showed slightly less efficient blocking than 0.8 %, which might be due to a rapid initial flux decrease that could not be captured during the experiments.

d) Fractionation of bi-disperse particle suspensions in dead end

We investigated the effect of changing particle size ratio with constant particle volume fraction of small and large particles of 1:1 w/w (total concentration 0.082 %).

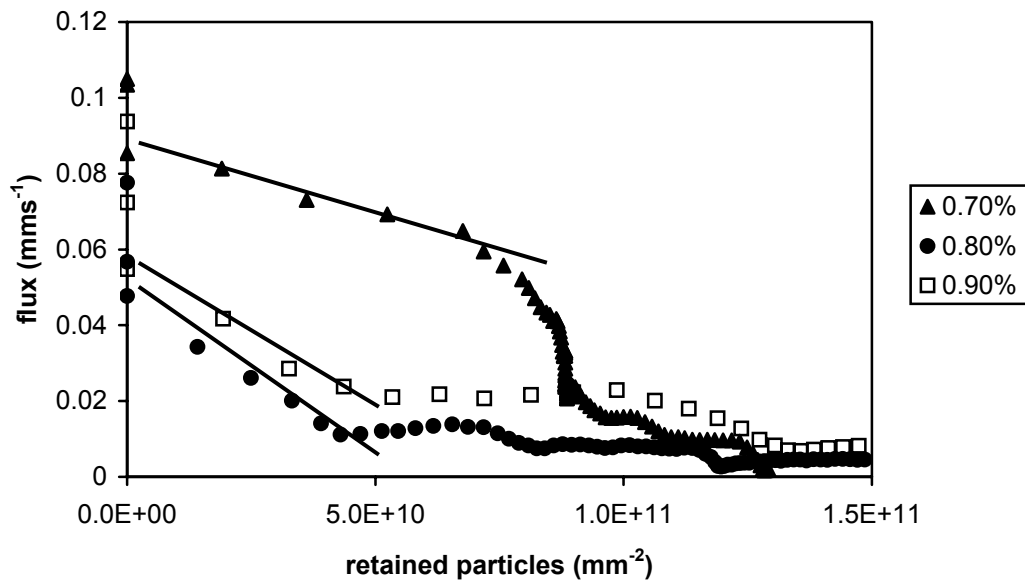


Figure 9: The effect of retained particles by the membrane on the flux in cross flow filtration of 0.1 μm latex particles with 0.2 μm polymer cellulose acetate membrane. The straight lines are fits with the pore blocking model in the first 3 minutes (same experiment as fig. 7).

Experiments were performed under conditions (transmembrane pressure and cross flow velocity) at which full transmission of the small particles was expected. In the fractionation experiments, 0.1 μm particles were separated from a larger co-particle with a diameter between 0.3 and 1.4 μm , using a 0.2 μm cellulose acetate membrane.

In figures 10a and 10b, fluxes and particle transmission are shown. Both the flux and transmission decrease in time for all particle size combinations. The bi-disperse suspensions of 1.4 and 0.1 μm , and 1.0 and 0.1 μm showed relatively high initial transmission, but for the bi-disperse suspensions of 0.6 and 0.1 μm , and 0.3 and 0.1 μm , transmission decreased rapidly. The large particles are retained by the membrane and form a cake layer, which in its turn affects the flux and transmission of small particles. It can be calculated that small particles need to be at least a size seven smaller to move through a bed of large particles, otherwise they will be captured.

Based on that, it was expected that the small particles were transmitted best in company of the largest particles, and this was the case. Transmission indeed decreased with decreasing co-particle size. Surprisingly, the fluxes did not show significantly different behavior.

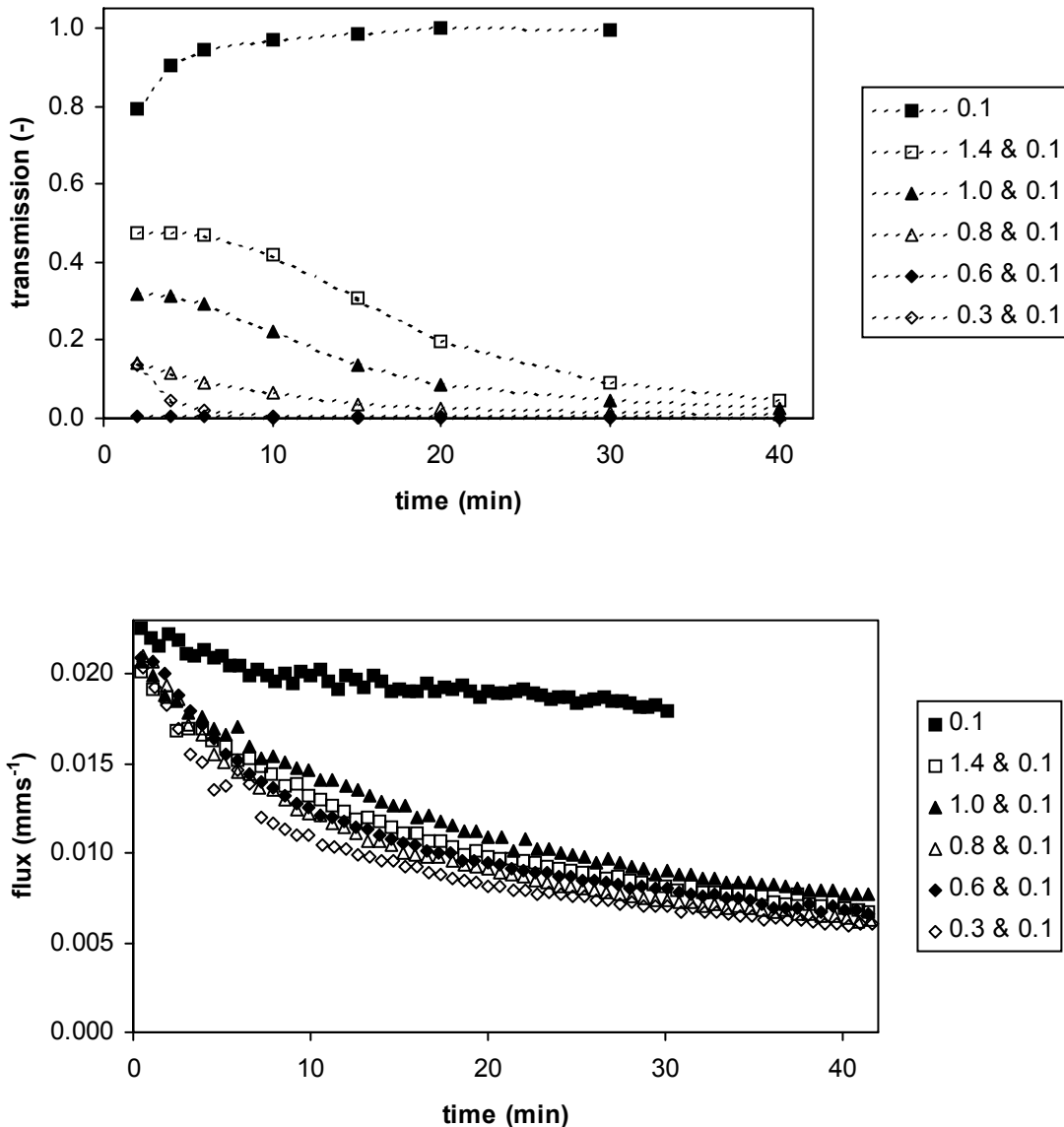


Figure 10a and 10b: The effect of particle size ratio on flux and transmission during dead end fractionation of bi-disperse latex particle suspensions. Transmembrane pressure was 0.7 kPa, total latex concentration 0.082 % of 0.1 μm and larger co-particle of 1.4, 1.0, 0.8, 0.6 and 0.3 μm with ratio 1:1 (w/w).

e) Fractionation of bi-disperse particle suspensions in cross flow

Similar to the dead end experiments, 0.1 μm particles were separated in cross flow mode from larger particles of size between 0.3 and 1.4 μm , at transmembrane pressure of 0.7 kPa. In figure 11a and 11b, the flux and transmission are depicted. The fluxes reach a steady value, despite the slight increase of the concentration of large particles due to recirculation of the feed (a maximum increase of 15 % was allowed). Unlike the dead end fractionation experiments where transmission

decreased to zero, the transmission reached a steady state value. As mentioned before, the cross flow promotes dynamic behavior of the cake layer, therewith enabling higher transmission and fluxes than in dead end filtration. Fluxes were higher than predicted with backtransport mechanisms [12], based on the large particles alone.

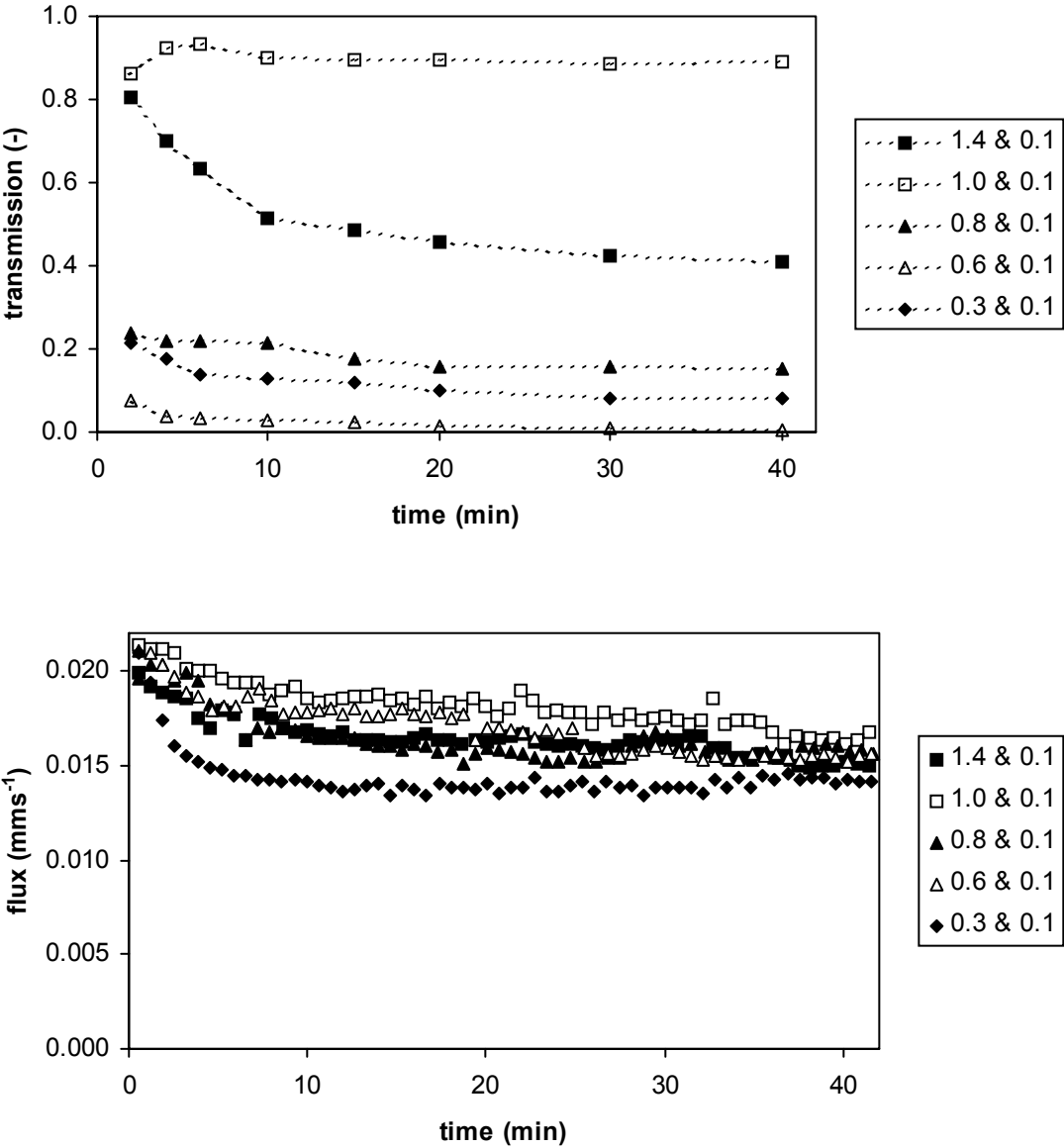


Figure 11a and 11b: The effect of particle size ratio on flux and transmission during cross flow fractionation of bi-disperse latex suspensions of 0.1 μm particles and larger co-particle with ratio 1:1 (w/w). Transmembrane pressure was 0.7 kPa, total latex concentration 0.082 %, cross flow velocity 0.074 ms^{-1} .

Fractionation of 1.0 and 0.1 μm particles gave the highest fluxes and almost full transmission (0.85), while the 1.4 and 0.1 μm suspension had a stable transmission around 0.45 (and a somewhat lower flux). It is thought that the presence of large particles near the membrane might explain the difference in transmission: since back transport by shear-induced diffusion of 1.4 μm particles is larger than for 1.0 μm particles, fewer particles will be present at the membrane surface for micro-mixing to ensure higher flux and transmission.

Transmission was almost negligible for the suspension with 0.6 and 0.1 μm particles. Apparently, this size combination leads to such a specific cake composition (size difference of six while seven is required for transmission) that transmission of small particles is hindered.

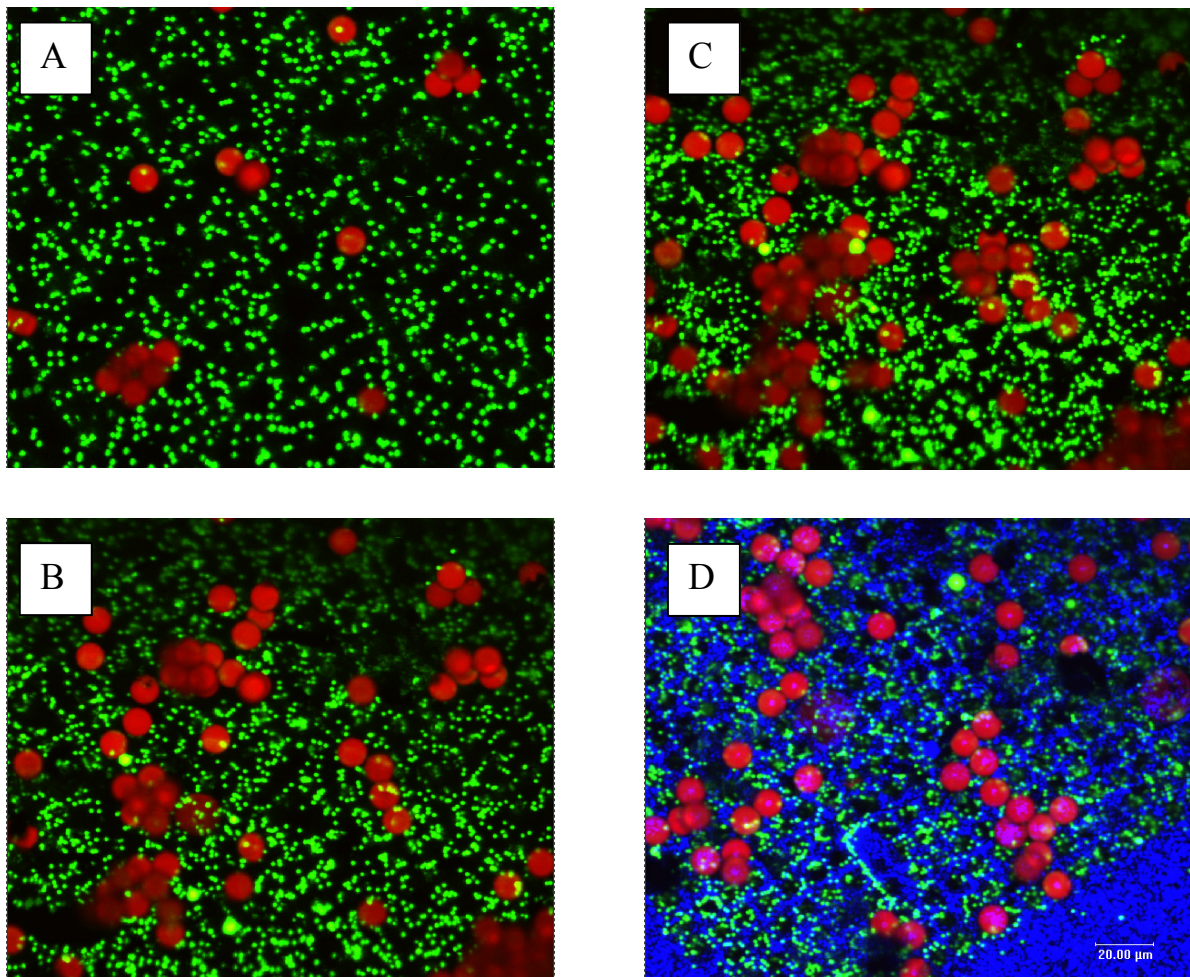


Figure 12: CSLM images of polymer microsieve during fractionation of bi-disperse suspension with $5.3 \cdot 10^{-7} \%$ 1.0 μm (green) and $2.3 \cdot 10^{-5} \%$ 9.7 μm particles (red). Snapshots A to C on $t = 6, 18$ and 30 min (without visualization of the microsieve), and D $t = 30$ min with microsieve on different location. The cross flow velocity was 0.047 ms^{-1} and the transmembrane pressure 0.55 kPa.

f) Particle deposition during fractionation of bi-disperse suspension in cross flow

Similar to the transmission experiments, particle deposition during fractionation of a bi-disperse suspension was monitored with CSLM. A suspension of $5.3 \cdot 10^{-7}$ % 1.0 μm green particles and $2.3 \cdot 10^{-5}$ % 9.7 μm red particles was fractionated with a 5.0 μm polymer microsieve at a transmembrane pressure of 0.55 kPa and a cross flow velocity of 0.047 ms^{-1} .

The CSLM images (fig. 12) indicate that both particle sizes deposited on the polymer microsieve, and particle deposition increased in time. The small green particles adsorbed to the pore edges and inside the pores, as seen previously for mono-disperse suspensions, and the large red particles deposited exactly on a pore. The presence of large particles near the membrane indicates that both particle sizes are involved in pore blocking and cake formation during particle fractionation.

g) Fractionation of tri-disperse particle suspensions in cross flow

In reality, feed suspensions often contain multiple components that need to be separated into multiple fractionations. This introduces two new variables: firstly the effect of poly-dispersity on both the flux and transmission of particles through the membrane, and secondly the order of separation.

To investigate the fractionation of a poly-disperse suspension, fractionation experiments were performed with a tri-disperse latex suspension, consisting of 0.1, 1.0 and 10 μm latex particles in equal volume fraction (1:1:1 w/w), using membranes of 0.2 μm and 3.0 μm under optimized process conditions (transmembrane pressure, cross flow velocity).

The flux of a mono-disperse 0.1 μm suspension through the 0.2 μm membrane was equal to the clean water flux and had almost full particle transmission (between 0.8 and 0.9, fig. 13a). The direct separation of 0.1 μm particles from the tri-disperse suspension with the 0.2 μm membrane gave a higher flux than the separation of 0.1 μm particles from a bi-disperse 0.1 and 1.4 μm suspension (fig. 13b). This could be explained by shear-induced migration of large particles towards the center of the cross flow channel, which promotes the transmission of small particles through the membrane [14].

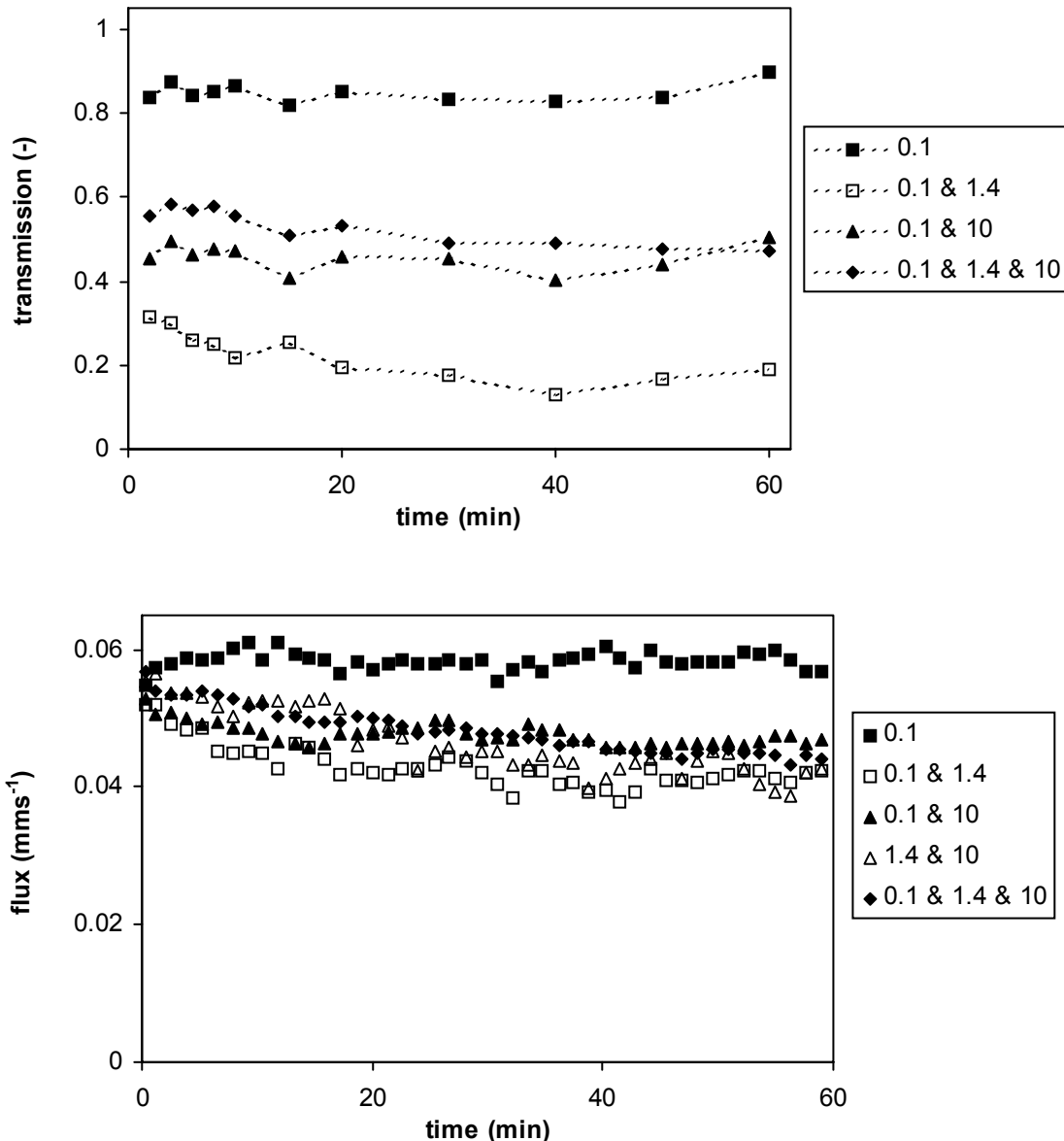


Figure 13a and 13b: Fluxes and particle transmission during filtration of different particle composition (0.1, 1.4 and 10 μm) with a 0.2 μm cellulose acetate membrane. Concentration was 0.0042 % for each particle size, ratio 1:1:1 w/w, transmembrane pressure was 2.0 kPa, and cross flow velocity 0.032 ms^{-1} .

The addition of 1.4 μm particles to a bi-disperse suspension of 0.1 and 10 μm particles did not affect flux and transmission, while the 0.1 and 1.4 μm bi-disperse suspension had the lowest flux and transmission (0.2). Fluxes and transmission with a 3.0 μm membrane are shown in figure 14a and 14b.

Please note, that only the concentration of a mono-disperse suspension could be measured in the permeate. Filtration of a mono-disperse 0.1 μm suspension with the 3.0 μm membrane resulted in a flux similar to the clean water flux and full particle

transmission. Although process conditions were optimized for the transmission of 1.4 μm particles, the transmission was 0.6 at most and the flux was only 50% of the clean water flux. The addition of 0.1 μm particles to a bi-disperse suspension of 1.4 and 10 μm particles caused faster initial flux decrease, probably because of enhanced particle interactions with the membrane. This implies, that the order in which particles are fractionated are an essential ingredient for design of a fractionation stack.

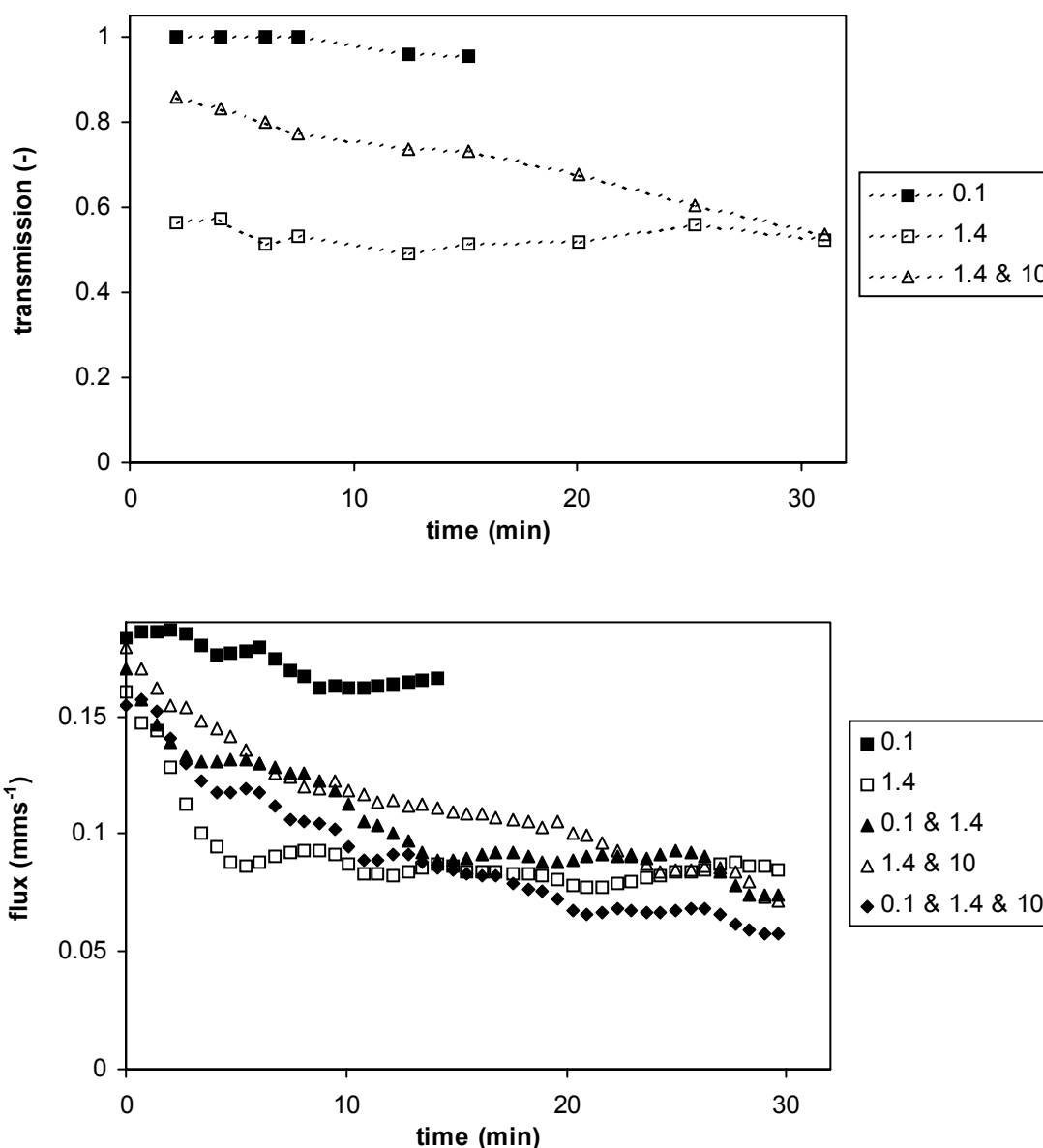


Figure 14a and 14b: Fluxes and particle transmission during filtration of different particle composition (0.1, 1.4 and 10 μm) with a 3.0 μm cellulose acetate-nitrate membrane. Concentration was 0.0042 % for each particle size, ratio 1:1:1 w/w, transmembrane pressure was 0.7 kPa, and cross flow velocity 0.049 ms^{-1} .

Conclusion

Fractionation of poly-disperse particle suspensions is not a trivial problem. Transmission of small particles in dead end filtration showed four transmission regimes depending on the transmembrane pressure, indicating that both colloidal interactions and hydrodynamic forces are involved.

Application of cross flow velocity strongly influenced these transmission regimes, but they could still be discerned. Membrane morphology was found to play a role in particle deposition, as was visualized with SEM and CSLM. Polymer membranes showed depth fouling, while microsieves had in-pore fouling. Higher particle concentrations were found to increase the risk of pore blocking by bridging.

For fractionation, a suitable combination of transmembrane pressure and cross flow velocity should be applied, which ensures full particle transmission, while keeping the larger particles away from the membrane. Especially for small particle size ratios, both particle sizes interact with the membrane, leading to decreasing flux and transmission. Therefore, periodic removal of deposits seems inevitable.

Clearly, more research is needed on the selective membrane separation of poly-disperse particle suspensions. Membranes with a narrow pore size distribution and minimal particle adsorption, such as microsieves, seem most suited for high-demanding separations.

Acknowledgements

We would like to acknowledge the support of the Dutch foundation of Economy, Ecology and Technology (EETK20033). Further, we like to thank the D-force project team (Friesland Foods BV, Aquamarijn microfiltration BV and the Membrane Technology Group, University of Twente) for interesting discussions. We are grateful to Míriam Girones of the Membrane Technology Group (University of Twente) for kindly providing the polymer microsieves. Anno Koning of Friesland Foods BV is greatly acknowledged for performing the CSLM measurements. Martijn Terlingen, Emmanuel Boussion and Zhang Chun Ya are thanked for experimental work.

References

- [1] G. Brans, C.G.P.H. Schroën, R.G.M. van der Sman, R.M. Boom, Membrane fractionation of milk: state of the art and challenges. *J. Membrane Sci.*, 243 (2004) 263.

-
- [2] P. Apel, Track etching technique in membrane technology. *Radiation Measurements* 34 (2001) 559.
- [3] C.J.M. van Rijn, M.C. Elwenspoek, Micro filtration membrane sieve with silicon micro machining for industrial and biomedical applications, *Micro Electro Mechanical Systems (MEMS)* (1995) 83, Amsterdam, the Netherlands.
- [4] A.J. Bromley, R.G. Holdich, I.W. Cumming, Particulate fouling of surface microfilters with slotted and circular pore geometry. *J. Membrane Sci.*, 196 (2002) 27.
- [5] V. Ramachandran, H.S. Fogler, Plugging by hydrodynamic bridging during flow of stable colloidal particles within cylindrical pores. *J. Fluid Mech.* 385 (1999) 129.
- [6] E. Iritani, Y. Mukar, Y. Toyoda, Properties of a filter cake formed in dead-end microfiltration of binary particulate mixtures. *J. Chem. Eng. Japan* 35 (2002) 226.
- [7] E.M. Tracey, R.H. Davis, Protein fouling of track-etched polycarbonate microfiltration membranes. *J. Colloid Interface Sci.* 167 (1994)
- [8] J. W. Goodwin, J. Hearn, C.C. Ho, R.H. Ottewill, Studies on the preparation and characterization of monodisperse polystyrene lattices. III preparation without added surface active agents. *Colloid and Polymer Sci.* 252 (1974) 464.
- [9] C.J.M. van Rijn, L. Vogelaar, W. Nijdam, J.N. Barsema, M. Wessling, Method of making a product with a micro or nano size structure. WO0243937 (2002).
- [10] V. Ramachandran, R. Venkatesam, G. Tryggvason, H.S. Fogler, Low Reynolds number interactions between colloidal particles near the entrance to a cylindrical pore. *J. Colloid Interface Sci.* 229 (2000) 311.
- [11] M.J. Biggs, S.J. Humby, A. Buts, U. Tüzün, Explicit numerical simulation of suspension flow with deposition in porous media: influence of local flow field variation on deposition processes predicted by trajectory methods. *Chem. Eng. Sci.* 58 (2003) 1271.
- [12] G. Belfort, R.H. Davis, A.L. Zydney, The behavior of suspensions and macromolecular solutions in crossflow filtration. *J. Membrane Sci.* 96 (1994) 1.
- [13] V.B. Pandya, S. Bhuniya, K.C. Khilar, Existence of a critical particle concentration in plugging of a packed bed. *AIChE Journal* 44 (1998) 978.
- [14] J. Kromkamp, F. Faber, K. Schroën, R. van der Sman, R. Boom, Effects of particle size segregation on crossflow microfiltration performance. In press *J. Membrane Sci.* (2005).

Chapter 6: A suspension flow model for hydrodynamics and concentration polarization in cross flow microfiltration¹

Abstract

A new computer simulation model is proposed for suspension flow in microfiltration systems. In this model, the diffusion of the suspended micro particles is governed by the mechanism of shear-induced migration. Using a continuum Euler-Euler approach, hydrodynamics and convection-diffusion are simultaneously resolved according to the lattice Boltzmann method. The new suspension flow model allows the complete solution of the flow field (including calculation of the actual local shear rate) in systems with complex geometries and the application of a pressure gradient over the feed flow channel as well as over the membrane. The cake layer dimensions and permeability are explicitly taken into account.

For a simple cross-flow system, a comparison is made between the new suspension flow model and existing models. The more realistic approach of the suspension flow model is found to be especially significant for the calculation of the cake layer profile at the beginning and the end of the membrane. Also the effect of narrowing of the flow channel by cake formation on the suspension flow pattern (at a constant pressure gradient over the flow channel) is more realistically predicted. Finally, some examples are presented of the concentration polarization and cake layer formation in microfiltration systems with more complex geometries.

The newly developed suspension flow model has generic applicability as a design tool for microfiltration membranes, systems and processes. Extensions of the model to three-dimensional systems (including large parallel computations), as well as adaptations of the diffusion model to anisotropic diffusivity can be relatively easily achieved.

¹ This chapter is published as: J. Kromkamp, A. Bastiaanse, J. Swarts, G. Brans, R.G.M. van der Smán, R.M. Boom, *Journal of Membrane Science* 253 (2005) 67.

Introduction

The performance of microfiltration processes is in general mainly determined by concentration polarization, which arises from the simultaneous transport of non-permeable species towards and back from the membrane surface. Modelling of flow and concentration polarization in microfiltration systems is already often put forward as an important tool to help understand and optimize these systems. Although numerous filtration models of varying degrees of complexity and simplification have appeared in literature, most of them do not apply for microfiltration, due to the different diffusion mechanism in particulate suspensions as compared to molecular solutions.

As has been identified by Belfort and others [1], for particulate suspensions with particle sizes between 0.5 and 30 μm , shear-induced diffusion can often be considered the relevant back-transport mechanism in the concentration polarization process. Other back-transport mechanisms are Brownian diffusion and inertial lift, which are respectively dominant for particle sizes smaller than 0.5 μm and larger than 30 μm . This paper addresses modelling of flow and concentration polarization in the shear-induced diffusive regime. Shear-induced diffusion, also called hydrodynamic diffusion, is a transport mechanism that is caused by hydrodynamic particle interactions in a suspension in shear flow. Excluded volume effects can then lead to particle displacements. In contrast to inertial lift, which is only relevant in the regime where the Reynolds number based on the particle size is not negligible, shear-induced diffusion occurs in the slow laminar flow regime as well. A general property of shear-induced diffusion is that it increases proportionally with the shear rate.

About two decades ago, shear-induced diffusion was first introduced in relation to microfiltration theory by Zydney and Colton [2]. Their concentration polarization model is based upon the classical L  v  que solution for mass transfer in which they replaced the Stokes-Einstein diffusivity with the shear-induced diffusivity, as determined from experimental data of Eckstein and others [3]. In the same year as Zydney and Colton, Davis and Leighton presented a model that describes the transport of a concentrated layer of particles along a porous wall under laminar flow conditions [4]. In this model, shear-induced diffusion accounts for the lateral migration of particles away from the porous wall. Instead of the approximate fit to the data of Eckstein and others, Davis and Leighton applied data of Leighton and Acrivos [5] for shear-induced diffusion, which were about 25 times greater and were shown to better describe the viscous resuspension of a settled layer of rigid particles in shear flow.

Romero and Davis extended the model of Davis and Leighton from a local treatment of the particle layer to a global model of cross flow microfiltration [6]. This global model is able to predict the axial dependence of the permeate flux and the thickness of the concentrated particle layer under steady or quasi-steady operation. The model also describes under which conditions a stagnant layer of packed particles exists beneath the flowing layer. In a following step, the global model was converted into a transient model, which not only describes the steady-state behavior but also the time-dependent decline of the permeate flux due to particle layer buildup [7].

In the aforementioned models, particle convection parallel to the membrane walls was ignored. As a consequence, the models are only valid for very small particle volume fractions in the bulk of the suspension Φ_b . Davis and Sherwood overcame this limitation in their similarity solution for cross flow microfiltration under conditions where the stagnant particle layer provides the controlling resistance to flow [8]. In their solution, the stagnant particle layer grows like $x^{1/3}$, where x denotes the dimensionless distance from the filter entrance. Their solution is however only valid in the situation that the critical length needed for the stagnant layer to form is much smaller than the filter length. Pelekasis developed a model which does not have this limitation [9], although his solution is only valid in situations where the permeate flux can be considered constant over the membrane length. This model is valid over a wide range of bulk particle concentrations. It is shown that in the limit where the particle volume fraction in the bulk suspension approaches zero, the model of Davis and Leighton is recovered.

All the abovementioned models have in common that they assume the bulk flow to be fully developed Poiseuille flow with a time-independent flow rate. This is valid for a straight flow channel, when the permeate velocity is much smaller than the average downchannel velocity of the suspension and when the stagnant layer is much thinner than half the channel width. These conditions are often not met in reality. First of all, the flow channel may deviate from perfectly circular or rectangular, e.g. when turbulence promoters are present. Secondly, when suspensions are filtered with particles that have a relatively low cake resistance, the cake layer height can become significant compared to the channel half width. Poiseuille flow can still be considered present when the cake layer height does not vary much along the filter length (and the actual flow velocity profile can be adapted to the actual channel height). The flow pattern can however easily deviate from Poiseuille flow when the cake layer height strongly varies along the filter length, such as at the beginning and at the end of the filter. Thirdly, the flow pattern can also be time-dependent, such as when oscillating cross-flow or backpulsing is applied. One should moreover realize that, in contrast to

Brownian diffusion, shear-induced diffusion depends linearly on the shear rate. Local deviations of the flow field from Poiseuille flow will therefore have a large influence on the local morphology of the flowing and stagnant particle layer.

This indicates that a more generic model with broad applicability to membrane systems requires an accurate, more detailed solution of the fluid flow field. This is possible with Computational Fluid Dynamics (CFD). So far, this technique is not often applied to membrane systems. Recently, Wiley and Fletcher successfully developed a generic CFD model that incorporates the flow across the membrane wall. In their article, they also reviewed earlier attempts in this field, which in general lead to less generic solutions than their model [10]. Another recent approach is that of Richardson and Nassehi [11]. These authors developed a finite element model for the solution of concentration profiles in flow domains with curved porous boundaries. Although both models may be extensible to modelling of concentration polarization in microfiltration processes, with shear-induced diffusion as back-transport mechanism and with cake layer formation, up to now no results on this subject have been reported.

The present work is directed at the development of a CFD model for flow and concentration polarization in microfiltration systems with shear-induced diffusion as back-transport mechanism. We apply the lattice Boltzmann (LB) method for this aim, which is based on kinetic theory, the physical theory describing the dynamics of large systems of particles. The LB method, being a discrete version of the Boltzmann equation, is in special cases identical to the finite volume scheme as used by Wiley and Fletcher [10]. Both methods can be applied for laminar as well as turbulent flows. The LB method may however have some advantages when compared to other finite difference schemes. Complex geometries can be quickly set-up and easily used in the LB method, while in other methods, the use of complex geometries is a major issue. The LB method is also very convenient for systems with moving boundaries and multiphase systems such as fluid flow with suspended particles. In the present work, this may be relevant for the simulation of rapidly growing, flowing and stagnant layers. Finally, LB schemes can be very easily implemented on a parallel computer, which facilitates computations of large systems.

Although the LB simulations can be easily carried out in three dimensions, as a first step, the present work presents results on two-dimensional (2D) systems. In order to validate the model, the simulation results are compared with results of approximate models when appropriate. Hereafter, the effects of some variations in the geometry on the flowing and stagnant particle layers and the resulting flux will be shown.

Computer simulation method

The suspension flow model is based on an Euler-Euler description of the system, in which both the hydrodynamics and the suspension flow are completely resolved. The hydrodynamics are calculated according to the continuity and Navier-Stokes (NS) equations:

$$\frac{\partial \rho}{\partial t} = \nabla \cdot \rho u, \quad \frac{\partial \rho u}{\partial t} + u \cdot \nabla \rho u = -\nabla p + \nu \nabla^2 \rho u + F \quad [1]$$

where $-\nabla p$ is the pressure gradient and F is the body force. The LB method solves the NS equation for weakly compressible conditions, therewith behaving as a pseudo-compressible scheme [12]. An advantage of this approach is that the Poisson equation does not need to be solved for the pressure. For the calculation of the NS equation, the kinematic viscosity ν ($= \eta/\rho$, with η representing the dynamic viscosity) of the fluid needs to be known. In our suspension flow model, we took into account that the viscosity η depends on the local concentration of suspended micro particles. Hereto, a model is used that is also applied by Romero and Davis [6]:

$$\eta(\Phi) = \eta_0 \left[1 + 1.5 \frac{\Phi}{1 - (\Phi/0.6)} \right]^2 \quad [2]$$

where Φ represents the particle volume fraction and η_0 the viscosity of the particle free medium. In our suspension flow model, the feed for the microfiltration process consists of a particulate suspension with particles of a size between 0.5 and 30 μm . These suspended particles are described as a component that is continuously distributed in the fluid. Their distribution over the system is calculated according to the convection-diffusion equation:

$$\frac{\partial \Phi}{\partial t} + u \cdot \nabla \Phi = D \nabla^2 \Phi \quad [3]$$

The velocity field u is calculated according to the NS equation. In our simulations, the diffusion coefficient D represents the shear-induced diffusion coefficient, following the shear-induced migration model of Leighton and Acrivos [5, 6]:

$$D = 0.33 \gamma a^2 \Phi^2 (1 + 0.5 e^{8.8\Phi}) \quad [4]$$

where $\dot{\gamma}$ is the shear rate and a is the radius of the suspended particles. Both the viscosity η and the shear-induced diffusivity D are treated as time and location dependent variables in our suspension flow model. In order to resolve the NS equation as well as the convection-diffusion equation the LB method is followed, which is explained in the next two paragraphs.

For a general introduction to the LB method, we refer to Succi [13]. In this article, we will explain relevant aspects of our method, without going into much detail. Hydrodynamics and convection-diffusion were solved with two separate LB schemes. Here, we will first introduce the LB method for the case of hydrodynamics. The LB method discretizes kinetic theory by collecting fluid mass in discrete lattice gas particles, locating these particles on points of a regular lattice and moving the particles according to a finite, discrete set of velocities, taking them to adjacent lattice points. As a consequence of this discretization procedure space, time and particle velocity are discrete variables. Physical quantities are represented by moments of a particle distribution function, in contrast to finite volume schemes, where physical quantities are represented by continuous fields. The lattice gas particles behave like real particles: they move and collide on the lattice. Collision occurs when particles encounter each other at a lattice point. After collision they move to adjacent lattice points. If this is done within the constraints of physical conservation laws and with a lattice with sufficient symmetry, real physical phenomena can be modelled this way. In analogy with the Boltzmann equation of the classical kinetic theory, the state of the particles on a lattice point is characterized by the particle distribution function $f_i(x,t)$, describing the average number of particles at a particular node of the lattice x , at a time t , with the discrete velocity c_i , which brings the particles in one time step to an adjacent lattice node. In the simulations described in this paper, the hydrodynamics were solved with a D2Q9 LB scheme, which is defined on a 2D square lattice with rest particles and 8 non-zero particle velocities. The velocity directions link lattice sites to its nearest and next-nearest neighbors. The velocity vectors on this 2D lattice are defined as:

$$\begin{aligned}
 \mathbf{c}_i = & \quad (0,0) & \quad i=0 \\
 & \left(\cos \frac{i-1}{2} \pi, \sin \frac{i-1}{2} \pi \right) & \quad i=1..4 \\
 & \sqrt{2} \left(\cos \frac{i-0.5}{2} \pi, \sin \frac{i-0.5}{2} \pi \right) & \quad i=5..8
 \end{aligned} \tag{5}$$

The particle distribution function contains information on physical properties of the fluid. The hydrodynamic field's mass density ρ , momentum density j , and the momentum flux density Π , being identical to the field's in the NS equation, are moments of this velocity distribution:

$$\rho = \sum_i f_i, \quad j = \sum_i f_i c_i, \quad \Pi = \sum_i f_i c_i c_i = \rho c_{sf}^2 I + \rho uu = pI + \rho uu \quad [6]$$

The lattice gas particles evolve by collisions and subsequent propagation to neighboring lattice sites. This two-step process is described by the following equations:

$$f'_i(x, t) = f_i(x, t) - \frac{f_i(x, t) - f_i^{eq}(x, t)}{\tau_f} + \frac{c_{i\alpha} F_\alpha}{c_{sf}^2} \quad [7]$$

$$f_i(x + \Delta x_i, t + \Delta t) = f'_i(x, t) \quad [8]$$

Here $f'_i(x, t)$ is the post-collisional distribution function. The lattice spacing is defined as $\Delta x_i = c_i \Delta t$. F is the body force, and the speed of sound c_{sf} is defined by $c_{sf}^2 = c^2/3$. In our simulations, we applied the BGK model [14, 15], which is a simplification of the full LB model. In this BGK model, the distribution functions are simply relaxed at each time step towards the local equilibrium distribution $f_i^{eq}(x, t)$ with the relaxation time τ_f . This relaxation time controls the relaxation of the viscous stress in the fluid and is linked to the kinematic viscosity ν via:

$$\nu = c_{sf}^2 (\tau_f - 0.5) \Delta t \quad [9]$$

In our simulations τ_f , and therewith the kinematic viscosity ν ($= \eta/\rho$) of the fluid on each lattice point was dependent on the local particle concentration, according to equation 2. The equilibrium distribution $f_i^{eq}(x, t)$ is chosen such that the weakly compressible NS equations (eq. 1) are obtained [16]. It can be expressed as a series expansion in powers of the flow velocity u :

$$f_i^{eq} = \rho w_i \left(1 + \frac{u \cdot c_i}{c_{sf}^2} + \frac{\overline{uu} : c_i c_i}{2c_{sf}^4} - \frac{u^2}{2c_{sf}^2} \right) \quad [10]$$

where \overline{uu} is the traceless part of uu , and the double dot product is defined as $A:B = \sum_{\alpha,\beta} A_{\alpha\beta} B_{\beta\alpha}$. The weight factors are given by $w_0=4/9$, $w_1=w_2=w_3=w_4=1/9$ and $w_5=w_6=w_7=w_8=1/36$.

The computation scheme for convection-diffusion has a strong analogy with the scheme for hydrodynamics. The particle distribution function $g_i(x,t)$ now contains information on physical properties of the diffusive component, in our case the suspended particles. For reasons of clarity, we will refer to fluid particles for the lattice gas particles in the hydrodynamics scheme and to suspended particles for the lattice gas particles in the convection-diffusion scheme. The relevant continuum field derived from the latter scheme represents the concentration of suspended particles Φ :

$$\Phi = \sum_i g_i \quad [11]$$

The relaxation parameter in the collision operator of the convection-diffusion scheme is not related to the kinematic viscosity ν but to the diffusion coefficient D :

$$D = c_{sg}^2 (\tau_g - 0.5) \Delta t \quad [12]$$

Here, the speed of sound c_{sg} is also defined by $c_{sg}^2 = c^2/3$. In our simulations, this diffusion coefficient D represents the shear-induced diffusion coefficient, according to the shear-induced migration model of Leighton and Acrivos [5], which is given by equation 4. Since the diffusion coefficient is dependent on the time and location dependent variables $\dot{\gamma}$ and Φ , it is recalculated every time step at every lattice point. The shear rate $\dot{\gamma}$ is calculated from the diagonal vectors of the non-equilibrium part of the distribution function according to [17]:

$$-c_{sf}^2 \rho \dot{\gamma} \tau_{sf} = \sum_{i=0}^{i=8} c_{i,x} c_{i,y} (f_i - f_i^{eq}) \quad [13]$$

Because we considered the diffusion to be isotropic, the absolute value for $\dot{\gamma}$ was used for the calculation of the shear-induced diffusivity D . More recent investigations have shown that shear-induced diffusion is not an isotropic process, but that the diffusivity depends on the direction relative to the shear field [18, 19]. Moreover, improved models have become available for shear-induced migration [20]. Our model

can be easily adapted to implement such modifications of the shear-induced diffusivity models. We do however not expect that taking into account anisotropy will have a large effect, since convection is strongly dominant along the flow lines.

Typical for the LB scheme is that the resulting finite difference equation for the evolution of Φ is identical to the Lax-Wendroff (LW) finite volume scheme in case of $\tau_g=1$ [21]. Both the LW and the LB scheme automatically correct for numerical diffusion, for the LB scheme as a consequence of the constraints for the equilibrium distribution. If $\tau_g \neq 1$, spurious oscillations, which are present in the LW scheme, are damped in the LB scheme. The LB scheme therewith behaves like a third order accurate scheme (for $\tau_g \neq 1$) [21].

In order to have stable calculations, stability criteria have to be met. In the hydrodynamics scheme, the grid Courant number Cr , which is a measure for the relative flow velocity on the grid, should meet the following condition:

$$Cr = \frac{u\Delta t}{\Delta x} < 1 \quad [14]$$

Also the compression of the medium should be sufficiently small, such that the Mach number Ma :

$$Ma = \frac{u}{c_{sf}} \ll 1 \quad [15]$$

The abovementioned conditions are met by a proper choice of the model parameters in our system. For the convection-diffusion scheme, the criteria for the diffusivity need some more attention because of the variation of the diffusivity with the shear rate and the concentration of suspended particles. The Fourier number Fo^* is a measure for the diffusion velocity on the grid:

$$Fo^* = \frac{D\Delta t}{\Delta x^2} \leq 0.5 \quad [16]$$

We have chosen our model parameters such that even when D is maximal in our system, this condition is met. Also the ratio between convection and diffusion is subjected to a stability condition. The timescale of diffusivity needs to be sufficiently fast compared to convection, which is reflected in the grid Peclet number Pe^* :

$$Pe^* = \frac{u\Delta x}{D} \leq 25 \quad [17]$$

Because the LB method behaves as a third order accurate scheme, the limiting value can be higher than the common value of 2. We have estimated the value of 25 ourselves by carrying out simulations with different maximal values for Pe^* . When $Pe^* > 25$, spurious oscillations were sometimes found, leading to anomalous results. Because of its dependency on the shear rate and the concentration of suspended particles, the shear-induced diffusivity D can strongly vary in our system. In order to meet the condition for Pe^* , the value of Pe^* was calculated at every time-step and at every node of the lattice. When the condition $Pe^* < 25$ was not met, the diffusivity was locally adjusted such that $Pe^* = 25$. The consequence is that D cannot become zero (as e.g. in the center of the flow channel, where the shear rate is equal to zero), but has a certain minimum limit, depending on the actual flow velocity u . When u is relatively high, such as in the center of the flow channel, the minimum limit for D is also high. In our system, the maximal flow velocity in the channel and therewith the shear rate at the wall was so high, that D did not need to be adjusted in the largest part of the concentration polarization layer. Only in the center area of the flow channel with relatively high flow velocity and where the concentration of suspended particles Φ was lower than about 0.10, might the diffusivity be set slightly higher than according to the shear-induced migration model. The effect of this correction on the simulation results was however found to be negligibly small.

In figure 1, the geometry of the microfiltration system is depicted. Its geometry and dimensions are inspired on the newly emerging class of micro-engineered membranes, called microsieves [22]. The feed side consists of a rectangular flow channel with a length L of 90 μm and a height $2H_0$ of 36 μm . A cross-flow is induced by a pressure gradient $(p_{in}-p_{out})/L$ over the channel of 3.0 Pa μm^{-1} , which results in $U_0=0.32 \text{ ms}^{-1}$ and $\dot{\gamma}_{wall,0}=54000 \text{ s}^{-1}$. The permeate side consists of a rectangular box with a width L of 90 μm and a height H_p of 2.4 μm . At the wall underneath the membrane, a constant pressure is applied, such that the average TMP was 1780 Pa. The feed and the permeate side are separated from each other by a wall with a thickness δ_m of 1.2 μm . From the flow inlet side (left) up to the flow outlet side (right), this wall consecutively consists of 15 μm solid wall, 45 μm membrane (L_m) and 30 μm solid wall. The membrane resistance R_m was $1.62 \cdot 10^8 \text{ m}^{-1}$.

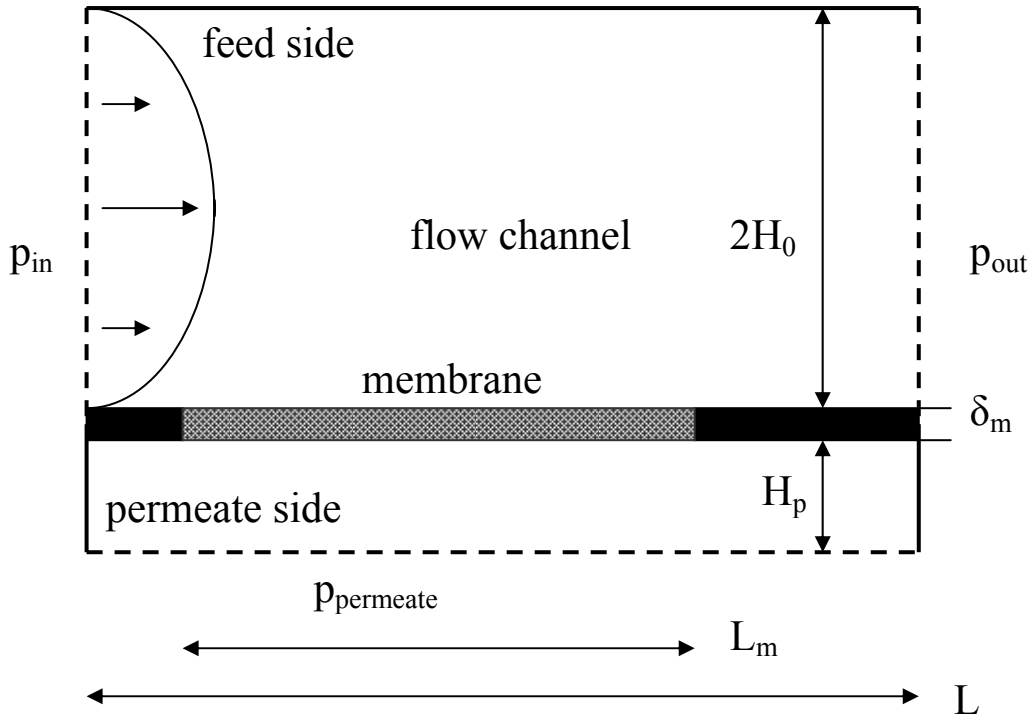


Figure 1: Lay-out of the 2D microfiltration system. Black lines indicate solid walls, whereas dashed lines indicate pressure boundaries. A detailed description is given in the text.

The feed suspension contained particles with a radius a of $2.5 \mu\text{m}$ in a volume fraction Φ of 0.05 . The viscosity ν and specific cake resistance R'_c were calculated according to equation 2 and 23. At the inlet and the outlet of the flow channel as well as at the permeate side, pressure boundary conditions are applied. This is done following the method proposed by Zou and He [23]. The pressure is kept constant at these boundaries:

$$p(x=0) = p_{in}, \quad p(x=L) = p_{out}, \quad p(y=0) = p_{permeate}, \quad [18]$$

The transmembrane pressure (TMP) is defined as the pressure difference between the flow channel and the permeate side at a position halfway the membrane, and when assuming a linear pressure gradient, is given by:

$$TMP = \frac{1}{2}(p_{in} + p_{out}) - p_{permeate} \quad [19]$$

For the suspended particles, boundary conditions with a fixed inlet concentration and a free outflow are applied at these boundaries, according to:

$$\Phi = \Phi(x = 0) = \Phi_b, \quad \frac{\partial \Phi(x = L)}{\partial x} = 0 \quad [20]$$

There is no need for a boundary condition for suspended particles at the permeate side ($y=0$), since a no-flux condition is applied at the membrane. At the solid walls at the topside of the feed side and at the left and right side of the permeate side no-slip conditions are applied to the fluid. The suspended particles are subjected to a no-flux condition at these boundaries.

The geometry is divided into a feed and a permeate side by the presence of a horizontally placed membrane. The membrane is placed between two solid walls at the beginning and the end of the flow channel. The suspended particles are fully retained by the membrane, by application of no-flux conditions. For the fluid, the membrane is described as a porous medium. The fluid experiences a hydraulic resistance when passing the membrane, because part of the fluid is retained. Hereto, a body force F is applied on the fluid when passing the membrane, following Darcy's law:

$$F = -\frac{\rho u}{K_{membrane}} \quad [21]$$

The coefficient $K_{membrane}$ is dependent on the membrane resistance R_m , the membrane thickness δ_m and the viscosity of the fluid phase, according to:

$$\frac{1}{K_{membrane}} = \eta \frac{R_m}{\delta_m} \quad [22]$$

During filtration, a high concentration of suspended particles may be reached at the membrane surface, which may subsequently lead to the formation of a stagnant cake layer. Suspensions with mono-disperse, hard spherical particles form a cake layer when the concentration reaches a value of 0.6. This cake layer behaves as a porous medium; suspended particles are fully retained by the cake, while the fluid experiences a flow resistance. In our simulations, this process of cake layer formation is simulated in a similar way. When the concentration of suspended particles locally exceeds a value of 0.6, the respective lattice point is described as a porous medium, in a similar way as the membrane. No-flux conditions are applied for the suspended particles, while the fluid experiences a body force as given by

equation 21 with the coefficient K_{cake} . This coefficient is chosen such that the Carman-Kozeny relation is obeyed:

$$\frac{1}{K_{cake}} = \eta R'_c = \eta \frac{C(1-\varepsilon_c)^2 S_c^2}{\varepsilon_c^3} \quad [23]$$

The Carman-Kozeny relation describes the specific cake resistance of a mono-disperse, non-compressible cake with porosity ε_c , specific surface $S_c=3/a$ and constant C . Randomly packed cake layers normally have a porosity $\varepsilon_c \approx 0.4$, while the constant $C \approx 5$. Not only the stagnant cake layer, but also the flowing concentrated layer can be considered a porous medium. In general, the flow resistance of this layer is negligibly small. Therefore, we have neglected this effect, as is usual in MF modelling [1].

The initial conditions of the simulations are consistent with a fully developed parabolic velocity profile for the fluid particles in the flow channel, following Poiseuille type flow by a downchannel pressure gradient:

$$-\frac{dp}{dx} = 3 \frac{\eta_b U_0}{H_0^2} \quad [24]$$

where η_b is the viscosity in the bulk of the suspension, U_0 is the average flow velocity, H_0 is the channel half width. The concentration of suspended particles in the flow channel was initially equal to the bulk concentration. At the permeate side of the membrane, the initial velocity of the fluid particles as well as the concentration of suspended particles was equal to zero.

Results and discussion

a) Simulation of microfiltration with the suspension flow model

In this section of the paper, we will first present results of the suspension flow model on the effect of transmembrane pressure. In this way, the development of the permeate flux in time is analyzed at conditions with and without the presence of a cake layer. It is also investigated whether a steady-state situation occurs. The suspension flow model is compared with the existing model of Romero and Davis [6] and Davis and Sherwood [8] to validate our model. This comparison is made on basis of the position-dependence of the flux and cake layer thickness in the steady-state regime so as to analyze the differences in cake layer profile along the

membrane between the different models. To make comparison with the similarity solution of Davis and Sherwood possible, the simulations were carried out in the regime where the cake layer is thin compared to the channel height.

Finally, we will step from a simple cross-flow system to systems with a more complex geometry, in order to illustrate the advanced possibilities of the suspension flow model compared to existing models. As examples of systems with a more complex geometry, simulation results of the steady-state flux will be presented of a system with a discontinuous membrane, a system with flow barriers and a system with a corrugated membrane. The permeate flux J in the simulation results is equal to the fluid velocity u underneath the membrane. The length-averaged flux $\langle J \rangle$ is the average permeate flux over the length of the membrane.

b) Effect of transmembrane pressure on flux and cake layer formation

In figure 2, the development of the length-averaged flux $\langle J \rangle$ in time is shown for different transmembrane pressures (TMP). The initial flux increases proportional to the TMP. At a TMP of 1180 Pa, the flux remains constant in time.

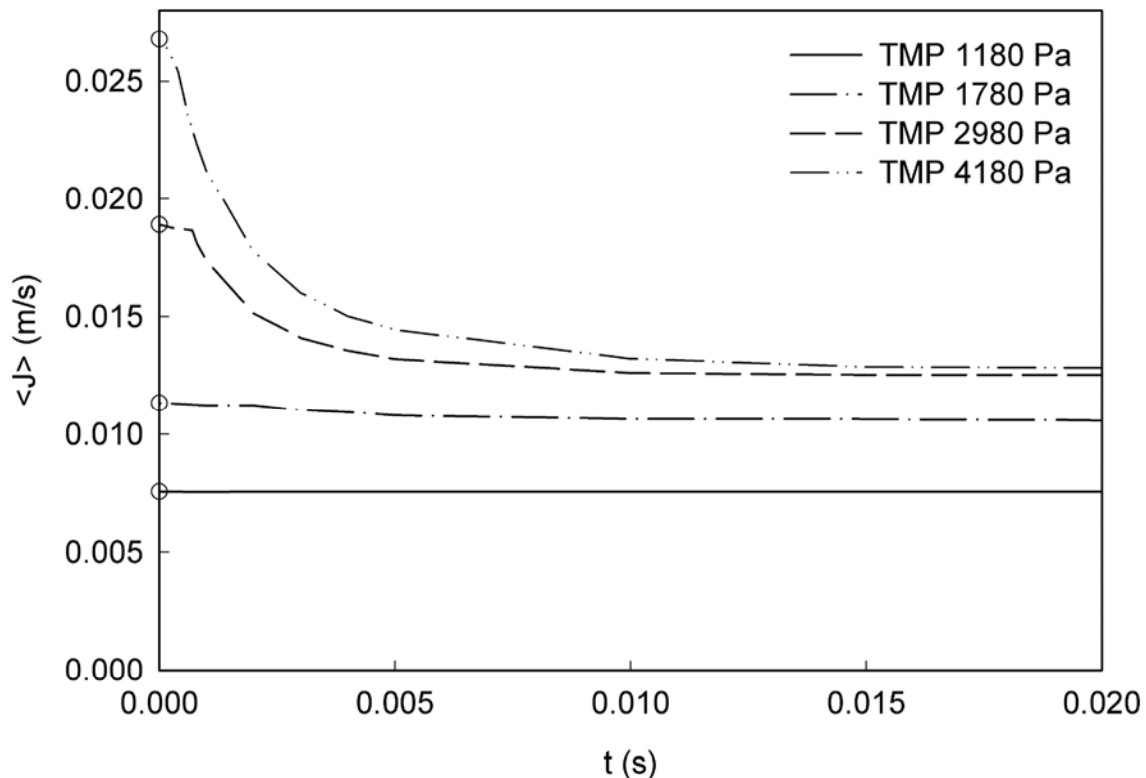


Figure 2: The length-averaged flux as a function of time for a transmembrane pressure of 1180, 1780, 2980 and 4180 Pa. Other system parameters as in figure 1. The calculated values for J_0 are depicted as circles on the Y-axis.

Here, the transport of suspended particles towards the membrane is too low to cause cake layer formation. At a TMP of 1780 Pa and higher however, the flux $\langle J \rangle$ declines initially, but reaches a steady-state at about 0.01 s. Figure 2 also shows the flux at $t=0$ as calculated from the membrane resistance and TMP (=flux particle-free medium J_0). This makes clear that the cake formation process does not start immediately at $t=0$, but about 1 ms later. This is due to the time required to develop the concentration polarization profile. The difference between the length-averaged steady-state flux $\langle J_{ss} \rangle$ at 1780 and 4180 Pa (fig. 3) can mainly be explained with the relative length of the cake-free zone at the beginning of the membrane, but differences in the cake-morphology at the end of the membrane and the narrowing of the flow channel by the cake formation may also have some effect.

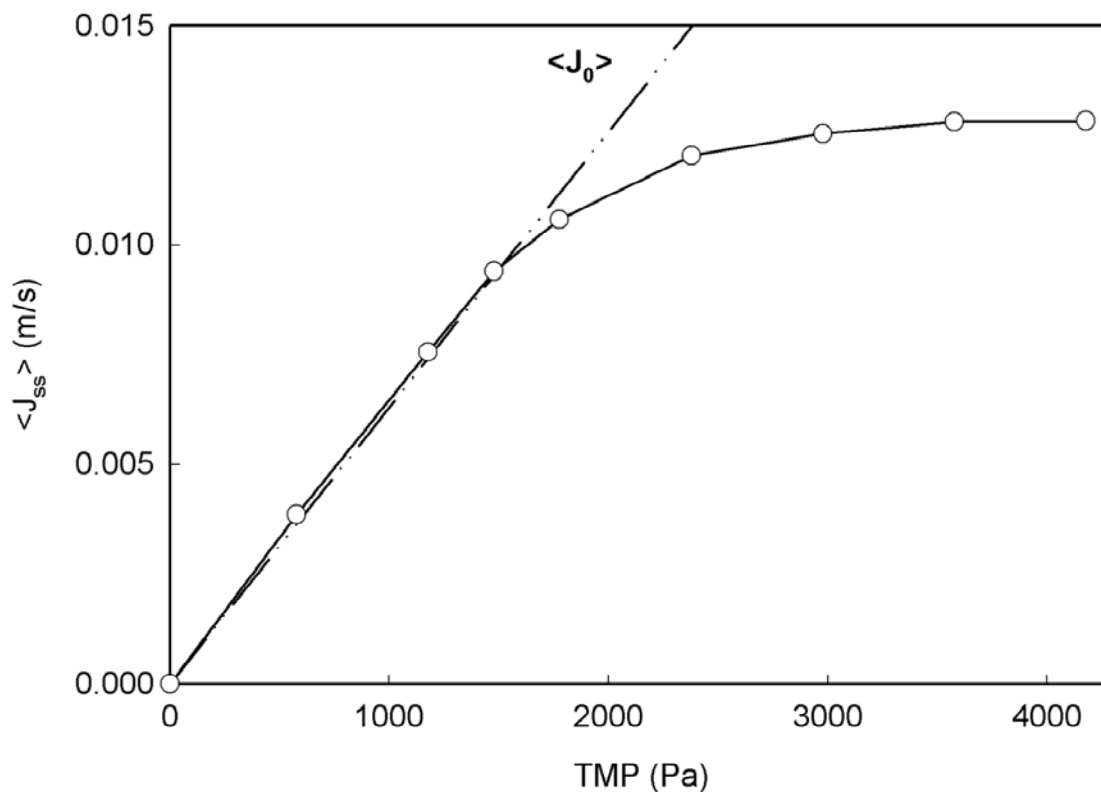


Figure 3: Length-averaged steady-state flux as a function of transmembrane pressure. Also indicated is the calculated line for the nominal flux $\langle J_0 \rangle$. System parameters as in figure 1.

At lower TMP, the length of the cake-free zone is relatively long so that in a large part of the membrane the maximum particle concentration at the membrane wall has not reached the value of 0.6, which leads to less back-transport of suspended particles and therewith to a lower steady-state flux. At higher TMP, the cake-free zone disappears completely (which is contrary to the model of Romero and Davis). In this

regime, the difference in cake height can also contribute to the difference in steady-state flux $\langle J_{ss} \rangle$. We can take the situation at a TMP of 2980 Pa as an example. Here the maximal thickness of the cake is 3.0 μm , which is about 8% of the total channel height. The pressure gradient Δp over the channel is kept constant, so if we assume that the channel height has decreased with 8% over the total channel length, the cross flow velocity U will decrease according to:

$$\Delta p = f \frac{L}{D_h} \frac{1}{2} \rho U^2 \quad [25]$$

where f is the friction factor, L the length of the flow channel, D_h the hydraulic diameter and ρ is the fluid density. Since it follows that the velocity only decreases with a factor $\sqrt{0.92}=0.96$, it becomes clear that according to:

$$\dot{\gamma}_{wall} = \frac{2U_{max}}{H_0} \quad [26]$$

The shear rate at the wall $\dot{\gamma}_{wall}$ will be raised locally with about 4% by the presence of the cake layer (compared to the situation without a cake layer). This higher shear rate can cause a thinner concentration polarization layer and faster particle back-transport (a higher shear-induced diffusivity), therewith resulting in a higher steady-state flux $\langle J_{ss} \rangle$ as a function of TMP as presented in figure 3. At low TMP, no cake layer is formed so that the flux follows the linear trend for the particle-free medium. At a TMP of 1780 Pa, a cake layer starts to be formed, so that the flux levels off and becomes almost constant at a TMP of 3600 Pa. These results show that the suspension flow model is not only able to simulate the flux and cake layer formation in time, but also the dependence on TMP. This is not only possible in the limits of infinitely thin cake layers or infinitely small flux decline, but also in transient regimes, as described in the model of Romero and Davis [6, 7].

c) Position dependence of flux and cake layer thickness

The suspension flow model incorporates a number of factors that are neglected in the model of Romero and Davis [6], such as: 1) the variation of TMP over the length of the membrane, 2) the fully resolved velocity field following NS and 3) the axial migration of suspended particles between the bulk phase and the concentration polarization layer (which e.g. enables the calculation of the dispersion of the concentration polarization layer at the end of the membrane). In this paragraph, we

will analyze which differences this brings about for the cake layer thickness and the flux. In the situation of an infinitely thin cake layer, and for a distance along the membrane $x \gg x_{cr}$, where x_{cr} is the length of the cake-free zone at the beginning of the membrane, Romero and Davis predict that the steady-state flux decreases along the membrane with the distance x , as given by:

$$J_{ss}(x) = J_0 \left[\frac{3(x - x_{cr})}{2x_{cr}} + 1 \right]^{-1/3} \quad [27]$$

where J_0 is the nominal transmembrane flux (=flux of particle-free medium). According to the similarity solution of Davis and Sherwood [8], under the conditions of $\Phi_b < 0.1$, cake-dominated resistance and $L \gg x_{cr}$, the length-averaged flux $\langle J_{ss} \rangle$ is given by:

$$\langle J_{ss} \rangle = 0.072 \dot{\gamma}_{wall,0} \left(\frac{\Phi_c a^4}{\Phi_b L_m} \right)^{1/3} \quad [28]$$

where $\dot{\gamma}_{wall,0}$ is the nominal shear rate at the wall, Φ_b the bulk particle volume fraction and L is the total membrane length. For the particle volume fraction in the cake Φ_c ($=1-\varepsilon_c$) a value of 0.60 was taken in our calculations.

First, the flux J_{ss} of the suspension flow model is compared with the model of Romero and Davis (fig. 4). The latter model does not take the pressure drop over the flow channel into account, so that the flux is equal to the flux of the particle-free medium (at the average TMP) from the beginning of the membrane until the critical distance x_{cr} . Behind this point, the flux declines as predicted by equation 27. In the computer simulations, conditions are chosen such that the cake layer did not become thicker than 10% of the channel height, so that $\dot{\gamma}_{wall}$ can be considered constant in time.

In the suspension flow model, the critical distance x_{cr} and the flux at the beginning of the membrane are dependent on the total membrane length. This can mainly be ascribed to the variation of TMP over the length of the membrane; since the average TMP is similar, the TMP at the beginning of the membrane is higher with longer membrane lengths. Due to these differences in TMP, the flux J_{ss} also drops off more quickly for longer membrane lengths. At the end of the membrane, the flux exhibits a peak due to the dispersion of the concentration polarization layer.

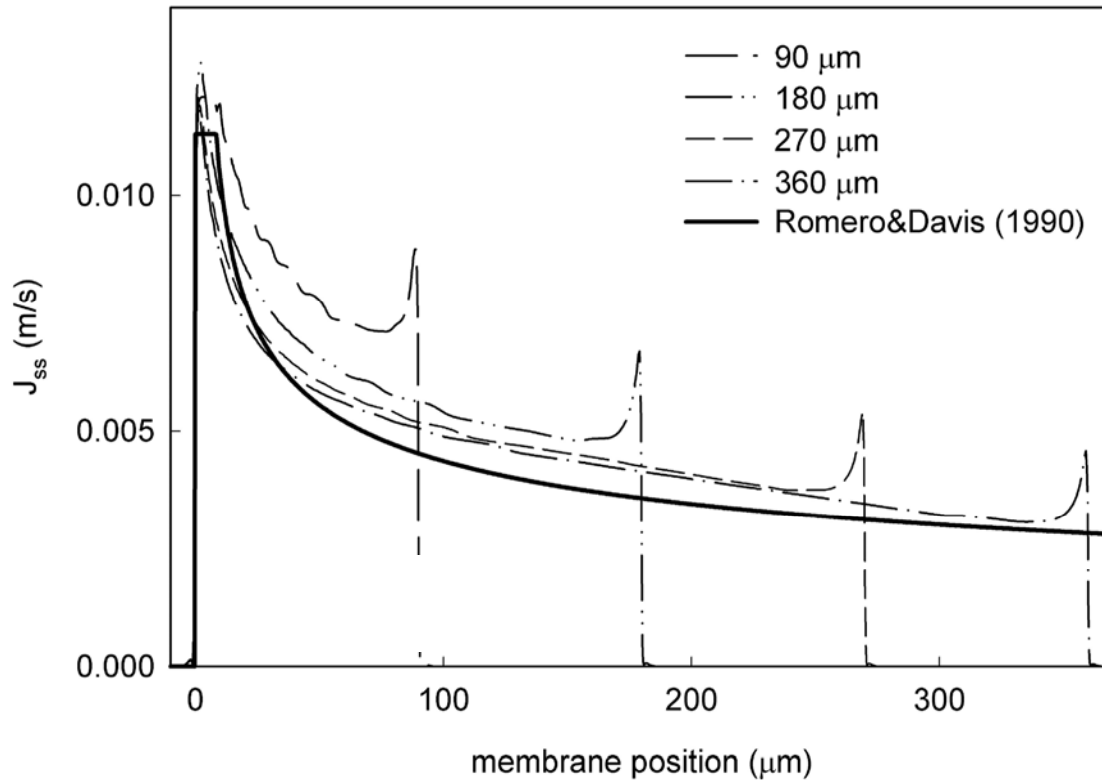


Figure 4: Steady-state flux as a function of position along the membrane for total membrane lengths between 90 and 360 μm . Also indicated is the calculated line for the steady-state flux as predicted by the model of Romero and Davis (eq. 27). Other system parameters as in figure 1.

In figure 5, it is shown how the length-averaged steady-state flux $\langle J_{ss} \rangle$ depends on the membrane length. For short membrane lengths, the difference between the suspension flow model and the model of Romero and Davis is relatively large. At a membrane length of 90 μm , the flux was almost 30% higher for the suspension flow model. The fluxes are however practically the same at longer membrane lengths, indicating that differences in cake layer formation between the models mainly occur at the beginning and the end of the membrane. This is in accordance with our expectations, since axial convective transport can be expected to be most relevant in these regions. With increasing membrane length, there is an increasing difference between the fluxes at different TMP. An increase of TMP can apparently lead to a more than proportional growth of the cake layer with eventually a lower flux. This may be due to the decrease of the mass flow rate $Q (=2U H_0)$ through the flow channel at higher TMP. The decrease of flux with increasing TMP does not agree with the expected effect of narrowing of the channel as explained earlier, since we then would expect an increase of $\dot{\gamma}_{wall}$ and therewith an increase of the flux as well.

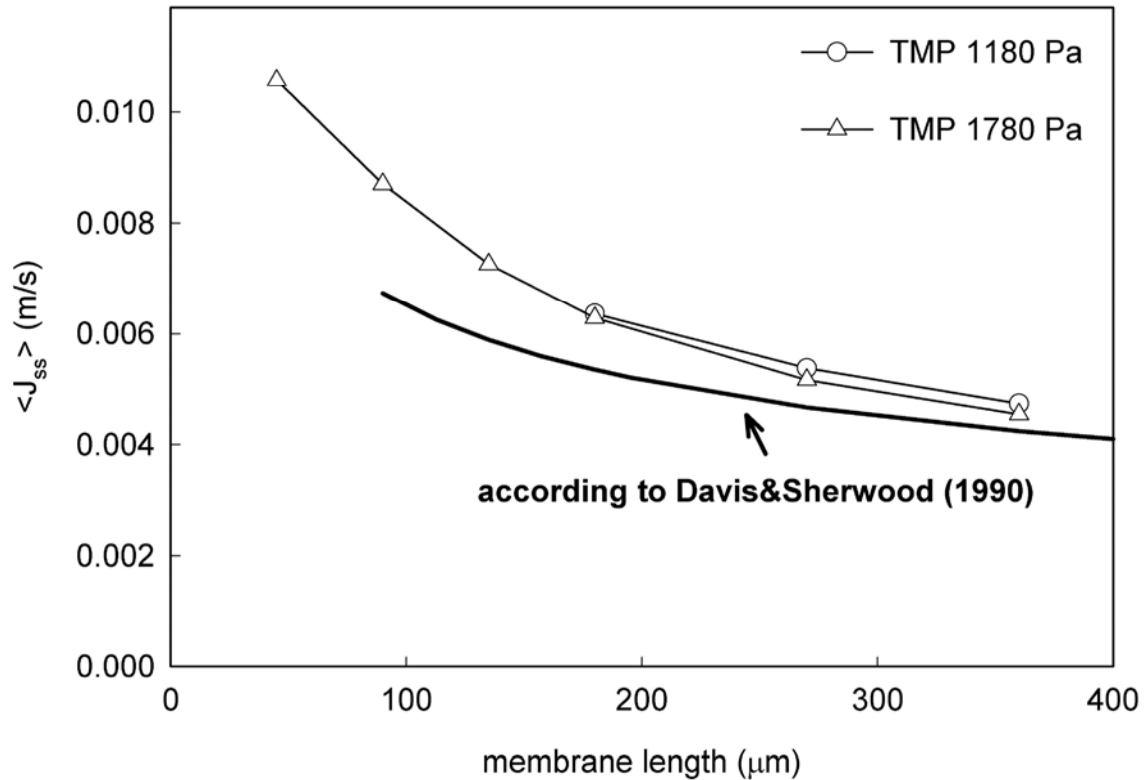


Figure 5: Length-averaged steady-state flux as a function of membrane length. Also indicated is the steady-state flux as predicted by the model of Davis and Sherwood (eq. 28). Other system parameters as in figure 1.

As explained before, the effect of narrowing of the channel by cake formation will lead to a lower cross-flow velocity but a higher shear rate at the place where the cake layer is at its highest point. At other places along the membrane however, where the cake layer is thinner, the cross-flow velocity will even be lower, which, in combination with the higher channel height, can now lead to a drop of the shear rate. Thus, at places along the membrane where the cake layer height is less than maximal, the drop of the shear rate can lead to a decrease of the flux J_{ss} .

The results in this paragraph show that for simple cross-flow systems with relatively long membranes, our suspension flow model predicts cake layer profiles that converge to the profiles that are predicted by the model of Romero and Davis. Differences between the predicted cake layer profiles mainly occur at the beginning and the end of the membrane, resulting in a higher $\langle J_{ss} \rangle$ for short membrane lengths with the suspension flow model. Since the suspension flow model incorporates extra features as compared to the model of Romero and Davis, the results of this model can be considered to be more accurate, which is particularly relevant to systems with

short membrane lengths and large variation of TMP over the length of the membrane.

d) Microfiltration in systems with different geometries

The solution of the flow field in the suspension flow model enables the calculation of concentration polarization in more complex flow geometries. In this paragraph, we will demonstrate some possibilities of the model by showing some examples. First, the effect of the presence of separate pore fields will be demonstrated. In such a situation, pore fields and solid walls alternate along the length of the membrane channel. This will result in extra membrane beginnings and ends, where the flux is relatively high. The passage of the concentration polarization layer over a piece of solid wall will namely lead to a (partial) dispersion, so that the flux at the start of the next membrane field will be higher than without the presence of the solid wall.

The division of a homogeneous membrane into pore fields and fields with solid walls might be used as a means to optimize the flux. The benefit of dispersion of the concentration polarization layer and the presence of repetitive membrane ends should then compensate for the diminished back-transport due to the reduced wall concentration at the solid walls. The suspension flow model enables an accurate flux prediction for these types of membranes. The presence of separate pore fields can also be an intrinsic property of some membrane types, such as the so-called microsieves [22], membranes prepared by micro-engineering which usually feature these distinct pore fields. The mechanical strength of these ultra thin microsieves is dependent on the size and division of the pore fields over the membrane surface. Here, the suspension flow model can be used to find the optimal lay-out of the pore fields as determined by both flux and mechanical strength.

In figure 6, the steady-state flux J_{ss} is presented for a homogeneous membrane with a total length of 135 μm and for a membrane with the same total length, which is divided into three evenly distributed membrane fields with a length of 33 μm and two solid walls with a length of 18 μm . It can be seen that the flux at the pore fields is clearly higher for the subdivided membrane. The length-averaged flux $\langle J_{ss} \rangle$ (membrane length similar to homogeneous membrane) is however about 5% lower. In this situation, the diminished back-transport is the dominant effect, which is unfavorable for the flux. In case of microsieves, the mechanical strength will however improve much by this subdivision [24].

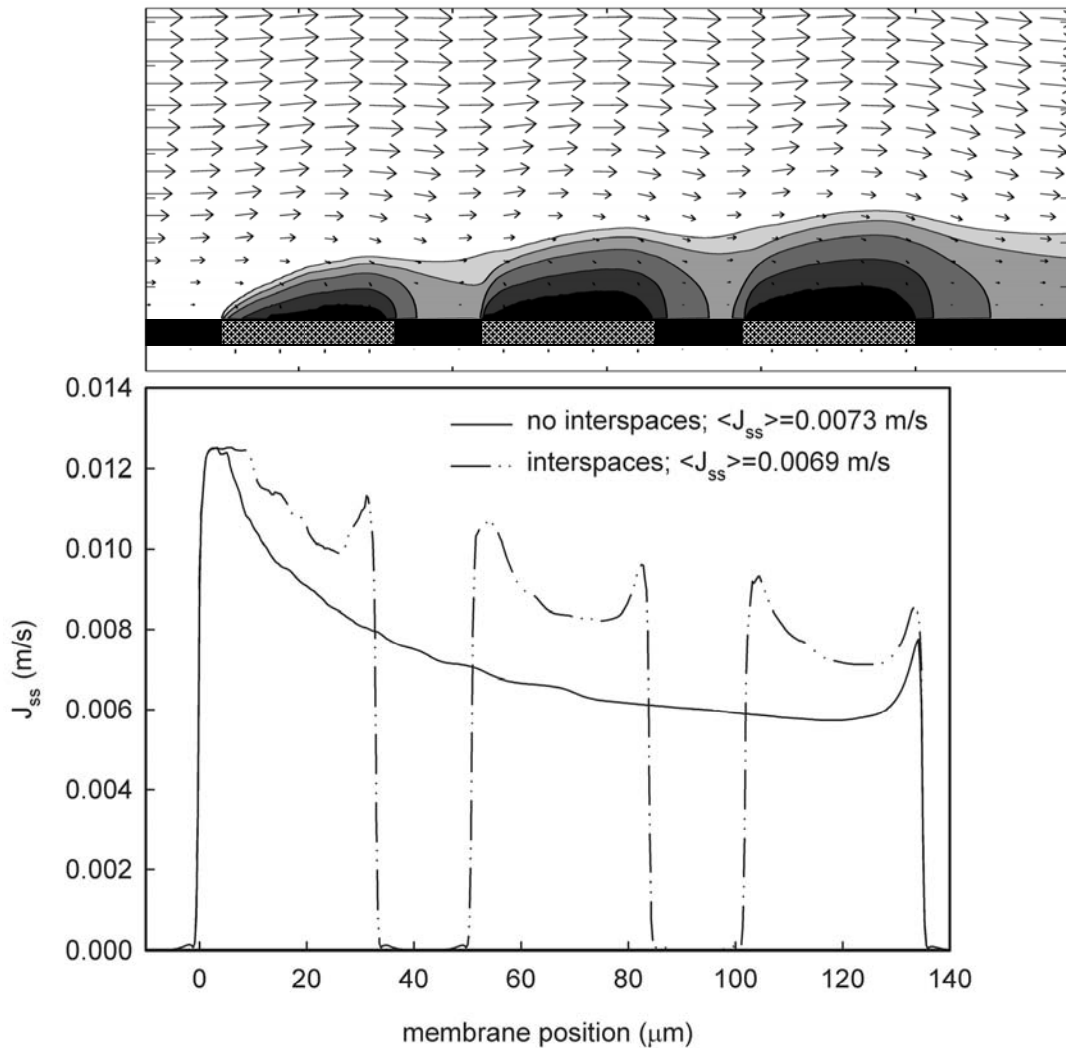


Figure 6: Steady-state flux as a function of position along the membrane for a homogeneous membrane with a total membrane length of 135 μm and for a membrane with the same total length, which is divided into three evenly distributed pore fields with a length of 33 μm and two solid walls with a length of 18 μm (see figure above graph). Also indicated is the length-averaged steady-state flux for both situations. The figure on top shows the concentration distribution and the flow field for the membrane with interspaces. Other system parameters as in figure 1.

The dispersion of the concentration polarization layer might improve with the presence of flow barriers at the solid walls. Whether or not this will render a positive flux effect is dependent on the trade-off between this improved dispersion on the one hand and the decreased wall shear rate on the other hand. With the suspension flow model, we are able to compute the effect of flow barriers. An example is given in figure 7. Here, triangles with a height of 2.7 μm were placed centrally on the solid walls. It can be seen that the flux is hardly influenced by the presence of these barriers, although their height exceeds the height of the cake layer. This might be

related to the microscale of the flow barriers. Because the Reynolds number is linearly dependent on the square height of the flow barrier, it will hardly be affected by the presence of these small flow barriers. The flow barriers do not induce flow disturbances such as vortices (fig. 7).

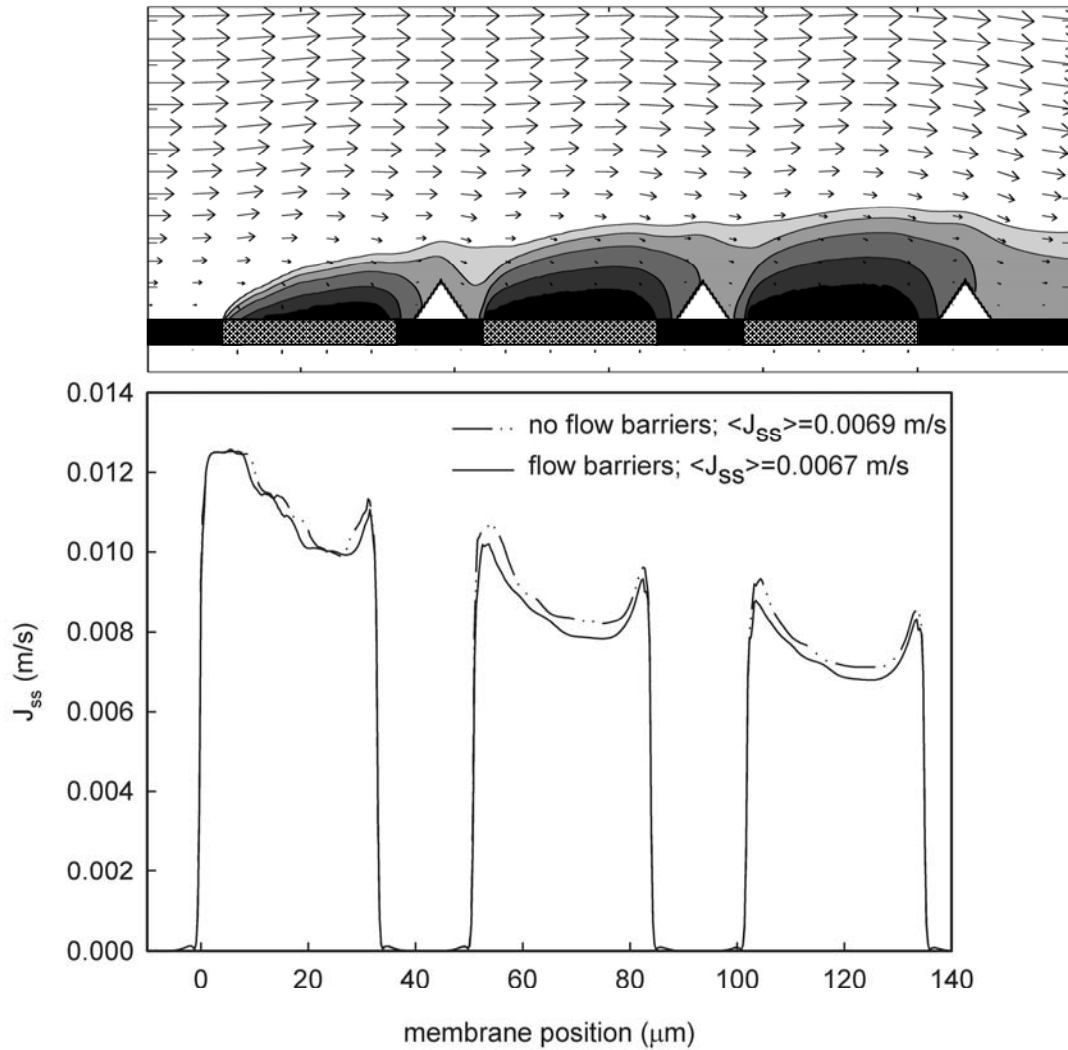


Figure 7: Steady-state flux as a function of position along the membrane for two different membranes: 1) a membrane with a total membrane length of $135 \mu\text{m}$, which is divided into three evenly distributed pore fields with a length of $33 \mu\text{m}$ and two solid walls with a length of $18 \mu\text{m}$ and 2) the same membrane but with flow barriers placed at the solid walls (see figure above graph).

The flow barriers had a triangular form, with a width of $9.9 \mu\text{m}$ at the bottom side to $0.3 \mu\text{m}$ at the top side. The height was $2.7 \mu\text{m}$. Three flow barriers were placed in total, each with the center at a distance of $9 \mu\text{m}$ after a piece of membrane. Also indicated is the length-averaged steady-state flux for both situations. The figure on top shows the concentration distribution and the flow field for the membrane with flow barriers; other system parameters as in figure 1.

On the other hand, because of the mechanism of shear-induced diffusion, the wall shear rate has a large effect on the flux. The decrease of the wall shear rate, due to an increased flow resistance of the flow channel, is the dominant effect in this example, such that the length-averaged steady-state flux $\langle J_{ss} \rangle$ was about 3% lower. Although more research is needed, this example might indicate that microscale flow barriers are not effective for flux improvement.

Another possibility for a higher flux would be the use of corrugated membranes. These corrugations are expected to lead to a better dispersion of the concentration polarization layer and increased flow resistance, as for the system with triangles, but would also affect the shear rate profile at the membrane wall for the total membrane length. More information on the application of corrugated membranes can e.g. be found in [25].

In our example, the membrane corrugations consist of triangles of membrane material, which are placed centrally on the membranes. The size was such that the membrane surface area was increased with 1.8%. Because the membrane has become much thicker at the position of the triangles, application of a similar TMP as for the aforementioned computations would lead to a suboptimal flux. Therefore the TMP was increased to 5340 Pa.

Figure 8 shows the flux along the membrane in steady-state situation. At the beginning and the end of the membrane, the steady-state flux J_{ss} is about 1.5 times higher than without the membrane corrugations. Because of the reduced cake formation in these regions, the relatively high TMP results in this high steady-state flux J_{ss} . This result also indicates that the membrane corrugations are particularly favorable in a system with membrane interspaces, where we have an increased number of membrane beginnings and ends. In the center region of the membrane pieces, the flux is lower than without corrugations. The presence of the corrugations apparently results in a lower mean wall shear rate, which leads to a lower steady-state flux J_{ss} . The length-averaged flux $\langle J_{ss} \rangle$ is however higher in the system with membrane corrugations, suggesting that further research in this direction would be worthwhile. Clearly, the suspension flow model presented in this article can be a very helpful tool for these types of optimizations.

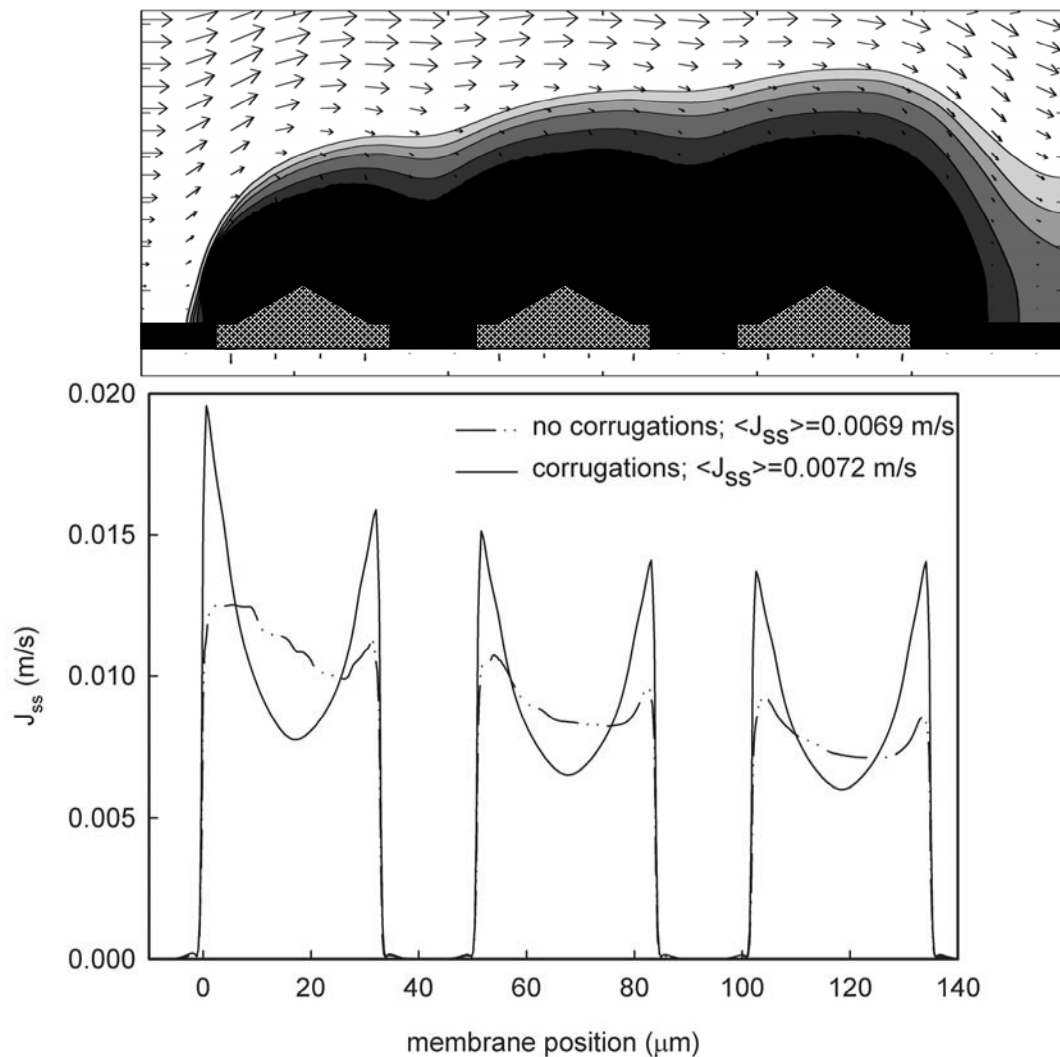


Figure 8: Steady-state flux as a function of position along the membrane for two different membranes: 1) a membrane with a total membrane length of 135 μm , which is divided into three evenly distributed pore fields with a length of 33 μm and two solid walls with a length of 18 μm and 2) the same membrane but with a corrugated structure (see figure above graph). The corrugations consist of triangular pieces of membrane, which are put on top of the pore fields. The triangular pieces had a width of 24.3 μm at the bottom side to 0.3 μm at the top side. The height was 2.7 μm . Three triangular pieces were placed in total, each with the center at a distance of 16.5 μm from the beginning of a pore field. Also indicated is the length-averaged steady-state flux for both situations. The figure on top shows the concentration distribution and the flow field for the membrane with corrugations; other system parameters as in figure 1.

Conclusion

In this article, a new computer simulation model is proposed which enables the study of concentration polarization behavior and cake layer formation in cross flow microfiltration systems. The new model solves the NS equations for the suspension

flow together with the convection-diffusion equation for the suspended particles and follows the lattice Boltzmann method. Diffusion of the suspended particles takes place according to the mechanism of shear-induced migration, which describes the migration of particles in a suspension in shear flow. The shear-induced migration velocity increases linearly with the shear rate and is strongly concentration-dependent.

Upon application for simple cross flow systems, the new suspension flow model yields more realistic results for the flux and cake layer profile than existing models. This is due to the fact that the suspension flow model totally resolves the suspension flow and the shear-induced diffusion behavior of the suspended particles, including a time- and location-dependent shear rate, whereas the existing models normally assume a Poiseuille flow profile and neglect axial transport between the bulk phase and the concentration polarization layer. In contrast to existing models, the new suspension flow model moreover accounts for pressure loss in the flow channel.

From comparison with results of the model of Romero and Davis [6], it became clear that the more realistic approach of the suspension flow model is especially significant for the calculation of the cake layer profile at the beginning and the end of the membrane. Also the effect of narrowing of the flow channel by cake formation on the suspension flow pattern (at a constant pressure gradient over the flow channel) leads to a substantial improvement of the predictions. In the situation of long membrane lengths and thin cake layers, the solution of the suspension flow model converges to that of the model of Romero and Davis.

The suspension flow model has a wider applicability than the existing models. Besides the use for simple cross flow systems, the suspension flow model allows for application in microfiltration systems with complex geometries and moving boundaries. In order to exemplify these possibilities, calculations are presented on systems with a discontinuous membrane, with flow barriers and with corrugated membranes. From these examples, it became clear that this model can be a valuable tool for the design of microfiltration membranes, systems and processes.

Acknowledgements

Friesland Foods is greatly acknowledged for supporting this research. The authors would like to acknowledge the support of the Dutch Ministries of Economic Affairs, Education, Culture and Sciences and of Housing, Spatial Planning and the Environment through a grant of the Dutch Program Economy, Ecology and Technology.

References

- [1] G. Belfort, R.H. Davis, A.L. Zydney, The behavior of suspensions and macromolecular solutions in crossflow microfiltration. *J. Membrane Sci.* 96 (1994) 1.
- [2] A.L. Zydney, C.K. Colton, A concentration polarization model for the filtrate flux in cross-flow microfiltration of particulate suspensions. *Chem. Eng. Commun.* 47 (1986) 1.
- [3] E.C. Eckstein, D.G. Bailey, A.H. Shapiro, Self-diffusion of particles in shear flow of a suspension. *J. Fluid Mech.* 79 (1977) 191.
- [4] R.H. Davis, D.T. Leighton, Shear-induced transport of a particle layer along a porous wall. *Chem. Eng. Sci.* 42 (1987) 275.
- [5] D.T. Leighton, A. Acrivos, Viscous resuspension. *Chem. Eng. Sci.* 41 (1986) 1377.
- [6] C.A. Romero, R.H. Davis, Global model of crossflow microfiltration based on hydrodynamic particle diffusion. *J. Membrane Sci.* 39 (1988) 157.
- [7] C.A. Romero, R.H. Davis, Transient model of crossflow microfiltration. *Chem. Eng. Sci.* 45 (1990) 13.
- [8] R.H. Davis, J.D. Sherwood, A similarity solution for steady-state crossflow microfiltration. *Chem. Eng. Sci.* 45 (1990) 3203.
- [9] N. Pelekasis, A convection-shear induced resuspension model for crossflow microfiltration, *Chem. Eng. Sci.* 53 (1998) 3469.
- [10] D.E. Wiley, D.F. Fletcher, Techniques for computational fluid dynamics modeling of flow in membrane channels. *J. Membrane Sci.* 211 (2003) 127.
- [11] C.J. Richardson, V. Nassehi, Finite element modeling of concentration profiles in flow domains with curved porous boundaries. *Chem. Eng. Sci.* 58 (2003) 2491.
- [12] X. He, S. Chen, G.D. Doolen, A novel thermal model for the lattice Boltzmann method in incompressible limit. *J. Comp. Phys.* 146 (1998) 282.
- [13] S. Succi, *The lattice Boltzmann equation for fluid dynamics and beyond.* Oxford university press, New York, 2001.
- [14] Y.H. Qian, D. d'Humières, P. Lallemand, Lattice BGK models for the Navier-Stokes equation. *Europhys. Lett.* 17 (1992) 479.
- [15] P.L. Bhatnagar, E.P. Gross, M.K. Krook, A model for collision processes in gases. I. Small amplitude processes in charge and neutral one-component systems. *Phys. Rev.* 94 (1954) 511.

- [16] U. Frisch, B. Hasslacher, Y. Pomeau, Lattice gas automata for the Navier-Stokes equation. *Phys Rev. Lett.* 56 (1986) 1505.
- [17] S. Hou, J. Sterling, S. Chen, G.D. Doolen, A lattice Boltzmann sub-grid model for high Reynolds number flows. *Fields Inst. Commun.* 6 (1996) 151.
- [18] V. Breedveld, D. van den Ende, M. Bosscher, R.J.J. Jongschaap, J. Mellema, Measurement of the full shear-induced self-diffusion tensor of non colloidal suspensions. *J. Chem. Phys.* 116 (2002) 10529.
- [19] A. Serou, J.F. Brady, Shear-induced self-diffusion in non-colloidal suspensions. *J. Fluid Mech.* 506 (2004) 285.
- [20] R.J. Philips, R.C. Armstrong, R.A. Brown, A.L. Graham, J.R. Abott, A constitutive equation for concentrated suspensions that accounts for shear-induced particle migration. *Phys. Fluids A* 4 (1992) 30.
- [21] R.G.M. van der Sman, M.H. Ernst, Convection-diffusion lattice Boltzmann scheme for irregular lattices. *J. Comp. Phys.* 160 (2000) 766.
- [22] C.J.M. van Rijn, M.C. Elwenspoek, Microfiltration membrane sieve with silicon micromachining for industrial and biomedical applications. *Proc. IEEE* (1995) 83.
- [23] Q. Zou, X. He, On pressure and velocity flow boundary conditions for the lattice Boltzmann BGK model. *Phys. Fluids* 9 (1997) 1591.
- [24] S. Kuiper, R. Brink, W. Nijdam, G.J.M. Krijnen, M.C. Elwenspoek, Ceramic microsieves: influence of perforation shape and distribution on flow resistance and membrane strength. *J. Membrane Sci.* 196 (2002) 149.
- [25] K. Scott, A.J. Mahmood, R.J. Jachuck, B. Hu, intensified membrane filtration with corrugated membranes. *J. Membrane Sci.* 173 (2001) 1.



Chapter 7: 3D Lattice Boltzmann sub-grid particle method for suspension flow

Abstract

In this paper, we present a simulation method for sub-grid particles with a radius between 0.1 and 0.35 times the grid size. The fluid flow is solved on a coarse grid by a lattice Boltzmann model for dispersed media with an excluded volume and body force term. The particle interactions are handled in more detail on a smaller time and length scale with soft sphere interactions and lubrication forces.

The sub-grid particle model provides more detail than continuum approaches, but with less computational effort than fully resolved particle methods. The current model is a first step towards a particle-based simulation method for suspension flows on mesoscale. The model was validated with the sedimentation of particle swarms, and the velocity profile of concentrated suspension flow.

Introduction

Computational Fluid Dynamics (CFD) has become an important tool to investigate the behavior of particulate suspension flows. Suspension flows are of interest in (petro-)chemical, food and pharmaceutical industries. Various effects have been subjected to research, such as shear induced migration and rheology, sedimentation of particle swarms, and the plugging of porous media. Roughly three modeling approaches can be distinguished for particulate flow [1]:

- 1) The continuum approach (Eulerian-Eulerian) with two-fluid model or a convection-diffusion model [2-3]. The particles are much smaller than the grid size and are treated as a continuous density field. Additional closure relations are required to describe the interaction between the phases.
- 2) Fully resolved particle methods (Eulerian-Lagrangian). The particles consist of several lattice sites and the momentum transfer is calculated numerically [4-6], and
- 3) The sub-grid particle approach (Eulerian-Lagrangian), where the particle diameter is in the same order of, or smaller than the grid size.

The momentum transfer is calculated with a drag force relation [7-9]. In microfiltration for example, suspended particles can be treated as a diffusive component that interacts with the fluid via viscosity relations in the concentration polarization layer, and porous media flow in the cake layer [10]. This continuum approach can provide useful information for the construction of membrane modules and the optimization of process parameters.

However, this approach is unable to predict interactions of particles with the membrane, such as retention and transmission, and pore blocking phenomena. These interactions need to be investigated in more detail and can be incorporated in the lattice Boltzmann (LB) model of Kromkamp *et al.* in a later stage [10]. A solution to this problem could be modeling of suspension flow with fully resolved particles in LB [6], but this method takes a lot of computer resources to study a statistically relevant system.

In this paper, we present a LB model with sub-grid particles with typical radius of 0.1 times the grid size. The fluid flow is solved on a coarse grid, while the particle behavior is handled in more detail on a smaller time and length scale. This approach is related to Particle-in-Cell methods [11] and simulation methods of fluidized beds in chemical engineering [7, 9, 12]. In most methods, particles are treated as point particles with two-way coupling to the fluid [1]. However, the excluded volume effect of the particles on hydrodynamics is often neglected, while this effect is important for the correct prediction of particle segregation and related effects caused by polydispersity. In the present method, we take into account the particle volume effect, two-way coupling and interactions between the particles. The sub-grid particle method is validated with the sedimentation velocity of particle swarms, and the velocity profile of concentrated suspension flow.

Theory

Because a single method is preferred for all scales, the fluid was simulated with the lattice Boltzmann (LB) method [13]. We used a LB model with three dimensions and 19 velocities (D3Q19). The volume effect of suspended particles was treated analogous to porous medium flow, with the extension that the solid phase, in this case the suspended particles, can be displaced by the fluid. Hence, the fluid volume fraction can change in time and space. A velocity difference between the fluid and the particle causes a drag force on the particle, which will be accelerated accordingly. The same force is acting in the opposite direction on the fluid (two-way coupling).

Our approach was inspired by the work of Guo and Zhao, who developed a LB model for flow through porous media with excluded volume effect and a body force [14]. However, their governing equations are invalid, because the assumption that the superficial velocity is divergence free is not true [8].

The model can be expressed by the following generalized Navier-Stokes equation, which is valid for both constant and variable porosity [7, 9]:

$$\begin{aligned} \frac{\partial(\varepsilon\rho)}{\partial t} + \nabla \cdot (\varepsilon\rho\mathbf{u}) &= 0 \\ \frac{\partial(\varepsilon\rho\mathbf{u})}{\partial t} + \nabla \cdot (\varepsilon\rho\mathbf{u}\mathbf{u}) &= -\varepsilon\nabla P + \nabla \cdot (\nu(\varepsilon)((\nabla\rho\mathbf{u}) + (\nabla\rho\mathbf{u})^T)) + F \end{aligned} \quad [1]$$

in which ε is the fluid volume fraction, defined as $\varepsilon = 1 - \Sigma V_p / \Delta x^3$, with ΣV_p the cumulative particle volume in the grid cell. ρ is the bulk fluid density, \mathbf{u} the (real) fluid velocity and P the pressure. ν is the kinematic viscosity and F the body force due to friction with the dispersed medium. This expression is similar to model A of Feng and Yu, who made a comparison between different types of governing equations for gas-solid fluidized beds [9].

In LB, imaginary fluid parcels move on a regular lattice by subsequent collision and propagation steps. In the collision step, the new equilibrium distribution is calculated from the actual local distribution. The collision operator ω controls the update of the local distribution from the calculated equilibrium distribution. In the propagation step, the fluid parcels are propagated into the direction of their corresponding velocity [13]. To describe fluid flow through the dispersed medium, fractional propagation was implemented. In this scheme, the pressure is a conserved quantity, and in the propagation the local distribution is corrected proportionally with the porosity of the new lattice cell. Global mass conservation was confirmed in tests. The similarity with eq. 1 will be shown in a forthcoming paper with inverse Chapman-Enskog analysis. The collision and propagation steps in the LB model are described by:

$$\begin{aligned} f_i'(x, t) &= f_i(x, t) - \omega(f_i(x, t) - f_{i,eq}(x, t)) + G_i \\ f_i(x + \bar{c}_i\Delta t, t + \Delta t) &= f_i'(x, t) \frac{\varepsilon(x)}{\varepsilon(x + \bar{c}_i\Delta t, t + \Delta t)} \end{aligned} \quad [2]$$

f_i is the local distribution; f_i' is the distribution after the collision step, but before propagation. Δx and Δt are the grid size and time increment, respectively. G_i is the distribution of the body force. The kinematic viscosity is defined as $\nu = c_s^2 (1/\omega - 0.5)\Delta t$ ($= \eta/\rho$ with η representing the dynamic viscosity). c_s is the speed of sound, equal to $c/\sqrt{3}$. The viscosity was chosen as a function of the particle volume fraction [8], according to Leighton [15]:

$$\eta(\varphi) = \eta_0 \left(1 + 1.5 \frac{\varphi}{1 - (\varphi/0.58)} \right)^2 \quad [3]$$

with η_0 the dynamic viscosity of the bulk fluid and φ the particle volume fraction ($= 1 - \varepsilon$). The equilibrium distribution function for fluid flow is defined as follows:

$$f_{i,eq} = w_i \varepsilon \rho \left(1 + \frac{\bar{c}_i \cdot \bar{u}}{c_s^2} + \frac{(\bar{c}_i \cdot \bar{u})^2}{2\varepsilon c_s^4} - \frac{\bar{u}^2}{2\varepsilon c_s^2} \right) \quad [4]$$

with body force [14]:

$$G_i = w_i \left(1 - \frac{\omega}{2} \right) \left(\frac{\bar{c}_i \cdot F}{c_s^2} + \frac{(\bar{c}_i \cdot \bar{u})(\bar{c}_i \cdot F)}{\varepsilon c_s^4} - \frac{\bar{u} F}{\varepsilon c_s^2} \right) \quad [5]$$

and fluid velocity:

$$\varepsilon \rho \bar{u} = \sum f_i \bar{c}_i + \frac{\Delta t}{2} F \quad [6]$$

ρ is the density of the fluid, defined as $\varepsilon \rho = \sum f_i c_i$, with $c = \Delta x / \Delta t$ the velocity of direction i , and u the (real) fluid velocity. The local pressure can be calculated by $P = (\rho - \rho_0) c_s^2$.

F is the sum of the particle drag force in the grid cell acting on the fluid ($F = -\sum F_{drag}$). The weight factors w_i were defined as $w_i = c_s^2 / 6 c^2$ for $i = 1, \dots, 6$, $w_i = c_s^2 / 12 c^2$ for $i = 7, \dots, 18$ and $w_0 = 1 - \sum w_i$. The particle drag force F_{drag} was calculated with the recently developed drag force relation of Van der Hoef *et al.* [16]:

$$F_{drag}^* = 10 \frac{(1 - \varepsilon)}{\varepsilon^2} + \varepsilon^2 \left(1 + 1.5 \sqrt{(1 - \varepsilon)} \right) \quad [7]$$

where F_{drag}^* is the dimensionless particle drag force defined as F_{drag} / F_{drag}^{St} and Stokes dragforce $F_{drag}^{St} = 6 \pi \eta \epsilon a |u-v|$, with particle velocity v , fluid velocity u and particle radius a .

This equation is a fit of drag force simulations with fully resolved particles in lattice Boltzmann and consists of the Carman equation and an additional term to correct for the limiting behavior when ϵ approaches 1. This relation was chosen, because it can easily be extended for bi-disperse suspensions [16]. However, also other drag force models could be implemented, such as the combined model of Wen&Yu and the Ergun equations, or Stokes drag force. For a comprehensive review on drag force relations, we refer to Li and Kuipers [7].

The fluid velocity and porosity at the position of the particle was calculated by 3D linear interpolation of the fluid velocity in the cell of the particle and in the seven closest neighboring grid cells, based on the position of the particle in the grid cell [12]. In figure 1, an example is given for interpolation in 2D. The fluid velocity U_x at the particle becomes $(0.25+0.5h_1+0.5h_2)U_{x_4} + (0.25-0.5h_1-0.5h_2)U_{x_1} + (0.25+0.5h_1-0.5h_2)U_{x_3} + (0.25-0.5h_1+0.5h_2)U_{x_2}$. In 3D, also the U_x velocities of the neighboring sites in the z-dimension are taken into account. This averaging method accounted for particles with multiple cell overlap and smoother behavior at low particle concentrations.

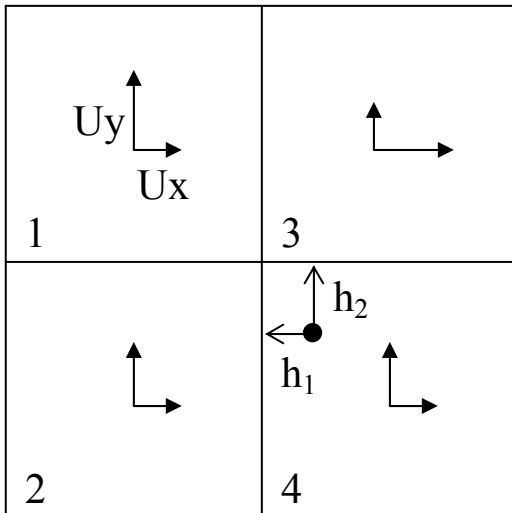


Figure 1: Interpolation of the fluid velocity and porosity at the position of the particle in 2D [12].

The force balance of particle i consists of the particle drag force and summation of interaction forces with other particles and rigid walls. Particle-particle interactions F_{ij} were described with a combination of soft-sphere interaction F_{soft} and lubrication

force F_{lub} , to account for excluded volume effects and hydrodynamic interactions [17, 18]. This particle interaction force was calculated pairs wise and started acting when the gap between the particles became smaller than the critical distance h_c , which is usually chosen in the order of one tenth of the particle radius:

$$\begin{aligned}
 F_{ij} &= F_{soft} + F_{lub} \\
 &= -k_c(h_c - h_{ij}) - 6\pi\eta \frac{a_i^2 a_j^2}{(a_i + a_j)^2} \left(\frac{1}{h_{ij}} - \frac{1}{h_c} \right) v_{ij} n_{ij}
 \end{aligned} \tag{8}$$

k_c is the stiffness parameter or spring constant, a the particle radius, h_{ij} the gap between the particles, and n_{ij} the unit vector. v_{ij} is the velocity difference between the particles. For reasons of simplicity, only the normal force between the particles was taken into account. The particle-wall interactions were handled accordingly. A neighborlist was implemented to find interacting particles quickly. Particle movement was calculated according to Newton's second law:

$$\begin{aligned}
 x(t + \Delta t) &= x(t) + v\Delta t + 0.5\Sigma F_p \Delta t^2 / m_p \\
 v(t + \Delta t) &= v(t) + \Sigma F_p \Delta t / m_p
 \end{aligned} \tag{9}$$

where m_p is the particle mass and F_p the total force acting on a particle, $F_p = \Sigma_j F_{ij} + F_{drag} / \varepsilon$ [9], with j' the neighboring particles within h_c . For high particle volume fractions, particle movement was solved on a smaller time scale by iteration, to maintain a stable system.

Results and discussion

The model was validated with sedimentation of particle swarms in various concentrations. Sedimentation has been studied very well with LB and fully resolved particle method [19]. The particles were placed on random positions in a periodic box of $3 \times 4 \times 4$ filled with stationary fluid. All boundaries were treated with periodic boundary conditions and sedimenting particles leaving the system at the bottom were re-introduced at the top.

The suspensions were allowed to settle by adding gravity force to the particles in the z-direction. Richardson and Zaki reported an empirical relation for the average sedimentation velocity of particle suspensions, as a function of the particle volume fraction [20]:

$$\frac{v(\varepsilon)}{v_0} = \varepsilon^n \quad [10]$$

with ε the fluid fraction, $v(\varepsilon)$ the average swarm sedimentation velocity and v_0 the sedimentation velocity of a single sphere in an infinite system, which was calculated by balancing the Stokes drag force with gravity and buoyancy forces. n is an empirical coefficient of about 5 in the Stokes flow regime.

Based on the energy balance of a particle and the rate of energy dissipation, Snabre and Mills derived an analytical relation for sedimenting suspensions in the Stokes flow regime [21]:

$$\frac{v(\varepsilon)}{v_0} = \frac{\varepsilon}{1 + \alpha(1 - \varepsilon)/\varepsilon^3} \quad [11]$$

α is a measure for the angular dispersion of the fluid streamlines against the vertical direction and is taken 4.6 [21]. The model of Snabre and Mills showed good agreement with experimental results and computer simulations, and performed better than the empirical relation of Richardson and Zaki.

In figure 2, simulations of the average suspension sedimentation velocities are compared with the relation of Snabre and Mills and the experimental results of Buscall *et al.*, who studied the sedimentation of latex particles [22]. Below particle volume fraction 0.2, the sub-grid particle model slightly underpredicts the relation of Snabre and Mills, while between particle fraction 0.1 and 0.2 the sub-grid particle model is comparable with the experimental data of Buscall *et al.* [22].

Deviations at low volume fractions can be explained by the relative small box size and the spatial averaging method with linear interpolation. For a small number of particles, the fluid flow velocity and fluid volume fraction is not known accurately enough at the location of the particle, despite the interpolation method. For low particle volume fractions a combination with Stokesian dynamics or Direct Numerical Simulation (DNS) methods [23] might give better results, at the cost of substantially more computational effort.

Further, the effect of the size ratio of the sub-grid particles compared to the grid size was studied (fig. 3). At particle volume fraction of 0.1, the radius of the sub-grid particles was varied between 0.06 and 0.45 times the grid size to investigate the effect on the relative average sedimentation velocity. Upto a radius of 0.35 times the grid size, the average sedimentation velocity was hardly affected by the ratio of the

particle radius to the grid size. A larger particle radius than 0.35 times the grid size caused a deviating average sedimentation velocity, due to the fact that the particle diameter approaches the grid size. At large particle diameter, local velocity and porosity are not well enough described by the model, and the interpolation method becomes limiting.

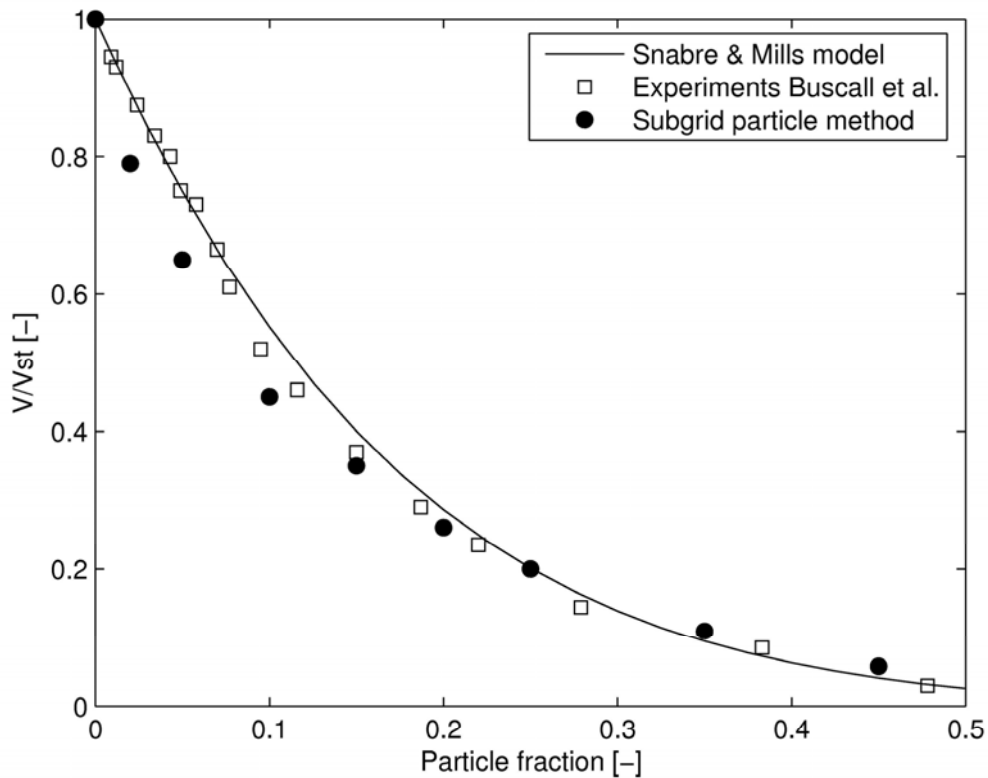


Figure 2: Comparison of the average suspension sedimentation velocity as a function of the particle volume fraction (ϕ) with the analytic relation of Snabre and Mills [21] and the experimental results of Buscall *et al.* [22]. The grid size Δx was $1.0 \mu\text{m}$ and particle radius was $0.1 \mu\text{m}$. Fluid density and viscosity were chosen equal to water: 1000 kgm^{-3} and $1.0 \cdot 10^{-6} \text{ m}^2\text{s}^{-1}$ respectively; particle density was 5000 kgm^{-3} .

The effect of the density ratio between the particles and the fluid was also evaluated (results not shown). A density ratio of factor 1.01 still resulted in stable simulations and a correct prediction of the average sedimentation velocity. It must be noted that sedimentation velocities become very small and small density ratios might cause more problems in simulations of suspension flows. The momentum transfer from the fluid to the particle could introduce fluctuating behavior of particles with very low mass.

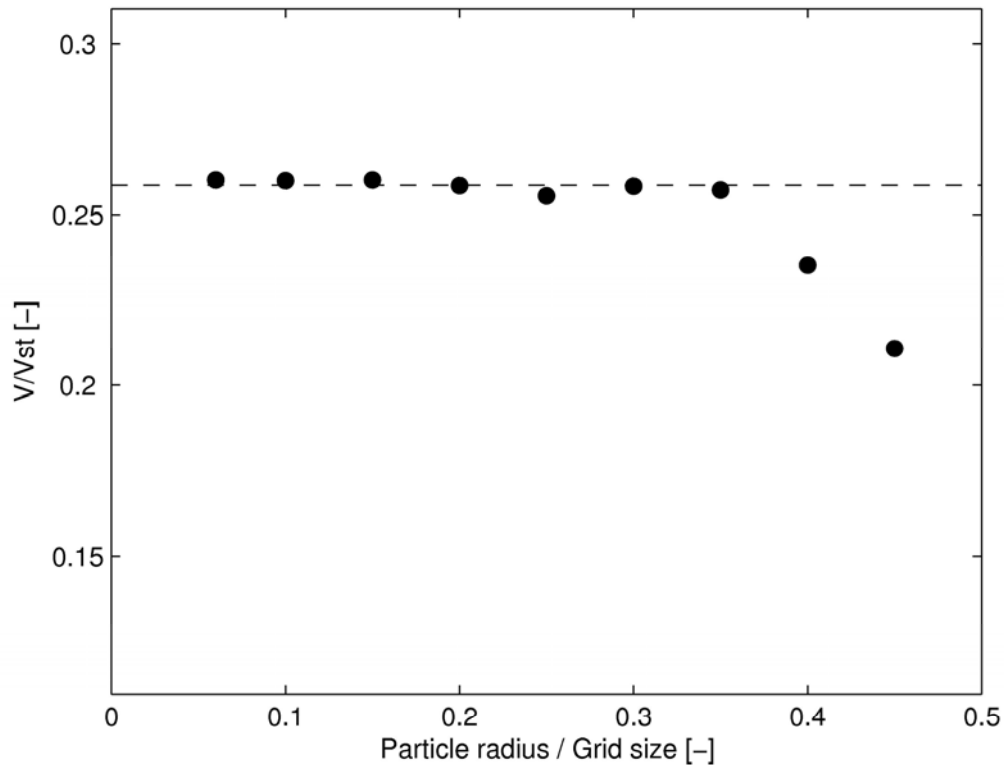


Figure 3: Effect of the particle radius on the relative average sedimentation velocity at a particle volume fraction (ϕ) of 0.1. Other parameters as in figure 2.

The second benchmark applies to concentrated suspension flow between two parallel walls. Above a particle volume fraction of 0.3, the velocity profile becomes blunted compared to the parabolic profile of a homogeneous Newtonian fluid, also known as Poiseuille flow. Further, a non-uniform particle concentration distribution develops into the channel. Both effects can be explained by irreversible interactions between the particles [24].

In the simulations, the suspension flow was driven by pressure periodic boundaries [25], providing a pressure drop over the channel. The upper and lower walls of the channel were implemented as rigid walls, while the sidewalls perpendicular to the flow had periodic boundaries.

The simulated velocity profiles in the channel were compared with the results of Lyon and Leal, who measured the particle velocity and concentration profiles with a modified laser-Doppler velocimetry method [24]. The velocity profiles were quite in agreement with the experimental results. For particle volume fraction of 0.4, the simulated velocity profile deviated from the parabolic profile of Poiseuille flow (fig. 4), which could be due to the fact that the model only roughly predicted particle

segregation effects. The accurate prediction of shear induced migration behavior, however, remains to be confirmed and will be subjected to further research.

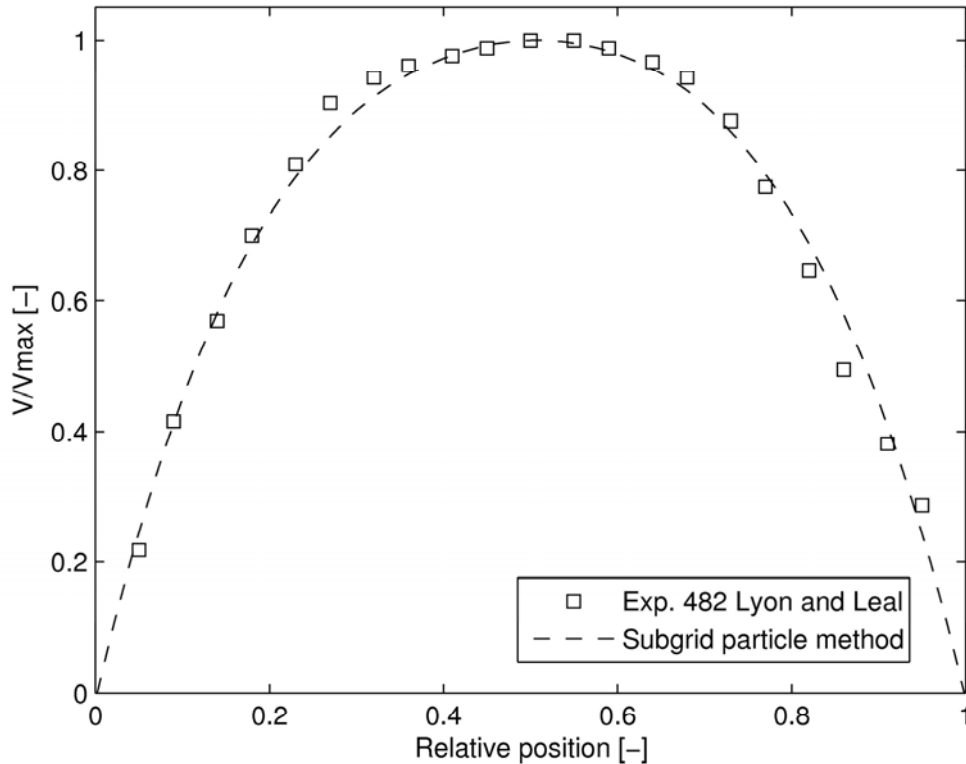


Figure 4: Velocity profiles of suspension flow between two parallel walls and experimental results of Lyon and Leal (exp. 482) [24]. The channel dimensions were 3x5x11 with $\phi=0.4$. The pressure drop over the channel was $1.0 \cdot 10^{-3}$ Pa. The grid size Δx was 1.0 mm, particle radius 0.229 mm, and the particle diameter to channel gap ratio was 24 in both the experiment and simulation. Fluid density and viscosity were 1000 kgm^{-3} and $1.0 \cdot 10^{-6} \text{ m}^2\text{s}^{-1}$ respectively; particle density was 5000 kgm^{-3} .

Conclusion

In this paper, we presented a Eulerian-Lagrangian sub-grid particle method for suspension flows in lattice Boltzmann, with excluded volume and particle interactions with a combination of lubrication force and soft-sphere interaction. The model was validated with the average sedimentation velocity of particle swarms, and is in agreement with an analytic relation and experimental data.

Below a particle volume fraction of 0.1 the prediction is less accurate, but quite satisfactory for the application of microfiltration, where at low volume fractions predominantly convective transport of the particles takes place. The radius of the sub-grid particles can be up to 0.35 times the grid size, before deviations from the

predicted average sedimentation velocity start to occur. The velocity profile of concentrated suspension flow (volume fraction 0.4) between two parallel walls was comparable with experimental data.

Acknowledgements

We would like to acknowledge the support of the European Commission through TMR grant ERB FMGE CT950051 (the TRACS programme at EPCC, Mike Cates and Kevin Stratford of the Physics and Astronomy department), and the support of the Dutch foundation of Economy, Ecology and Technology (EET). John F. Brady of Caltech Chemical Engineering (Pasadena, California) and Wim Briels of the Computational Dispersion Rheology group (University of Twente, the Netherlands) are thanked for interesting discussions about the sub-grid particle model. Martin van der Hoef and Renske Beetstra of the Fundamentals of Chemical Reaction Engineering group (University of Twente, the Netherlands) are thanked for discussions about the lattice Boltzmann model and particle dynamics. Further, we like to thank Luis Portela (Kramerslab Delft University, the Netherlands) for discussing particle interactions and comparison with Stokesian dynamics.

References

- [1] E. Loth (2000) Numerical approaches for motion of dispersed particles, droplets and bubbles, *Prog. Energy Comb. Sci.* 26, 161.
- [2] D. Gidaspow (1994) *Multiphase flow and fluidization: continuum and kinetic theory descriptions*. Academic Press, Boston, 1994.
- [3] D.Z. Zhang, A. Prosperetti (1997) Momentum and energy equations for disperse two-phase flows and their closure for dilute suspensions. *Int. J. Multiphase Flow* 23, 425.
- [4] J.F. Brady, G. Bossis (1988) Stokesian dynamics, *Ann. Rev. Fluid Mech.* 20, 111.
- [5] S. Lomholt, M.R. Maxey (2003) Force-coupling method for particulate two-phase flow: Stokes flow, *J. Comp. Phys.* 184, 381.
- [6] A. Ladd, R. Verberg (2001) Lattice Boltzmann simulation of particle-fluid suspensions, *J. Stat. Phys.* 104, 1191.
- [7] J. Li, J.A.M. Kuipers (2003) Gas-particle interactions in dense gas-fluidized beds, *Chem. Eng. Sci.* 58, 711.

-
- [8] N.A. Patankar, D.D. Joseph (2001) Modeling and numerical simulation of particulate flows by the Eulerian-Lagrangian approach, *Int. J. Multiphase Flow* 27, 1659.
- [9] Y.Q. Feng, A.B. Yu (2004) Assessment of model formulations in the discrete particle simulation of gas-solid flow, *Ind. Eng. Chem. Res.* 43, 8378.
- [10] J. Kromkamp, A. Bastiaans, J. Swarts, G. Brans, R.G.M van der Sman, R.M. Boom (2005) A suspension flow model for hydrodynamics and concentration polarization in crossflow microfiltration, *J. Membrane Sci.* 253, 67.
- [11] D.M. Snider (2001) An incompressible three-dimensional multiphase particle-in-cell model for dense particle flows, *J. Comp. Phys.* 170, 523.
- [12] B.P.B. Hoomans, J.A.M. Kuipers, W.J. Briels, W.P.M. van Swaaij (1996) Discrete particle simulation of bubble and slug formation in two-dimensional gas-fluidised beds: a hard sphere approach. *Chem. Eng. Sci.* 51, 99.
- [13] S. Succi (2001) *The Lattice Boltzmann equation for fluid dynamics and beyond*, Oxford University Press, England.
- [14] Z. Guo, T. Zhao (2002) Lattice Boltzmann model for incompressible flows through porous media, *Phys. Rev. E.* 66, 036304.
- [15] D.T. Leighton (1985) *The shear induced migration of particulates in concentrated suspension*, Ph.D. thesis, Stanford University.
- [16] M.A. van der Hoef, R. Beetstra, J.A.M. Kuipers (2005) Lattice Boltzmann simulations of low Reynolds number flow past mono-and bidisperse arrays of spheres: results for the permeability and drag force, *J. Fluid Mech.* 528, 233.
- [17] R.C. Ball, J.R. Melrose (1997) A simulation technique for many spheres in quasi-static motion under frame-invariant pair drag and Brownian forces, *Physica A* 247, 444.
- [18] N.Q. Nguyen, A.J.C. Ladd (2002) Lubrication corrections for Lattice Boltzmann simulations of particle suspensions, *Phys. Rev. E* 66, 046708.
- [19] N.Q. Nguyen, A.J.C. Ladd (2005) Sedimentation of hard-sphere suspensions at low Reynolds number, accepted *J. Fluid Mech.*
- [20] J.F. Richardson, W.N. Zaki (1954) Sedimentation and fluidization I, *Trans. Inst. Chem. Eng.* 32, 35.
- [21] P. Snabre, P. Mills (2000) Settling and fluidization of non Brownian hard spheres in a viscous liquid, *Eur. Phys. J. E* 1, 105.

[22] R. Buscall, J.W. Goodwin, R.H. Ottewill, Th.F. Tadros (1982) The settling of particles through Newtonian and non-Newtonian media, *J. Coll. Int. Sci.* 85, 78.

[23] T. Kajishima, S. Takiguchi (2002) Interaction between particle clusters and particle-induced turbulence, *Int. J. Heat Fluid Flow* 23, 639.

[24] M.K. Lyon, L.G. Leal (1998) An experimental study of the motion of concentrated suspensions in two-dimensional channel flow. Part 1. Monodisperse systems, *J. Fluid Mech.* 363, 25.

[25] T. Inamuro, M. Yoshino, F. Ogino (1999) Lattice boltzmann simulation of flows in a three-dimensional porous structure, *Int. J. Numer. Meth. Fluids* 29, 737.



Chapter 8: Concluding remarks, towards fractionation on production scale

Introduction

In the previous chapters, we reported on various aspects of a membrane based fractionation process for poly-disperse particle suspensions. In this chapter, we will summarize some of the main conclusions and put them into perspective for the design of a fractionation process. The relevant aspects are summarized in table 1. Further, an outlook is given for future research on (membrane) fractionation.

Table 1: Aspects of membrane fractionation that are discussed in this thesis.

Scale	Aspect	Chapter	E/S ¹⁾
Pore geometry / Particle (typical size 0.1 – 10 µm)	Pore shape and edge design	3	S
	Particle / Pore diameter ratio	3	S
	Inter pore distance	3	S
	Particle release	3	S
Pore field / Membrane morphology (typical size 10 – 100 µm)	Microsieve support structure	4	E, S
	Membrane and microsieve morphology (particle deposition)	5	E
	Surface properties (particle transmission)	5	E
Process / Module design (typical size > 100 µm)	Feed composition (flux and transmission)	5	E
	Process conditions and transmission regimes	5	E
	Process conditions and filtration regimes	3, 6	S
	Order of fractionation poly-disperse suspensions	5	E
	Channel design and inserts	6	S

¹⁾ experimentally determined (E), or by computer simulation (S).

Conclusions and perspective on pore geometry and particle scale

Microsieve technology offers much freedom in design that is unknown to any other type of microfiltration. It is characterized, amongst others, by very high hydraulic permeability compared to traditional membranes [1, 2], but also by the possibility to

manufacture pores with almost any shape, with a range of porosities. In chapter 3, the effect of pore geometry and porosity was studied by computer modeling. The forces on a deposited particle were evaluated and depending on the filtration regimes, various pore geometries could be recommended. For example, it was found that triangular pores pointing into the cross flow direction performed best (60 % increase in flux) in the sub-critical filtration regime, because the particles could be released easiest. Besides this, an important finding was that the membrane porosity influenced particle release. Particles can settle more easily behind a particle that has already deposited on top of a pore, if the next pore is right behind the blocked pore. These effects were quantified into an extended particle release criterion for different pore geometries, membrane porosities, and particle to pore diameter ratios. This criterion can be used for the design of microsieves to achieve better performance. Until now, the effect of particles on pores has been investigated, but for fractionation processes, it is essential that in further research, the effect of pore shape and membrane porosity on the transmission of particles be investigated as well. Flux and transmission will be determined by the particle to pore diameter ratio (hydrodynamic friction effect) if no other interactions are of importance. In a second step, colloidal forces can be included to describe the particle-pore wall interaction for different hydrodynamic regimes (see also chapter 5). These effects will be elaborated in the next paragraph.

Conclusions and perspective on pore field design and membrane morphology

The effect of the microsieve support structure on the flow through the membrane was evaluated with computer simulations and pore blocking experiments (chapter 4). Based on simulations, it was found that the substructure influences the flux behavior of the microsieve to a large extent, and a new design was proposed. The clean water flux of the improved sieve design was almost equal to the theoretical flux and the formation of separate particle layers on the membrane could even be distinguished. The specific resistance of these layers was in line with computer simulations (chapter 4).

The effect of membrane morphology on particle deposition in transmission experiments with polymer microsieves and with conventional polymer membranes was investigated in chapter 5. The fouling behavior of the conventional polymer membranes was comparable to deep bed filtration, while microsieves showed in-pore fouling. It is expected that the tortuous structure of the polymer membrane gradually

becomes filled with small particles in time, and will thus slowly become clogged internally. The microsieve probably adsorbs only a single layer of particles inside the pores. Even though a polymer membrane may initially show more stable fluxes, the microsieve will therefore have a better long-term behaviour.

The combination of hydrodynamic and colloidal forces [3] can explain the different transmission regimes found in chapter 5. Due to the relatively large hydrodynamic forces resulting from the high fluxes observed while using microsieves, particles can be adsorbed in the primary minimum of the particle-wall interaction curve (fig. 1). Figure 1 demonstrates the importance of colloidal interactions in transmission processes and the control of surface properties. Prior research showed that a silicon nitride surface suffers from aging, as was reflected in an increasing contact angle for water, which indicates a slow loss of hydrophilicity [4].

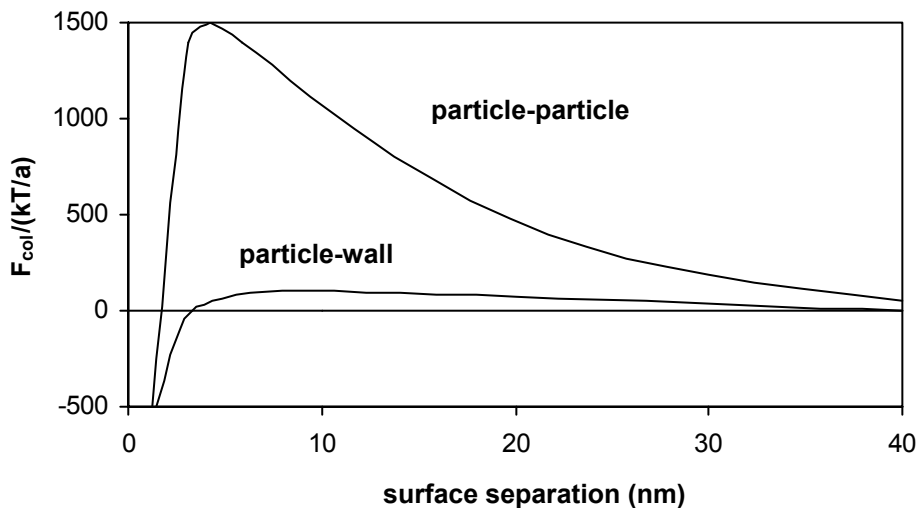


Figure 1: Particle-particle and particle-wall interaction forces for 0.22 μm carboxylate latex-particles, and polycarbonate Nuclepore membranes [3]. The primary minimum is located below 3 nm from the surface, $\Psi_{\text{particle}} = -50 \text{ mV}$, $\Psi_{\text{wall}} = -25 \text{ mV}$, 0.001 M 1:1 electrolyte, pH 6.

In general, a decreased hydrophilicity is correlated with an increased susceptibility to fouling of the microsieves. A more constant hydrophilicity can be achieved with surface modification, such as polymer coatings [4] or covalently attached hydrophilic groups [5].

An accurate experimental study into the interactions between particles and membrane and pore wall is not trivial, even when simple, reliable model systems are used, since many different phenomena act simultaneously. Computational Fluid Dynamics (CFD) methods can therefore be helpful tools for a further investigation of transmission phenomena on particle and pore scale. Besides this, in computer simulations, the conditions and variations that can be studied can be wider than

would be possible experimentally. The models in this thesis did not yet incorporate colloidal interactions, since this would extend the model to a level of complexity that would not be warranted by the current state of the art. However, as more knowledge on system behavior is being gathered, the colloidal (DLVO) interactions between particles and membrane should be incorporated in a model with fully resolved particles [6]. This would make the prediction possible of the different transmission regimes that were observed experimentally. Subsequently, the combined effect of transmembrane pressure and cross flow velocity on particle transmission can be investigated for different membrane morphologies, different particle to pore diameter ratios, and different particle concentrations. This will give a sound theoretical base for the transmission regimes that we found, and will open up the route towards the rational design of fractionation processes.

Conclusions and perspective on process scale and module design

For optimal transmission of mono-disperse particles, a stable transmission regime must be found. As chapter 5 shows, this is not as straightforward as it seems, because the transmission regime depends on the particle properties, particle-wall interactions and process parameters such as the transmembrane pressure and the cross flow velocity (regime 1 or 3, chapter 5). Different transmission regimes were found for different particle sizes, membrane pore sizes, colloidal interactions, and hydrodynamic forces. In addition, the concentration of the particles in the suspension influences the transmission behavior to a very large extent, and even in a transmission regime that seems suitable, transmission and flux decreased in time, probably due to bridging (chapter 5).

The situation becomes even more complex when considering the type of feed used in fractionation, which implies the presence of particles of various sizes. Besides the transmission regime that was described before, the transmembrane pressure and cross flow velocity also determine whether the filtration regime is sub-critical or critical [7]. In the sub-critical regime, large particles are taken up from the membrane by the cross flow. Experiments and simulations show that sub-critical fractionation of particle suspensions with small size differences is almost impossible, because particles with a size that is close to the membrane pore size can hardly be removed from the membrane surface by the cross flow, as we described in chapters 3 and 5. Alternatively, one could work in the critical filtration regime, but this implies that particle deposition on the membrane takes place rapidly. Therefore, additional means

are required to remove deposited particles, and therewith, to maintain high flux and transmission, such as pulsed cross flow or backpulsing. To evaluate various relevant effects, computations could be carried out that are in line with the model presented in chapter 6, but that the model would have to be extended considerably e.g. to incorporate the presence of poly-disperse particles. To validate the extended model, visualization of particle deposition and removal during a backpulse cycle with a high-speed camera would yield important information.

In chapter 5, the effect of particle size differences was studied mainly for bi-disperse suspensions at equal particle fractions of small and large particles. In practice, particles can be present at any ratio; therefore, one should incorporate this effect and relate it to flux and transmission. The ultimate aim should be a relation or model that predicts transmission of small particles in the presence of large particles, for different particle size ratios and different total concentrations. This relation will be the basis for the design of a sub-critical fractionation process.

Fractionation of poly-disperse suspensions (e.g. tri-disperse, chapter 5) is still a challenge, since the process has many variables. A better understanding of the fractionation of bi-disperse suspensions will be a starting point, but obviously more information will have to be added in order to describe poly-disperse suspensions. CFD simulations with a model for poly-disperse suspensions, based on multi-component convection-diffusion [8] are an interesting option. In this case, not just one fractionation step should be considered, but the complete process design should be considered as a whole. We showed in chapter 5 that the order in which particles are removed from each other is of essence for a successful fractionation.

The complete design of a well-performing process for fractionation of poly-disperse suspensions, based on a complete understanding of the underlying principles is not yet achieved. Even though a start has been made, it is clear that challenges remain to be answered both experimentally and computationally. Full membrane fractionation of natural feedstocks with high concentrations of particles and small particle size differences demand the utmost of current membrane technology regarding membrane choice, process conditions, and (minimal) fouling behavior. For some of the separation steps required for full fractionation encouraging results are available. Most of the building blocks for membrane fractionation (e.g. the effects of particle-membrane interaction, particle transmission and retention phenomena) are now present in a fundamental form; the integration into a consistent framework for process design is only a matter of time and continued research effort.

Perspective on new principles for fractionation

Lately, some other, new methods for fractionation of poly-disperse particle suspensions have emerged, which could be used as an alternative to or in combination with microfiltration, such as shear-induced migration [9], and lateral displacement in micro devices [10] (fig. 2). These methods could be beneficial for high demanding fractionation processes of feedstocks with high particle concentrations (shear-induced migration) or small particle size differences (lateral displacement).

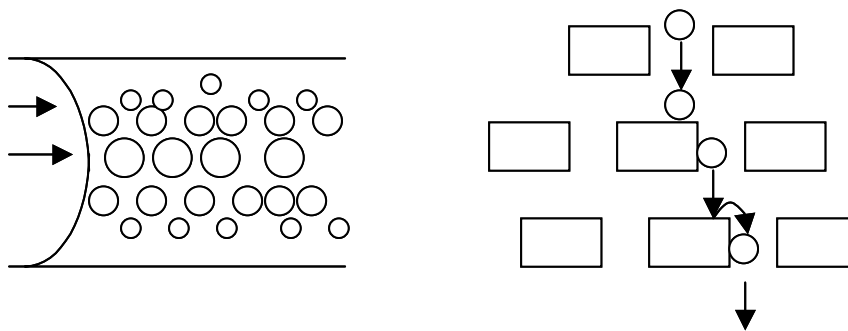


Figure 2: Principle of shear induced migration (left) and lateral displacement (right) in a so-called ratchet.

Shear induced migration implies the migration of suspended particles of a certain size towards the center of the channel in Poiseuille flow, due to the hydrodynamic interactions between particles of similar and of different sizes. With concentrated poly-disperse suspensions, the largest particles will migrate to the center of the channel, while smaller particles are excluded from the center and will be concentrated towards the wall of the channel. Kromkamp *et al.* achieved fractionation of poly-disperse suspensions based on this principle [9].

In lateral displacement in a ratchet, a particle chooses its path through a micro device with a repeating structure deterministically based on its size. Depending on the particle size, and the actual layout of the device this causes a deviation of the particle from its original streamline [10]. Since this effect is dependent (amongst others) on the size of the particle, this effect can be used to achieve fractionation.

It is too early to say whether these new methods will enable large-scale fractionation of poly-disperse suspensions. Significant research will be needed for the understanding and quantification of the mechanisms, and their subsequent translation into a practical process design. Similar to the microfiltration-based

processes that we reported on in this thesis, experimental studies of these new fractionation mechanisms are not trivial, and complementation with computer simulations would accelerate the progress of research in these fields. Both of these new particle segregation phenomena are well suited to study with computer simulations. The effects of (relative) particle concentrations, particle size difference, and process conditions can be investigated with the bi-disperse sub-grid particle approach described in chapter 7, that is based on the recently developed drag-force relation for bi-disperse particles [11]. This might open up the route towards the use of these mechanisms, either as an independent fractionation system for poly-disperse suspensions or as a hybrid fractionation process in combination with microfiltration technology.

References

- [1] C.J.M. van Rijn, M.C. Elwenspoek, Micro filtration membrane sieve with silicon micro machining for industrial and biomedical applications, Proceedings of Micro Electro Mechanical Systems (MEMS) (1995) 83, Amsterdam, the Netherlands.
- [2] C.J.M. van Rijn, Nano and micro engineered membrane technology, Elsevier Amsterdam (2004), ISBN 0444-51489 9.
- [3] V. Ramachandran, R. Venkatesam, G. Tryggvason, H.S. Fogler, Low Reynolds number interactions between colloidal particles near the entrance to a cylindrical pore. *J. Colloid Interface Sci.* 229 (2000) 311.
- [4] M. Girones, Z. Borneman, R.G.H. Lammertink, M. Wessling, The role of wetting on the water flux performance of microsieve membranes. *J. Membrane Sci.* 259 (2005) 55.
- [5] A. Arafat, K. Schroën, L.C.P.M. de Smet, E.J.R. Sudhölter, H. Zuilhof, Tailor-made functionalization of silicon nitride surfaces. *J. Am. Chem. Soc.* 126 (2004) 8600.
- [6] A. Chatterji, J. Horbach, Combining molecular dynamics with Lattice-Boltzmann: A hybrid method for the simulation of (charged) colloidal systems. *J. Chem. Phys.* 122 (2005) 184903.
- [7] J.A. Howell, Sub-critical flux operation of microfiltration, *J. Membrane Sci.*, 107 (1995) 165.
- [8] A. Shauly, A. Wachs, A. Nir, Shear-induced particle migration in a polydisperse concentrated suspension. *J. Rheol.* 42 (1998) 1329.
- [9] J. Kromkamp, F. Faber, K. Schroën, R. van der Sman, R. Boom, Effects of particle size segregation on crossflow microfiltration performance. In press *J. Membrane Sci.* (2005).

[10] L.R. Huang, E.C. Cox, R.H. Austin, J.C. Sturm, Continuous particle separation through deterministic lateral displacement. *Science* 304 (2004) 987.

[11] M.A. van der Hoef, R. Beetstra, J.A.M. Kuipers, Lattice Boltzmann simulations of low Reynolds number flow past mono- and bidisperse arrays of spheres: results for the permeability and drag force. *J. Fluid Mech.* 528 (2005) 233.

Summary

Within the food and chemical industry, there is a strong drive towards more sustainable production methods from renewable sources. Since the desired components are often part of heterogeneous mixtures, this has led to an increased interest in separation technology. In this thesis, the fractionation of suspended micro particles in a liquid is investigated, which can in principle be realized with membrane technology. However, the current state of knowledge on membrane processes is not yet detailed enough to warrant large-scale application. On top of that, the intrinsic fact that membranes have pore size distributions instead of one pore size complicates the design of a process meant to yield pure components. The use of innovative types of membranes, such as microsieves that have a uniform pore size, and computer modeling that could help in the detailed evaluation of process conditions seem a logic route to make membrane-based fractionation of milk feasible in the future.

The emergence of microsieve technology has opened up the possibility to design a membrane in all its aspects. The effects of pore to particle size ratio, pore geometry, and inter-pore distance (porosity) were evaluated with lattice Boltzmann (LB) simulations in chapter 3. Triangular pores pointing into the cross flow direction could give a 60 % higher flux than circular pores. High membrane porosities were found disadvantageous for particle uptake by the cross-flow, because of shielding by previously deposited particles. All investigated effects, such as pore to particle size ratio, pore geometry and porosity were captured in a single criterion for critical flux, which relates the microsieve pore design to the process conditions. This led to recommendation of different membrane designs for filtration, and fractionation purposes.

Besides the pore (field) design, we evaluated the microsieve as a whole (chapter 4). LB simulations and experiments showed that the support structure had a large effect on the flux. During dead end filtration of a particle suspension, the flux decreased initially faster than the prediction of a pore blocking model, while later on the flux decreased slower than predicted. This confirmed that the pore field had a non-uniform flux distribution, due to the substructure. The effect of the support structure only became negligible when the channel height under the pore field was increased to at least 150 μm .

The combination of particle transmission through the membrane with particle retention distinguishes membrane fractionation from other membrane filtration processes. In chapter 5, we described the transmission mechanisms of mono-

disperse latex particles through a polymer membrane. The effects of process parameters, such as transmembrane pressure, cross flow velocity and feed concentration were investigated. We identified four particle transmission regimes with polymer membranes, which could be related to the location of particle deposition.

Particle deposition was investigated in-line with Confocal Scanning Laser Microscopy. It was observed that random depth deposition took place in the polymer membrane (tortuous path), while the polymer microsieve exhibited in-pore fouling (cylindrical pores). It is expected that microsieves are better suited for fractionation purposes because the location of deposited particles is still within reach.

In fractionation of bi-disperse suspensions, it was found that the particle size ratio affected transmission of the smaller particle, but both particle sizes were involved in flux decrease. In fractionation of the tri-disperse suspension, the order in which particles are separated is of clear importance for optimization of the fluxes and transmissions (chapter 5).

To study the effect of process conditions on module scale, and to design the module, a new method for modeling 2D suspension flow was introduced in chapter 6. Suspended particles were treated as a second continuous density field and the mass transfer was described with a convection-diffusion model in LB. Concentration polarization and cake layer formation could be described accurately and were in agreement with an analytical model. Unlike analytical models, the LB model uses the actual local shear rate to calculate the local diffusivity, and can be used for complex geometries and dynamic systems. The model was used to evaluate the effect of turbulence promoters and corrugated membranes.

For suspension flows on intermediate scale, this continuum approach is too coarse to capture all relevant phenomena, such as particle segregation effects and particle-membrane interactions. Therefore, a 3D discrete particle simulation method was developed (chapter 7). Because these particles are smaller than the grid cells on which the fluid flow is solved, this approach is called sub-grid particle method, contrary to fully resolved methods, where particles consist of several grid cells. The method was validated with two benchmark studies. Ultimately, the method is to be used for modeling the fractionation of bi-disperse suspensions in microfiltration.

Finally, we discussed the practical implementations of our findings for membrane fractionation, and gave an outlook on the use of practical experiments and computer simulations in the design of fractionation processes (chapter 8).

Although considerable progress was made in this study, we feel that fractionation of particle suspensions will remain a challenge for future research, both experimentally and computationally, but at the same time we also feel that fractionation is within reach when given sufficient research effort.

Samenvatting

Binnen de chemische en levensmiddelenindustrie wordt gestreefd naar duurzame productiemethoden met hernieuwbare grondstoffen. Omdat deze grondstoffen vaak gewonnen worden uit complex samengestelde mengsels, is er groeiende aandacht voor scheidingstechnologie. In dit proefschrift wordt het fractioneren van gesuspendeerde micro deeltjes in vloeistof onderzocht, hetgeen kan worden bereikt met membranen. De huidige kennis van membraanprocessen is echter vaak onvoldoende voor grootschalige toepassingen. Bovendien hebben bestaande membranen een porie-grootteverdeling, in plaats van een uniforme poriegrootte, wat het scheiden in verschillende fracties moeilijker maakt. Door gebruik te maken van nieuwe typen membranen, zoals microzeven, en computer simulaties voor het optimaliseren van de procesparameters wordt het fractioneren van melk met membranen waarschijnlijk beter haalbaar in de toekomst.

Vanwege hun uniforme poriegrootte lijken microzeven de meest geschikte membranen voor fractioneren. Tevens kunnen de microzeven beter worden geoptimaliseerd voor een bepaald proces, omdat de productie een grote vrijheid van het ontwerp biedt. Hoofdstuk 3 beschrijft computer simulaties voor verschillende porie/deeltjes grootteverhouding, porievorm en afstand tussen de poriën (porositeit). Deze simulaties zijn uitgevoerd met de rooster Boltzmann methode (lattice Boltzmann, LB). Met driehoekige poriën (wijzend in de richting van de langsstroom) kon een 60% hogere flux worden behaald dan met ronde poriën. Een hoge membraan porositeit was nadelig voor het resuspenderen van neergeslagen deeltjes, omdat de deeltjes elkaar afschermen van de langsstroom. Alle effecten van porie/deeltjes grootteverhouding, porievorm en porositeit zijn samengebracht in een criterium voor kritische flux, dat de procesparameters relateert aan het membraanontwerp. Hiermee konden voor zowel fractioneren van deeltjes als tegenhouden van alle deeltjes verschillende membraan ontwerpen worden aanbevolen.

Behalve het ontwerp van de zeefvelden, is het ontwerp van de gehele microzeef bestudeerd (hoofdstuk 4). LB simulaties en experimenten toonden aan dat de onderliggende structuur een negatief effect had op de flux. Tijdens dead end filtratie van een deeltjessuspensie daalde de flux eerst sneller dan voorspeld met een porie-blokkeringsmodel, en daarna langzamer dan voorspeld. Dit bevestigde de ongelijke fluxverdeling door de zeefvelden. Met simulaties vonden we dat het effect van de

onderliggende structuur verwaarloosbaar wordt, als het kanaal onder het zeefveld minstens 150 μm is.

De combinatie van deeltjestransmissie en retentie onderscheidt fractioneren van andere membraanfiltratie processen. In hoofdstuk 5 wordt de transmissie van mono-disperse latex deeltjes door een polymeer membraan beschreven. De effecten van verschillende procesparameters, zoals transmembraandruk, langsstroomsnelheid en deeltjesconcentratie werden bestudeerd. We vonden vier verschillende transmissieregimes, afhankelijk van de aanhechtingsplaats van de deeltjes op het polymere membraan. De deeltjesafzetting op verschillende membranen werd tijdens het proces gevolgd met CSLM (Confocal Scanning Laser Microscopy). Bij het polymere membraan trad willekeurige dieptevervuiling op in de tortueuze structuur, terwijl de microzeef vervuild raakte in de cilindrische poriën van de toplaag. Men kan verwachten dat microzeven beter geschikt zijn voor fractioneren, doordat de aangehechte deeltjes beter toegankelijk zijn en gemakkelijker verwijderd zouden kunnen worden.

Tijdens het fractioneren van bi-disperse suspensies werd de transmissie van het kleine deeltje beïnvloed door de deeltjes-grootteverhouding. Beide deeltjesgroottes zijn echter bepalend voor het fluxverloop. Tijdens het fractioneren van een tri-disperse suspensie wordt de volgorde van het fractioneren van belang voor het optimaliseren van de fluxen en transmissies (hoofdstuk 5).

Om het effect van de procesparameters op moduleschaal en het moduleontwerp te bestuderen werd in hoofdstuk 6 een nieuwe 2D simulatiemethode ontwikkeld voor stroming van deeltjessuspensies. Massatransport van de gesuspendeerde deeltjes werd beschreven met een convectie-diffusie vergelijking in LB. Concentratie-polarisatie en koekopbouw waren in overeenstemming met analytische modellen. In tegenstelling tot de analytische modellen, gebruikt het LB model de lokale afschuifsnellheid voor de diffusiecoëfficiënt en kan het model worden gebruikt voor complexe geometriën en dynamische processen. Het model is toegepast voor het beoordelen van turbulentie promotoren en gecorrigeerde membranen.

Voor deeltjesstroming op mesoschaal is deze aanpak niet gedetailleerd genoeg om alle belangrijke effecten te beschrijven, zoals deeltjessegregatie en deeltjes-membraaninteractie. Daarom is een 3D discrete deeltjes simulatiemethode ontwikkeld in LB (hoofdstuk 7). Omdat de deeltjes kleiner zijn dan de roostercellen waarin de vloeistofstroming wordt opgelost, wordt deze aanpak de 'sub-grid particle' methode genoemd. Dit in tegenstelling tot volledig opgeloste methoden, waarbij de deeltjes een aantal roostercellen beslaan. Het model is vergeleken met twee

benchmarks en kan verder worden uitgewerkt voor het simuleren van bi-disperse suspensies.

Tenslotte gaan we in op de praktische gevolgen van dit onderzoek en geven we een toekomstvisie op het ontwerpen van membraan fractioneerprocessen met behulp van praktische experimenten en computersimulaties. Hoewel in dit onderzoek veel vooruitgang is geboekt, zal het fractioneren van deeltjessuspensies een uitdaging blijven, zowel in praktisch opzicht als in computer simulaties. Verder onderzoek zal het fractioneren van deeltjes met microfiltratie binnen bereik brengen.

Dankwoord

Na vier jaar en een paar maanden is het gelukt: mijn proefschrift is af. Ik ben blij dat ik geen grote tegenslagen heb gehad; al vind ik het jammer dat het niet gelukt is om met de originele microzeven deeltjessuspensies te fractioneren. Al begrijpen we nu wel een stuk beter waarom dat niet lukte. De tijd is snel voorbij gevlogen en ik heb het idee dat ik gisteren ben begonnen met dit promotie onderzoek. Dit onderwerp was een grote uitdaging en gaf aanleiding om de hersens te kraken op allerlei problemen, zowel wat betreft praktische experimenten als computer simulaties. Ik moet zeggen dat ik in dit project echt mijn ei kwijt kon en dat ik in deze periode veel heb bijgeleerd.

Uiteraard heb ik het niet kunnen doen zonder de hulp van anderen, die ik hierbij graag wil vernoemen. Als eerst gaat mij dank uit naar mijn begeleiders (promotor en co-promotoren) Remko, Karin en Ruud.

Remko bedankt dat je de kans bood om te promoveren. Ik vond het erg leuk om met je te discussiëren over praktische resultaten en simulaties. Daarbij ben je een grote bron van inspiratie die visie uitstraalt; en heb je oog voor detail om een artikel net wat extra inhoud te geven en naar een hoger niveau te tillen. Karin, ik vond het plezierig om met je samen te werken; door je grote theoretische en praktische kennis van membranen en de manier waarop je de afstudeerders mee hebt begeleid. Daarnaast kwam je (Engelse) taalgevoel goed van pas om mijn soms warrige alinea's logisch achter elkaar te zetten. Ruud, bedankt voor het opzetten van de lattice Boltzmann methode en jouw functie als vraagbaak hierbij. Ik waardeer je fysische kennis enorm en zonder jouw hulp had het nooit wat geworden met de simulaties (en al helemaal niet het sub-grid particle model). Ik hoop dat de kennis over lattice Boltzmann binnen de vakgroep zal blijven voortbestaan en er nog vele mooie dingen uit voortkomen.

Vervolgens wil ik de projectpartners van het D-force project bedanken:

Friesland Foods: Rolf, Albert en Frank voor hun visie op het onderzoek waarbij ze op inspirerende wijze de praktische relevantie binnen het D-force project wisten te belichten. Janneke voor de prettige samenwerking ook als collega bij proceskunde; ik vind het erg leuk dat we samen twee artikelen hebben geschreven. De jongens op het lab in Deventer, Bas en Reinier, voor allerlei praktische zaken met microzeven en Anno Koning voor de CSLM opnamen. Ik heb met veel plezier met jullie mogen

samenwerken en waardeer jullie bereidwilligheid om mee te werken aan mijn onderzoek heel erg.

Aquamarijn Micro Filtration: Cees en Wietze voor discussies over het ontwerp van microzeven en het van specifieke verschijnselen die microzeven zo speciaal maken. Membrane Technology Group in Twente: Matthias, Rob, Zandrie en Míriam voor interessante discussies over fluxen en 'fouling' van microzeven, en het beschikbaar stellen van de polymere microzeven. Deze polymere zeven hebben wezenlijk bijgedragen aan de begripsvorming van fractioneringssystemen.

Verder ben ik dank verschuldigd aan Jos en Gerrit voor het oplossen van allerlei praktische problemen met membraan modules, pompen, computers en printers. Aan Boudewijn voor je hulp met microscopie.

Aan Jan, Hans R. en Hans M. van de technische werkplaats voor het ontwerpen van mooie membraanmodules en alle elektronische randapparatuur. Aan Pieter, Olivier en Hylke voor ondersteuning van waardoor ik de nodige simulaties heb kunnen doen op het PC cluster van proceskunde. Aan Lorenzo de la Fuente, Alfons Hoekstra (Universiteit van Amsterdam), en Mike Cates, Kevin Stratford (EPCC Edinburgh, Schotland) voor hulp tijdens het programmeren.

Daarnaast wil ik graag de afstudeerders bedanken die aan dit project hebben meegewerkt: John, Benedict, Jan-Harm, Kirsten, Emmanuel, Martijn, Chun Ya en Anna. Membraanfiltratie van latex deeltjes met microzeven en polymeer membranen bleek een pittig onderwerp en de resultaten waren vaak lastig te verklaren. Desondanks heeft jullie werk geresulteerd in een interessant artikel.

Dankzij de goede sfeer op het werk was het elke dag weer een plezier om de berg op te fietsen. Met kamergenoten Marieke B., Marieke W., Eira, Marisca, René D., Michel, Dominik, Gosia zijn we samen alle ups en downs doorgekomen op kamer 620. Met Sandra en Eduard heb ik leuke momenten beleefd tijdens congressen; vooral NYM was erg geslaagd! Martijn bedankt voor je ski-lessen op de wintersport; Maarten, Julita, Sebastiaan Hoekema, Detmer en Jeroen: Ik genoot van de talrijke partijtjes squash om lekker los te gaan.

Uiteraard de hele vakgroep proceskunde bedankt voor alle mooie vakgroep-activiteiten: aio-reizen, labuitjes, we-day, promotiefeesten, kerstdiners, hap-en-stap avonden ("MG": Marleen, Cynthia, Sandra) en ga zo maar door. Ik vond het erg gezellig om in het begin van mijn promotie te carpoolen met Mark ("als je mee helpt opletten, zorg ik dat we lekker snel thuis zijn"). Ik zal het allemaal erg missen.

Ik vond het eveneens erg gezellig om af te spreken met de oud-huisgenoten van Nobelweg 6: Remko, Ype, Meinou, Carl en Lenie, Pieter en Jeanine, Harry, Jan-Jelle, Tineke om te barbeque-en aan de Rijn of te RISK-en, en met mijn huisgenoten op de Hoogstraat: Mieke, Marije en Arnaut, Tim, Eelke, Femke en Louis, Kathelijn, Jop.

Met de kaartvrienden van de middelbare school Marc, Edwin en Theo bracht ik gezellige avonden door met “potjes rikken” tot vroeg in de nacht. De mannen van Zomerlust en TCW A1 zorgden voor de nodige ontspanning op de racefiets en mountainbike. Daarnaast heeft Rogier de geocache wandeltochten geïntroduceerd, waarover ik erg enthousiast geworden ben.

Verder wil ik iedereen bedanken die op welke manier dan ook heeft meegewerkt aan de totstandkoming van dit proefschrift.

Tenslotte wil ik mijn ouders (pa en ma) en mijn broer Roland bedanken voor hun onvoorwaardelijke steun. En tevens voor het gevoel dat ik altijd thuis welkom ben in Wouwse Plantage.

Curriculum Vitae

Gerben Brans was born on September 2, 1976 in Wouwse Plantage. He attended primary school at “Basisschool De Stappen” in Wouw, and secondary school (VWO) at “Norbertus College” in Roosendaal.

In 1994, he started the Bioprocess Engineering study at Wageningen University and graduated in 1999 with technological specialization. Between 1999 and 2001, he worked for Cargill BV R&D in Bergen op Zoom as research technologist. Gerben started his Ph.D. project in September 2001 at the Food and Bioprocess Engineering group of Wageningen University on the subject of fractionation of particle suspensions with membrane technology.

Since December 2005, he is employed by Applikon BV in Schiedam and is involved in bioreactor development for tissue engineering.

This work was financially supported by the Dutch ministries of education, culture, science, economics and environmental affairs. This research was part of the EET program, project EETK 20033.